

Diss. ETH No. 16299

Pozzolanic activity of natural clay minerals with respect to environmental geotechnics

A dissertation submitted to the
SWISS FEDERAL INSTITUTE OF TECHNOLOGY ZURICH

for the degree of
Doctor of Technical Science

presented by

CHRISTIAN JÖRG MÜLLER

Dipl. Mineralogist, University of Karlsruhe

born 15.12.1969

citizen of Esslingen (Germany)

accepted on the recommendation of

Prof. Dr. Sarah Springman, examiner
Dr. Rita Hermanns Stengele, co-examiner
Prof. Dr. Ruben Kretschmar, co-examiner
Dr. Michael Plötze, co-examiner

Zurich 2005

Acknowledgements

My special thanks go to my examiners, Prof. Dr. Sarah Springman, Dr. Rita Hermanns Stengele, Prof. Dr. Ruben Kretzschmar and Dr. Michael Plötze, for their professional, technical supervision and for offering me the possibility of writing this thesis. In this context, my hidden supervisor, Dr. Günter Kahr, has to be mentioned and thanked for numerous technical discussions on our way home.

Dr. Gianluca Ambrosini, Ernst Bleiker, Dusan Bystricky, Fredi Ehrbar, Ildiko Fonyo, Beat Hornung, Hermann Moench, Inge Reichenbach, Matthias Schwotzer, Dr. Peter Wägli and Andrea van der Zande helped and supported me in the laboratory whenever I had problems that had to be solved. I gratefully acknowledge that and “thanks for the good times”. Many thanks to Dr. Sven Friedel who supported me with the mathematics of the evaluation model for thermal analysis.

I would like to thank the Swiss Federal Institute of Technology Zurich and the Institute for Geotechnical Engineering for financial support.

Last but not least, I want to mention my family, Gaby, Fabio, Leoni and Jascha who sometimes had to suffer from a “mentally” absent partner and father. Many thanks to them for always supporting me in the past several years.

List of Contents

ABSTRACT

ZUSAMMENFASSUNG

LIST OF FIGURES

LIST OF TABLES

ABBREVIATIONS AND DEFINITIONS

CHAPTER 1 Introduction and goals 1

CHAPTER 2 Clay-lime interactions 5

2.1 Historical Introduction 5

2.2 Definitions. 7

2.3 Natural clay minerals as pozzolans? 9

2.4 Importance of pozzolanic properties of clay minerals to geotechnics 10

2.5 Chemical aspects associated with the pozzolanic reaction 12

2.5.1 Pozzolanic reaction of clay minerals I: cation exchange, swelling and rheology. 14

2.5.2 Pozzolanic reaction of clay minerals II: dissolution, precipitation and pore refinement 21

CHAPTER 3 Analytical methods, materials and sample preparation/handling . 27

3.1 Standard analytical methods 27

3.1.1 Loss-on-ignition 27

3.1.2 Inductively coupled plasma atomic emission spectroscopy 28

3.1.3 Wavelength dispersive X-ray fluorescence. 28

3.1.4 Cation exchange capacity and exchangeable cations 28

3.1.5 X-ray diffraction 29

3.1.6 Rheological measurements 30

3.1.7 Extraction of remaining clay minerals 32

3.1.8 (Environmental) Scanning electron microscopy (ESEM and SEM) 33

3.1.9 Mercury intrusion porosimetry 33

3.2 Thermal gravimetry with evolved gas analysis 34

3.2.1 Evaluation model for quantification of TG-EGA data 34

3.2.2 Determination of portlandite and clay minerals by their evolved crystal or hydroxyl water . 38

3.3 Calculation of results 40

3.3.1 Calculation of consumed contents of clays and lime 40

3.3.2 Standard deviation and standard error of the mean. 41

3.4 Materials and their characterisation 41

3.4.1 Kaolin 'China Clay' 42

3.4.2 Illitic clay from Massif Central (Le Puy) 43

3.4.3 Bentonite Volclay 44

3.4.4 Decarbonated water. 46

3.4.5 Calcium hydroxide 46

3.4.6 Other chemicals. 47

3.5 Sample preparation and handling 47

3.5.1 Pozzolanic reaction of clay minerals I 47

3.5.2 Pozzolanic reaction of clay minerals II. 50

CHAPTER 4 Quantitative X-ray diffraction and calibration of internal standard method	53
4.1 Introduction to the internal standard method	53
4.2 Determination of portlandite content	55
4.2.1 Internal standard	55
4.2.2 Calibration line for portlandite quantification	56
4.2.3 Calculation of results in the reacted samples	58
4.2.4 Summary	59
4.3 Flexible structure models	59
4.4 Flexible structure model of triclinic kaolinite	63
4.5 Flexible structure model of triclinic portlandite	66
4.6 Flexible structure models applied to swelling montmorillonite	69
4.6.1 Summary	73
CHAPTER 5 Pozzolanic reaction of clay minerals I: cation exchange, swelling and rheology	75
5.1 Results and discussion	75
5.1.1 Cation exchange	75
5.1.2 Swelling measurements at controlled relative humidity	80
5.1.3 Rheology	81
5.2 Conclusions	84
CHAPTER 6 Pozzolanic reaction of clay minerals II: dissolution, precipitation and pore refinement	85
6.1 Results and discussion	85
6.1.1 Comparison of initial and after reaction extracted clays	85
6.1.2 Reaction products	89
6.1.3 Extent of pozzolanic reaction and passivation effects	91
6.1.4 Estimation of reaction equations	95
6.1.5 Pore refinement	96
6.1.6 Porosity development	99
6.2 Conclusions	101
CHAPTER 7 Relevance of results to geotechnics	103
7.1 Pozzolanic reaction of clay minerals I: cation exchange, swelling and rheology	103
7.1.1 Cement-stable bentonites	103
7.2 Pozzolanic reaction of clay minerals II: dissolution, precipitation and pore refinement	106
7.2.1 Soil lime solidification	106
7.2.2 Cut-off wall materials	106
CHAPTER 8 Summary and outlook	109
8.1 Summary	109
8.2 Outlook	111

APPENDICES

CURRICULUM VITAE

Abstract

This study is addressed to the chemical reactions that occur in engineered geo-materials during the interaction of clay minerals and lime (e.g. pozzolanic reaction). These reactions were investigated on three different clay minerals (kaolinite, illite and montmorillonite) in the system clay mineral-lime-water. Due to the solidifying, cementing character of the pozzolanic reaction, the study is subdivided into the period before substantial solidification occurs, mainly influenced by cation exchange phenomena, and into the period after, mainly influenced by dissolution and precipitation phenomena. The impact of these chemical reactions on physical properties (rheology, microstructure) of engineered geo-materials are shown.

The addition of lime to aqueous sodium-montmorillonite-dispersions results in the short-term in an equilibrium shift towards the calcium form of the montmorillonite. This is mainly because of the high aqueous calcium concentration in equilibrium with lime. An intensifying effect due to the calcium speciation at high pH appeared very probable. In either case, re-adsorption of sodium on lime-treated montmorillonite was hindered. The different sorption behaviour of the clay mineral's edge and outer surface sites on the one hand, and interlayer sites on the other hand, greatly influences the crystalline swelling behaviour of the montmorillonite and the yield point of its dispersions. The preferred sorption of calcium into the interlayers causes sodium to sorb primarily on the outer surfaces of the clay mineral. Sodium enters the interlayer space and causes interlayer expansion only after occupancy of these outer surfaces. These effects resulted in a significant increase of the dispersions' yield point at around 20% of adsorbed sodium. Further addition of sodium reduced the yield point again due to the contraction of interlayers' space and of the diffuse ion layer.

In practical applications, sodium-montmorillonite dispersions in the presence of lime are therefore in a calcium-montmorillonite-like state without additional sodium dosages. Even with subsequent sodium additions, this state is irreversibly fixed on the time-scale relevant for practical applications. Sodium salts, which reduce the calcium concentration in equilibrium with lime (e.g. sodium carbonate and sodium hydroxide), seem to be an

exception. From practice, it is known that these salts are capable of increasing the yield point even after lime has been added. The inclusion of other sodium salts with no such effect (e.g. NaCl), prior to the addition of cement or lime, would be an alternative approach to increase the dispersion's yield point. For this purpose, the necessary amount can be estimated from the cation exchange behaviour determined in this study.

The continuous dissolution of clay minerals in the presence of lime leads in the long-term to the cementation of the materials by the formation of cement hydrates. The cementation has proceeded after one to two months as far as the surfaces of the clay mineral-lime aggregates were completely covered with reaction products. This led to the cessation of the dissolution reaction. Whether dissolution proceeds further after the seven months investigated (e.g. through the development of steady-state diffusion profiles), was not resolved in this study. In analogy to long-term investigations on the strength development of lime-stabilised soils, this seems however very probable. In either case, the precipitation of reaction products additionally leads to a reduction of porosity as a result of the filling or closure of the macro- respectively inter-aggregate pores. Mass balance derived reaction equations show that the estimated composition of the reaction products is realistic in comparison with literature data and that a major part of the measured porosity reduction can be ascribed to the pozzolanic reaction.

It follows with respect to soil solidification techniques, at least for fine grained soils with mainly clay minerals, that the lime fixation point as defined for soil improvement (~4%) is not sufficient by far for a sustainable, long-lasting solidification. At least 9% of lime for illite and 11% for kaolinite have to be added in order to solidify the material in a sustainable form. For montmorillonite, this necessary lime content may even be as high as 20%. Only a fraction of this 20% is used for the solidification process by the pozzolanic reaction. Implications of this significantly increased lime demand can not be discussed further from the results obtained.

With respect to barrier materials rich in clay minerals, it follows that no extensive dissolution of these active (e.g. contaminant-sorbing) components is to be expected in the presence of cement. The content of the three clay minerals was reduced in the first three to seven months by 7% to 9% in absolute terms. Much more crucial for the choice of clay minerals as active components in an environmental geotechnical sense is the passivation

of their reactive surfaces. Contaminants entering the barrier can only contact the clay minerals' surfaces by slow diffusion through the overgrown reaction products (cement hydrates). The performance of engineered barrier materials made of clays and cement is thus not only influenced by the cementing and pore-filling action of the cement hydrates, the resulting strength development and also by the associated increase in brittleness and reduction of permeability. The retention of contaminants by cement hydrates becomes also a major function of such materials which has to be considered for the design of engineered barriers in respect of optimising environmental protection.

For mixtures of clay and cement in general, there are consequences for a necessary lime addition in some instances. If the cement content in the mixture is chosen to be low (< 30%), the lime content produced during cement hydration (< 9%) may become limiting for the pozzolanic reaction. Thus, additional benefits arising from the cementing and pore refinement potential of the pozzolanic reaction can not be fully used. In that case, lime addition to the clay-cement mixture should be carried out.

Zusammenfassung

Die vorliegende Arbeit befasst sich mit den chemischen Reaktionen, die während der Tonmineral-Kalkhydrat-Wechselwirkung (u.a. puzzolanische Reaktion) in geotechnischen Baumaterialien auftreten. Diese Reaktionen wurden modellhaft im System Tonmineral-Kalkhydrat-Wasser an drei verschiedenen Tonmineralien (Kaolinit, Illit und Montmorillonit) untersucht. Aufgrund der verfestigenden, zementierenden Wirkung der puzzolanischen Reaktion wurde die Arbeit zweigeteilt, in die Zeit vor einer wesentlichen Verfestigung, beeinflusst durch Kationenaustausch-Phänomene, und in die Zeit danach, beeinflusst durch Auflösungs- und Ausfällungs-Phänomene. Auswirkungen dieser chemischen Reaktionen auf physikalische Eigenschaften (Rheologie und Mikrostruktur) der geotechnischen Baumaterialien werden aufgezeigt.

Kurzfristig betrachtet, bewirkt die Zugabe von Kalkhydrat zu wässrigen Natrium-Montmorillonit-Dispersionen eine Verschiebung des Gleichgewichtes in Richtung der Calcium-Form des Montmorillonits. Dies ist v.a. begründet in der hohen Löslichkeit von Kalkhydrat. Ein verstärkender Effekt aufgrund der Calcium-Speziierung bei hohem pH erscheint als sehr wahrscheinlich. In jedem Fall war die erneute Natrium-Adsorption an Kalkhydrat-behandeltem Montmorillonit gehemmt. Das unterschiedliche Sorptionsverhalten der Kanten und äusseren Oberflächen einerseits und der Zwischenschichten des Tonminerals andererseits hat einen wesentlichen Einfluss auf das kristalline Quellverhalten des Montmorillonits und auf die Fliessgrenze der Dispersionen. Die bevorzugte Sorption von Calcium in der Zwischenschicht hat zur Folge, dass Natrium zuerst auf den äusseren Oberflächen sorbiert wird. Erst nach der Belegung dieser äusseren Oberflächen dringt Natrium in die Zwischenschichten ein und bewirkt eine Aufweitung des Zwischenschichttraumes und ein Aufbrechen der Taktoide des Montmorillonits. Diese Effekte hatten eine deutliche Erhöhung der Fliessgrenze der Montmorillonit-Dispersionen bei ungefähr 20% adsorbiertem Natrium zur Folge. Bei weiterer Zugabe von Natrium verringerte sich die Fliessgrenze wieder aufgrund der Kontraktion des Zwischenschichttraumes und der diffusen Ionenschicht.

Für praktische Anwendungen ergibt sich daraus, dass Natrium-Montmorillonit-Dispersionen in Anwesenheit von Kalkhydrat ohne zusätzliche Natrium-Zugabe in einem Calcium-Montmorillonit-ähnlichen Zustand vorliegen. Auch bei nachträglicher Natriumzugabe ist dieser Zustand in für praktische Anwendungen relevanten Zeiträumen irreversibel festgelegt. Eine Ausnahme scheinen Zugaben von Natrium-Salzen zu bilden, die die Calcium-Konzentration im Gleichgewicht mit Kalkhydrat erniedrigen (z.B. Natriumkarbonat oder Natriumhydroxid). Von diesen ist aus praktischen Erfahrungen bekannt, dass sie die Fließgrenze auch nach erfolgter Kalkhydrat-Zugabe erhöhen können. Eine alternative Möglichkeit zur Erhöhung der Fließgrenze von Montmorillonit-Dispersionen wäre die Zugabe von anderen Natrium-Salzen (z.B. NaCl), bevor Zement oder Kalkhydrat zudosiert werden. Abschätzungen über die notwendige Menge an Natrium können über das in dieser Arbeit bestimmte Kationenaustauschverhalten vorgenommen werden.

Die kontinuierliche Auflösung der Tonminerale in Anwesenheit von Kalkhydrat führt langfristig zur Zementierung der Materialien durch die Bildung von Zementhydraten. Diese Zementierung war nach ein bis zwei Monaten soweit abgelaufen, dass die Oberflächen der Tonmineral-Kalkhydrat-Aggregate mit Reaktionsprodukten vollständig überwachsen waren. Dies führte zum Stillstand der Auflösungsreaktion. Ob diese Auflösungsreaktion nach mehr als den sieben untersuchten Monaten weiter fortschreitet (z.B. durch Ausbildung von steady-state Diffusionsprofilen) konnte nicht geklärt werden, erscheint aber in Analogie mit Langzeitmessungen zur Festigkeitsentwicklung von Kalkhydrat-stabilisierten Böden sehr wahrscheinlich. In jedem Fall führt die Ausfällung der Reaktionsprodukte durch das Verfüllen oder den Verschluss der Makro- bzw. Interaggregatporen zusätzlich zu einer Porositätsreduktion. Mittels Massenbilanz abgeleitete Reaktionsgleichungen zeigen, dass die berechnete Zusammensetzung der Reaktionsprodukte im Vergleich mit Literaturdaten realistisch ist und dass ausserdem ein Grossteil des gemessenen Porositätsverlustes auf die puzzolanische Reaktion zurückzuführen ist.

Im Hinblick auf Bodenvermörtelungsmassnahmen ergibt sich daraus, dass in feinkörnigen Böden mit überwiegend Tonmineralen der minimale Kalkhydratgehalt, der zur Bodenverbesserung empfohlen ist (~4%), in keinem Fall für eine nachhaltige, langan-

haltende Bodenverfestigung ausreichend ist. Für eine nachhaltige Bodenverfestigung müssen einem solchen Boden mindestens 9% Kalkhydrat für Illit und 11% für Kaolinit zugegeben werden. Für Montmorillonit ergibt sich sogar ein hierfür notwendiger Kalkhydratgehalt von 20%, wobei nur ein Teil dieser 20% für die Verfestigung durch die puzzolanische Reaktion verwendet wurde. Die Konsequenzen aus diesem stark erhöhten Kalkhydratbedarf können jedoch mit den erhaltenen Ergebnissen nicht weiter diskutiert werden.

Im Hinblick auf tonmineralreiche Barrierematerialien resultiert, dass keine weitgehende Auflösung der Tonminerale in Gegenwart von Zement zu erwarten ist. Der Gehalt der drei Tonminerale verringerte sich in den ersten drei bis sieben Monaten um 7% bis 9% absolut. Viel bedeutender für umweltgeotechnische Massnahmen und entscheidender für die Wahl von Tonmineralen als aktive (z.B. Rückhalt von Schadstoffen) Komponenten ist die Passivierung ihrer reaktiven Oberflächen. Schadstoffe, die in die Barriere eindringen, können die Tonmineraloberflächen nur noch durch langsame Diffusion durch die aufgewachsenen Reaktionsprodukte (Zementhydrate) erreichen. Die Funktionalität technischer Barrierematerialien aus Ton und Zement wird also nicht nur durch das Zementierungs- und Porenverfüllungsvermögen der Zementhydrate, den resultierenden Festigkeitszuwachs und den damit verbundenen Anstieg der Sprödigkeit und die Reduktion der Permeabilität bestimmt. Der Rückhalt von Schadstoffen an Zementhydraten muss als weitere wichtige Eigenschaft solcher Materialien betrachtet und bei der Konzeption technischer Barrieren zum Schutz der Umwelt berücksichtigt werden.

Für Mischungen aus Tonmineralen und Zement allgemein ergeben sich Konsequenzen für eine unter Umständen notwendige Kalkhydratzugabe. Wenn der Zementgehalt in der Mischung niedrig gewählt wird ($< 30\%$), kann der während der Zementhydratation entstehende Kalkhydratanteil limitierend für die puzzolanische Reaktion werden. Somit kann das Zementierungs- und Porenverfüllungspotential der puzzolanischen Reaktion nicht vollständig genutzt werden. In diesem Fall sollte ein Kalkhydratzusatz zur Ton-Zement Mischung erfolgen.

List of Figures

CHAPTER 2 Clay-lime interactions	5
Figure 2-1. The ancient harbour of Puteoli (more than 2000 years old). Today the structures have been covered by the modern harbour. The drawings below may give an impression (a) what the original structure looked like and (b) how it deteriorated later on (left: drawing by G. P. Bellori 1764, right: drawing by P. A. Paoli 1768) [CNR 2005].	6
Figure 2-2. (a) Predominance area diagram in the system Ca^{2+} - H_2O - $\text{Ca}(\text{OH})_2$ as a function of pH and $[\text{Ca}^{2+}]$ concentration and (b) fractions of soluble calcium-species with pH in this system; calculated with the chemical equilibrium program Medusa [Puigdomenech, 2000].	15
Figure 2-3. Crystalline swelling of the sodium and calcium form of montmorillonite: (a) water content with relative water pressure (relative humidity), (b) basal distance between clay mineral's layers with relative humidity [modified from Plötze & Kahr, 2003]	17
Figure 2-4. Phase diagram showing the different states of a bentonite dispersion as a function of ionic strength and solid content [modified from Abend & Lagaly, 2000].	18
Figure 2-5. Thickness of the diffuse ion layer for monovalent ions approximated as five times the reciprocal Debye-Hückel length [data taken from Lagaly et al., 1997] and measured basal spacing [data taken from Norrish, 1954b], both as a function of the normality of solution.	19
Figure 2-6. Schematic representation of the four states of a bentonite dispersion; solid content and ionic strength lead to transitions between the states; the influence of solid content is symbolised through the number of tactoids in black, the one of ionic strength through the thickness of the diffuse ion layer in grey surrounding the particles.	20
Figure 2-7. Aggregation of elementary clay particles [modified from Touret et al., 1990].	20
CHAPTER 3 Analytical methods, materials and sample preparation/handling ..	27
Figure 3-1. XRD sample chamber (without the closure unit) for experiments at controlled humidity and temperature.	30
Figure 3-2. Determination of the Cross-Over Point of a bentonite dispersion with 100g/l bentonite: Storage and loss moduli of a bentonite dispersion with shear stress.	31
Figure 3-3. Schematic representation of a mass loss and the associated signal from the mass spectrometer due to an evolved volatile component.	35
Figure 3-4. Calibration lines for the carbon dioxide evolving from decomposing calcite (left) and for the water from decomposing kaolinite (right); the slope of the lines is the effective sensitivity.	35
Figure 3-5. Two mixtures of clay and calcite analyzed by their evolved gases from decomposition; Volclay with calcite (a) fitted with the primitive model and (c) with the temperature dependent model; China Clay with calcite (b) fitted with the primitive model and (d) with the temperature dependent model.	37
Figure 3-6. TA data for a 7 month reacted China Clay-lime-water mixture (15 g/70 g/100 g); calcite content 1.5%. Simulation of used mineral fractions per total ignited mass ($\text{CaO}/\text{oxide}_{\text{clay}} = 1.4$) gives a consumed content of 12.0% for lime and 8.6% for the clay. The solid lines in the upper figure indicate the cut-offs used as a first estimate for the determination of lime water and China Clay hydroxyl water.	39
Figure 3-7. Particle size distribution of the China Clay calculated from mercury intrusion porosimetry.	42
Figure 3-8. TG-MS data of the kaolin China Clay; the first water peak of the illite corresponds to ~1 % water loss.	43
Figure 3-9. Particle size distribution of the illite MC calculated from mercury intrusion porosimetry.	43
Figure 3-10. TG-MS data of the illitic clay.	44

Figure 3-11.	Particle size distribution of the bentonite Volclay calculated from mercury intrusion porosimetry.	45
Figure 3-12.	TG-MS data of the < 20 μm sieve fraction of the bentonite Volclay.	45
Figure 3-13.	Particle size distribution of the calcium hydroxide calculated from mercury intrusion porosimetry.	46
Figure 3-14.	TG-MS data of portlandite; the small loss of CO_2 corresponds to $\sim 1.5\%$ of calcite.	47
Figure 3-15.	Schematic picture of the experimental setup for the cation exchange experiment.	48
Figure 3-16.	Schematic adsorption isotherm showing the two different preparation steps.	49
Figure 3-17.	Automatic control of relative humidity and temperature during a desorption and adsorption measurement in the humidity chamber.	50

CHAPTER 4 Quantitative XRD and calibration of internal standard method 53

Figure 4-1.	Calibration line for the measured portlandite content versus the actual content; error bars correspond to the 1-s estimated standard deviation, as calculated by the program BGMN.....	57
Figure 4-2.	The original montmorillonite structure of Tzipursky & Drits (1984) and the expanded ones in bc projection, with basal distances of 9.85 \AA (left), 12.4 \AA (middle) and 15.2 \AA (right).	59
Figure 4-3.	Schematic representation of a flexible structure model for a triclinic 2:1 layer clay mineral. In this example, the unit cell is defined (as commonly) such as the lower and upper half part of an individual solid layer may slide over each other with the interlayer as the sliding plane.	60
Figure 4-4.	Starting crystallographic angles α and β and fitted ones (dots), the stars indicate the fits with the best R_{wp} values < 0.7 of the mean R_{wp}	63
Figure 4-5.	Shifts in the crystallographic a and b direction calculated from the fitted unit cell parameters.....	64
Figure 4-6.	The original kaolinite structure in bc projection and the -b/3 and +b/3 translationally disordered ones.	65
Figure 4-7.	Rietveld refinement plot of the raw China Clay.....	65
Figure 4-8.	Three different structure models refined on the same profile. top: triclinic portlandite with isotropic crystallite size ($R_{\text{wp}} = 24.8\%$); middle: triclinic portlandite with anisotropic crystallite size ($R_{\text{wp}} = 22.7\%$); bottom: hexagonal portlandite with anisotropic crystallite size ($R_{\text{wp}} = 23.2\%$).....	67
Figure 4-9.	Portlandites from the ICSD (some numbers identified at the data points); left: cell dimensions a versus c; right: cell dimension c as a function of z coordinate of oxygen atom.....	68
Figure 4-10.	Schematic picture of the average development of an interstratified sample of one- and two-layer hydrates of montmorillonite with increasing humidity	70
Figure 4-11.	Basal spacing with relative humidity of the pristine Volclay material in desorption; open circles: desorption measurements of an at 75 % RH pre-equilibrated sample, crosses: basal spacing of either one of the flexible structure models supposed to represent discrete one- or two-layer hydrate crystallites; the arrow indicates the extracted transition point discussed in the text.	71
Figure 4-12.	Top: Basal spacing of the two flexible structure models with relative humidity; bottom: Fractions of quartz (crosses) and of the two flexible structure models with relative humidity.	72
Figure 4-13.	Development of the basal spacing of a sodium montmorillonite with relative humidity; measured data in dark blue, baseline in red, fitted data in green and the residuals in light blue.....	72

CHAPTER 5 Pozzolanic reaction of clay minerals I..... 75

Figure 5-1.	Double logarithmic plot of the sodium isotherm at constant calcium concentration but variable ionic strength.....	75
Figure 5-2.	Correlation between sorbed sodium and calcium amounts on the bentonite samples.	76

Figure 5-3.	TG-MS curve under nitrogen of the sample with sorbed sodium (7 mmol/100g) and calcium (142 mmol/100g).....	77
Figure 5-4.	Indirect adsorption data from measured solution values in addition with the direct data from Fig. 5-1 (without error bars); note: first sample series adsorbed sodium below detection limit.	79
Figure 5-5.	Transition from one- to two layer hydrate depending on the relative humidity as a function of the adsorbed amount of sodium.	81
Figure 5-6.	Cross-over points as a function of the calculated amounts of adsorbed sodium; note: first sample series adsorbed sodium below detection limit. The three tactoid regions refer to the schematic picture at the end of this chapter.	82
Figure 5-7.	Schematic picture of the evolution of tactoids in dispersions with constant solid content (number of primary layers), constant calcium (solubility of CH) but varying sodium concentrations; the grey shaded area symbolises the diffuse ion layer.....	83

CHAPTER 6 Pozzolanic reaction of clay minerals II 85

Figure 6-1.	Comparison of thermal gravimetry patterns of initial and after reaction extracted clays: (a) illite MC, (b) China Clay and (c) Volclay. Y-axis: differential mass loss in arbitrary units.....	86
Figure 6-2.	Comparison of X-ray diffraction patterns of initial and after reaction extracted clays: (a) illite MC, (b) China Clay and (c) Volclay. Y-axis: X-ray intensity in arbitrary units.....	87
Figure 6-3.	Major reaction products after three months for reacted Volclay-lime mixtures at a water to solid ratio of 13, (a) lath-shaped AFm phase, (b) platy hexagonal AFm phase, (c) bundle of ettringite needles, (d) AFm and C-S-H phases intergrown, (e) foil-shaped C-S-H phase and (f) huge hexagonal AFm phase in an aggregate of a China Clay-lime mixture at a water to solid ratio of 2.	88
Figure 6-4.	X-ray diffractograms of the three initial clays and clay-lime mixtures (39/13/100) reacted for 3 months: (a) illite MC, (b) China Clay and (c) Volclay. Y-axis: X-ray intensity in arbitrary units.....	90
Figure 6-5.	TG-MS data of the initial and clay-lime mixtures in fig. 6-4: (a) illite MC, (b) China Clay and (c) Volclay. Y-axis: differential mass loss in arbitrary units.....	91
Figure 6-6.	Reacted fractions of China Clay and lime with their initial contents in the solid mixture: upper figure metal oxides _{China Clay} from extract, lower figure CaO _{CH} from XRD. The number at each data point gives the reaction time in days.....	92
Figure 6-7.	Aggregates of reacted clay-lime mixtures after three months cemented and surrounded by pozzolanic reaction products (w/s = 13). (a) Illitic clay-lime mixture, (b)-(d) Volclay-lime mixture.	93
Figure 6-8.	Released silicon with median particle diameter of the clay mineral.	95
Figure 6-9.	Fragments of freeze-dried China Clay-lime specimens (15/70/100), reacted for 1 month (left), 2 months (middle) and 7 months (right); scale is in centimeters.	97
Figure 6-10.	Temporal development of the pore size distribution in the China Clay-lime mixture (15/70/100); (a) 1 month, (b) 2 month, (c) 3 month, and (d) 7 month hydrated samples. Relative pore volume shown as histogram.	98
Figure 6-11.	Development of total porosity in mixtures with compositions given in Table 6-5; the error bars correspond to the standard error of the mean, missing error bars indicate a single determination only.....	100

CHAPTER 7 Relevance of results to geotechnics 103

Figure 7-1.	Diagram showing the bentonite content versus the total amount of sodium (i) introduced through a pure sodium bentonite, (ii) necessary to maintain an exchangeable sodium percentage ESP of 15 or 25 % in the presence of lime.	104
-------------	--	-----

List of Tables

CHAPTER 2 Clay-lime interactions	5
Table 2-1. Pozzolans	7
CHAPTER 3 Analytical methods, materials and sample preparation/handling ..	27
Table 3-1. Comparison of LOIs determined at 1000°C either by standard method or by thermal analysis (TA).....	28
Table 3-2. Initial mass before and percentage of material recovery after extraction.	32
Table 3-3. Comparison of contents of added calcite with the fitted values.	38
Table 3-4. Molar volumes calculated from the mineral densities and their molar masses	52
CHAPTER 4 Quantitative X-ray diffraction and calibration of internal standard method	53
Table 4-1. Second series of mixtures prepared for the calibration of portlandite quantification with XRD	58
Table 4-2. Unit cell parameters for the original kaolinite structure and the -b/3 and +b/3 translationally disordered ones.	64
Table 4-3. Linear relationships obtained by analysing crystal structure data of the portlandites in the ICSD	68
CHAPTER 5 Pozzolanic reaction of clay minerals I: cation exchange, swelling and rheology	75
Table 5-1. Crystalline Ca-phases and equivalent amounts of calcium.....	77
CHAPTER 6 Pozzolanic reaction of clay minerals II: dissolution, precipitation and pore refinement	85
Table 6-1. Hydroxyl water content [%] referred to the ignited mass	85
Table 6-2. Averaged consumption of clay minerals and lime in all of the clay-lime mixtures of each clay	92
Table 6-3. Chemical formulas of the minerals with the molar masses of the ignited dehydroxylated minerals.....	94
Table 6-4. Released amounts of silicon, aluminium and iron by clay mineral dissolution.....	94
Table 6-5. Phenomenological description of the specimen.....	96
Table 6-6. Estimated volume changes per mole of clay mineral due to the pozzolanic reaction. ..	99

Abbreviations and Definitions

General Definitions

Cement Latin caementa meant 'stone chips used for making mortar'; etymologically, the notion behind it was originally caedmenta, a derivative of caedere 'cut' (from which English gets concise and decide). In due course the signification of the Latin word passed from 'small broken stones' to 'powdered stone (used for mortar)', and it was in this sense that it passed via Old French ciment into English [www.makersgallery.com/concrete/defs.html].

Concrete The word comes, via Old French concret, from Latin concretus, the past participle of concrecere 'grow together', hence 'harden'. This was a compound verb formed from the prefix com- 'together' and crescere 'grow' (source also of English crescent, increase and accrue). Its original application in English was fairly general referring to that which is solid or material; its use for the building material did not emerge until the early 19th century [www.makersgallery.com/concrete/defs.html].

Loam Loam, also known as earth, is a mixture of clay, silt, sand and larger aggregates such as gravel and stones. Rammed Earth is dampend earth compressed within a removable framework [www.diamondhead.net/waeds.htm].

Physico-chemical Abbreviations and Definitions

H H₂O

C CaO

S SiO₂

A Al₂O₃

F Fe₂O₃

\bar{C} CO₂

\bar{S} SO₃

Mole The amount of substance that contains as many objects (atoms, molecules, formula units, ions, or other specified entities) as there are atoms in exactly 12 g of carbon-12 [Atkins, 1994].

Avogadro's constant $N_A = 6.02 \cdot 10^{23} \text{ mol}^{-1}$, the number of objects in one mole.

Molar mass Mass per mole of objects.

Molar volume Volume per mole of objects.

Density Mass per unit volume of a substance.

Air void content Volume percent of air in a sample.

Porosity Volume percent of pore space in a sample: $p = \frac{V_{pores}}{V_{total}}$

1 Introduction and goals

This study is attributed to investigating clay mineral-lime interactions with respect to improving geo-materials for use in environmental geotechnics. These are primarily chemical interactions at high pH values and high aqueous calcium concentrations. The clay minerals partially dissolve and combine with the lime's calcium to cement hydrates (pozzolanic reaction). The study is subdivided into two periods because of the solidifying action of the newly-formed minerals: into the periods before and after solidification, i.e. into short-term and long-term chemical interactions. The influence of the chemical reactions on physical properties (rheology, microstructure) of engineered geo-materials are shown.

Prior to solidification, the rheological and mechanical behaviour of clay mineral-lime mixtures is mainly determined by the clay minerals and their plasticity; and for bentonite, by the outstanding ability to form gel-like dispersions, even at high water contents. Bentonite-lime dispersions are used in geotechnics e.g. for the sealing and solidification of ground used for construction. Nevertheless, scientific knowledge about the rheological behaviour of such dispersions at the high pH values in the presence of lime is very scarce. For these conditions, even less is known about the sodium-calcium exchange, which significantly influences the rheological behaviour.

As soon as sufficient cement hydrates are formed by the pozzolanic reaction, the material solidifies and is characterised by the typical brittle, mechanical behaviour of cements. This solidification and the related microstructural development is used in geotechnics for soil solidification and, in environmental geotechnics, for the design of cut-off walls for waste encapsulation. Nevertheless, scientific knowledge about the pozzolanic reaction of clay minerals is scarce. Any previous attempts to produce a quantitative description of reaction progress have not been located in the literature to date. However, quantitative knowledge about the reaction progress allows the microstructural development of such solidifying mixtures to be estimated or predicted. From quantitative mineralogical data,

the temporal evolution of porosity may be calculated and estimates of the development of permeability and strength may be given.

In summary, there is a significant lack of knowledge about clay mineral-lime interactions in terms of (i) the extent of cation exchange, (ii) the extent of dissolution of clay minerals and lime and the role of their mineral surfaces, (iii) the extent of formation of new cement hydrates and (iv) the influence of these chemical processes on the physical properties of engineered geo-materials.

The general goal of this study is to provide quantitative information about the chemical and mineralogical interaction of clay minerals and lime. The specific goals are:

- (i) to show the importance of sodium-calcium cation exchange and its influence on the rheological and swelling properties in order to assess:

the role of sodium, which is always present in natural soils and technical cement systems.

- (ii) to quantify consumption rates for portlandite and clay minerals in order to assess:

the loss/gain in active material properties through decomposition of clay minerals respectively through formation of cement hydrates

- (iii) to identify reaction products in order to calculate:

the approximate amount and composition of reaction products by mass balance

- (iv) to provide an insight into microstructural features of the reaction between clay minerals and lime in order to:

estimate the extent of pore refinement through the pozzolanic reaction

The knowledge about sodium-calcium cation exchange in clay mineral-lime systems, about reaction rates and stoichiometry of the pozzolanic reaction, is essential in order to explain and predict some observed, yet unexplained, effects in clay-lime applications.

This hypothesis seeks to address the following questions:

Why must sodium be added to slurries of cement and bentonite? Is it possible to predict the amount of sodium needed to be added to such a slurry?

How extensively do natural clay minerals react with lime? Is it possible to derive criteria for mixture design in clay-lime applications as e.g. soil lime stabilisation and cut-off wall design?

This study is organised as follows:

Chapter 2 is a literature review on the clay mineral-lime interactions, on the relevance of these interaction to geotechnics and on the chemical processes occurring during these interactions.

Chapter 3 briefly summarises the standard analytical techniques used. A more detailed report is given on the thermal analysis, and especially on a new model developed for semi-quantification of evolved carbon dioxide and mineral water. This model was used then to determine the amount of calcite in the solid samples. The chapter also describes the chosen materials and the sample handling steps applied.

Chapter 4 gives a short introduction to quantitative mineral analysis by X-ray diffraction combined with Rietveld analysis. An extra chapter was dedicated to the Rietveld technique which has been the most appropriate method for quantitative clay mineral analysis carried out in this study. Although the goal of clay mineral quantification could not be achieved yet due to problems arising from the real structures of clay minerals, nonetheless flexible (crystal) structure models were developed successfully. These flexible models might pave the way for a complete yet simple description of the real structures and imperfections in crystals with layered structures. Such a model was successfully applied to the problem of swelling montmorillonite in this study.

Chapter 5 refers to the results of the short-term bentonite-lime interactions. Chemical data together with rheological measurements show the influence of sodium-calcium cation exchange on the rheology of bentonite-lime/cement dispersions. Together with literature data, the rheological effects observed are interpreted in terms of volume changes of the solid fraction inside the dispersions.

Chapter 6 refers to the results of the long-term clay-lime interactions. Chemical and mineralogical data show that the dissolution of clay minerals and lime and the formation of cement hydrates does not proceed significantly between one and a half and seven months. Porosity and pore size distribution data show the influence of the mineralogical transformations on the pore properties of engineered geo-materials.

In Chapter 7, the results obtained in Chapter 5 and 6 are discussed with respect to selected geotechnical applications, namely injection grouting, soil-lime improvement/solidification and the design of technical barriers for environmental protection.

In Chapter 8, a summary of the most important results, implications and an outlook is given.

2 Clay-lime interactions

2.1 Historical Introduction

Clay minerals and cement hydrates are the major constituents of clays and hardened cements. They ensure binding and dimensional stability in clay-based (e.g. loam or earth) or cement-based materials and have been used since thousands of years for building construction. Such building materials are usually composites of coarse, well graded grains, held together by the fine-grained binding agents. The coarser grains are e.g. the sand in loam, or the aggregate in concrete. The fine grains with the cohesive and adhesive properties ensure dimensional stability and are not visible to the eye due to their sub-micrometer sizes.

The oldest recorded cases of loam brick construction date back to about 10,000 BC in Mesopotamia [Heathcote, 1995]. The Great Wall of China was built of rammed earth (loam) and stone during the Third Century BC. In Europe, there is also a long, more or less continuous tradition of the use of loam as a building material, evidenced since the Bronze age [Burroughs, 2001].

The use of loam today is limited due to its main disadvantages: poor erosion resistance to water and poor dimensional stability. These disadvantages were overcome with the use of hydraulic materials [Klemm, 1989]. A hydraulic material not only sets and hardens as a result of chemical reactions with water, but continues to harden when placed under water and forms a water-resistant product [Taylor, 1997, Mehta & Monteiro, 1993]. It is therefore particularly suitable for construction in **moist environments**. The water resistance and exceptional performance of hydraulic mortars made of lime and a pozzolanic material (pozzolan) are demonstrated by the use of these materials for the construction of Roman aqueducts and waterfront retaining walls. The good state of preservation of the old harbour wall in Pozzuoli, Southern Italy, (fig. 2-1) exemplifies the longevity and durability of pozzolan-lime mortars [Ziegler, 2004]. Some remains are still incorporated into the modern pier of Pozzuoli and have thus lasted over 2,000 years, even in the aggressive sea water environment.

Figure 2-1. The ancient harbour of Puteoli (more than 2000 years old). Today the structures have been covered by the modern harbour. The drawings below may give an impression (a) what the original structure looked like and (b) how it deteriorated later on (left: drawing by G. P. Bellori 1764, right: drawing by P. A. Paoli 1768) [CNR 2005].



Modern Portland cement is also a hydraulic material. Portland cement clinker is manufactured by heating a calcareous material, typically limestone, and an argillaceous one, typically clay or shale. The products from the partial fusion process are the so-called clinker minerals. The final product of Portland cement is gained by inter grinding sulphate minerals with the clinker [Taylor, 1997].

Today, pozzolanic materials are enjoying a renaissance as supplementary cementing materials in Portland cements and may replace part of the clinker in order to enhance the performance of the hydrated cement [Taylor, 1997]. Such composite or blended cements are employed for their economic, ecological and technological benefits [Malhorta & Mehta, 1996]. Energy consumption, as well as CO₂ emissions, are reduced. Supplementary cementing materials reduce the lime content in hydrated Portland cements and replace it with pore-filling cement hydrates, which is known to improve the ultimate strength, impermeability and durability to chemical attack of the cement [Mehta & Monteiro, 1993]. Additionally, resistance to the deleterious alkali-silica reaction can be reduced with supplementary cementing materials [e.g. CSA A23.2-28A].

This study focuses on the pozzolanic properties of natural clay minerals in clay-lime composites. To some extent, the results will be transferable to clay-cement composites, as pozzolanic materials consume mainly the calcium provided by the lime of the hydrated Portland cement and, only to an unknown small extent, the calcium from other cement hydrates [Taylor, 1997].

2.2 Definitions

Pozzolan materials

A pozzolanic material or **pozzolan** or pozzolana is a “siliceous or siliceous and aluminous material, which in itself possesses little or no cementitious property but which will, in a finely divided form and in the presence of moisture, chemically react with calcium hydroxide at ordinary temperatures to form compounds possessing cementing properties” [Malhorta & Mehta, 1996].

The denomination “pozzolan” is derived from the volcanic tuff of Pozzuoli, which was used by the Romans as a mineral admixture to lime mortars. A distinction is drawn between pozzolanic materials and latent hydraulic materials. The latter contain a considerable amount of calcium, which is the basis for the development of self-cementing properties after alkaline activation. Ground granulated blast furnace slag is a typical example of a latent hydraulic material. Pozzolans are classified into natural materials and artificial ones: the latter are mostly industrial by-products [Malhorta & Mehta 1996]. Examples for both types are given in Table 2-1 [modified from Liebig, 1997].

Table 2-1. Pozzolans

	pozzolan	active components
natural	volcanic tuff	aluminosilicate glasses, zeolites, clay minerals
	rock from meteorite impact	aluminosilicate glasses, zeolites, clay minerals
	diatomaceous earth	fine grained skeletal remains of diatoms
	bauxite	aluminium hydroxides
artificial	calcined ^a clays or shales	unstable dehydroxylation products of clay minerals
	low-calcium fly ash	glasses, calcined silicates
	condensed silica fume	silica glasses
	rice husk ash	silica glasses

^a to calcine: to heat an inorganic material to a high temperature but without fusing in order to drive off volatile matter or to effect changes (as oxidation or pulverization) [Merriam-Webster Online]

Lime

In the building material technology, **lime** usually refers to oxides and hydroxides of calcium and magnesium [e.g. DIN 1060-1]. In this study, the magnesium component is disregarded, as it is of minor importance in geotechnics.

Quicklime (calcium oxide) is produced from limestone (calcium carbonate). Decarbonation of limestone leads at a decomposition temperature of $\sim 900^{\circ}\text{C}$ to the thermal dissociation into quicklime and carbon dioxide.

“**Slaked lime** is produced by reacting, or slaking quicklime with water, and consists mainly of calcium hydroxide. The term includes **hydrated lime** (dry calcium hydroxide powder), milk of lime and lime putty (dispersions of calcium hydroxide in water); the generic term, lime includes quicklime and slaked lime; lime is, however, sometimes used incorrectly to describe limestone products;” [Oates, 1998]. All kinds of slaked lime are sensitive to atmospheric carbon dioxide and are easily converted back to limestone (chemical cycle).

In this study, the term lime refers only to hydrated lime or dry calcium hydroxide powder with the mineral name **Portlandite** (CH^1).

Clays and clay minerals

Clays are sedimentary deposits/soils, which consist mainly of fine-grained mineral particles. These fine grains are mostly in the size fraction smaller than $2\ \mu\text{m}$ ($10^{-6}\ \text{m}$), the so-called clay fraction. Clays show plastic behaviour at an appropriate water content and harden when dried or fired.

Clay minerals are the major constituents in the clay size fraction of clays and soils, and are responsible for the material's plastic behaviour. According to the chemical nomenclature of silicates, they belong to the group of phyllosilicates or sheet silicates. Their individual **layers** are comprised of tetrahedral (T) silicate or aluminosilicate sheets and octahedral (O) sheets containing, in the majority of cases, aluminium or magnesium. Such a layer contains either a condensed TO sequence (1:1 layer) or a condensed TOT sequence (2:1 layer). These individual layers are stacked onto each other and are separated by an interlayer. Depending on the type of clay mineral and its chemical composition, the individual layers may be charge deficient, resulting in a permanent negative layer charge, which is compensated by exchangeable cations in the interlayer. The special group of

¹ In cement chemical nomenclature H_2O is abbreviated by H, CaO by C, SiO_2 by S, Al_2O_3 by A, Fe_2O_3 by F, CO_2 by $\bar{\text{C}}$ and SO_3 by $\bar{\text{S}}$.

expandable clay minerals is capable of changing their volume (swelling) caused by water uptake through the hydration of interlayer cations.

2.3 Natural clay minerals as pozzolans?

Clay minerals have typical characteristics that preclude their use as pozzolans in common cement/concrete technologies [He et al., 2000] for the following reasons:

- (i) they have stable crystal structures of low chemical solubility. This results in a small release rate of silicon and aluminium, which explains the poor pozzolanic reactivity. Malhorta & Mehta (1996) even judge clay minerals as not pozzolanic,
- (ii) their layer structure and the resulting cleavage might have a negative impact on the strength of the cementitious building product,
- (iii) they have small particle sizes resulting in high specific outer surface areas. In aqueous systems, these surfaces are always covered with layers of relatively immobile water molecules. Addition of clay minerals leads thus to a high water demand which lowers the density and strength of the building products [He et al., 2000]. This water demand is increased even more by expandable clay minerals, as these contain several layers of interlayer water,
- (iv) their high sorption capacity influences the chemical composition of the aqueous medium with possible negative effects on the technological properties of cements (e.g. rate of setting).

As a result, the research activity on composite cements (blended cements) focused on calcined clay minerals as pozzolanic blendings. Thermal treatment or calcination of clay minerals leads below 250°C to a loss of the sorbed water from the surfaces (dehydration), then at temperatures between 250°C and 800°C to a loss of the hydroxyl water from the crystal structure (dehydroxylation) accompanied by a structural reorganisation [e.g. Emmerich, 2000, and ref. therein]. The dehydroxylation temperature is characteristic for the type of clay mineral. Further temperature increase leads to a destruction of the crystal structure and recrystallisation of metastable transition phases before the stable phases crystallise. These metastable transition phases often show improved pozzolanic reactivity [e.g. Liebig, 1997]. The high surface area and non-crystalline nature of these metastable phases leads to a high pozzolanic reactivity [Malhorta & Mehta, 1996]. A typical representative of such a metastable phase is the extensively investigated metakaolinite [Strätling & zur Strassen, 1940; Murat, 1983; Serry et al., 1984; de Silva & Glasser, 1992; Dunster et al., 1993; He et al., 1994a, b; Salvador, 1995; Heide et al., 1996; Liebig & Althaus, 1997]. Data on the pozzolanic properties of other calcined clay minerals may be

found in Ambroise et al. (1985, 1987), Ghorab et al. (1991), He et al. (1995, 1996a,b, 2000) and Liebig & Althaus (1997).

Calcined “meta”-clay minerals have lost the typical clay properties enumerated above; it might thus be considered misleading to name them as clay minerals. In this study, the term clay mineral refers only to **natural, non-calcined** clay minerals.

2.4 Importance of pozzolanic properties of clay minerals to geotechnics

In environmental engineering, applications of interest include engineered barrier systems for landfill, contaminated land and nuclear repositories. Such systems are often designed as multi-barriers consisting of a natural geological and an artificial barrier(s). In general, clays and, in particular, swelling clays, are used for the artificial barrier design. As a result of the above mentioned physico-chemical characteristics of clay minerals, clay-based materials show e.g. self-healing, contaminant-adsorbing, water-transport-reducing and plastic properties. These technological properties are mandatory for disposal techniques. The development of active barrier materials based on these properties is an important issue [Hermanns & Bucher, 1990; Hermanns, 1993; Hermanns Stengele & Plötze, 2000]. For waste encapsulation purposes, barrier (cut-off wall) materials are often designed as mixtures of cement and/or lime¹ together with active clay materials [e.g. Hermanns, 1993]. The cement is added to ensure sufficient strength and to prevent particle erosion. However, there is much concern about the physico-chemical stability of clays under highly alkaline conditions. The active material properties may not be guaranteed in the aggressive chemical environment of the high pH cement pore solution. An increase in porosity, hydraulic conductivity and diffusive transport could result in leakage through the barrier and in environmental hazard. Exposure of the clay minerals’ reactive surfaces to the cement pore solution leads to high reactivity, and, possibly, high yields of clay mineral dissolution/transformation.

In the field of geotechnical engineering, the pozzolanic properties of clay minerals are relevant to **injection grouting** and soil lime-improvement/stabilisation techniques. Grouting describes the procedure of pressing a slurry or paste into the cavities and pores of soils or

¹ As mentioned earlier, lime is also a major reaction product of Portland cement hydration.

into the fissures and cracks of rocks for the purpose of sealing and solidification [Amann, 1997]. A wide variety of grouting agents are used in the construction industry, only dispersions or slurries made mainly of cement and bentonite¹ will be considered in this study. Such slurries may be also used for the construction of slurry-trench walls. In general, they have a higher cement than bentonite content and are therefore in the long-term identified by those of hardened cement.

In the short-term, such composites benefit mainly from the typical clay properties as long as the cement is not fully hydrated. Bentonite is added to improve workability and suspension-stability of the fresh slurries and pastes and is, in some grouting techniques, used as a sealing compound to lower the permeability in soils or fractured rocks. The bentonite content highly influences the flowability of the slurries: higher contents decrease the final strength and increase the water demand and the dispersion-stability, but also the yield point and the dynamic viscosity. Nevertheless, dispersion stability and quality may be poor, leading to segregation and bleeding (settlement of the solid particles). Bentonites are thus classified as “cement-stable” or not, according to their ability to form stable dispersions [Pulsfort & Walz, 2000]. First, after addition of sodium and subsequent sodium-calcium cation exchange, the dispersions show improved properties. Such additions occur on an empirical basis, as the extent of sodium-calcium cation exchange is not yet fully known in cementitious environments.

Another field of relevance, is the **modification of soils by lime addition** for the purpose of construction on or in the soil. The chemical effects of the added lime cause immediate changes in soil plasticity and workability and allow for easy ramming of the soil and a good compaction rate. This facilitates further construction work. Addition of lime for immediate **soil improvement/stabilisation** is often required in the humid seasons when soils are muddy.

In **soil solidification**, the addition of higher lime proportions generates a soil-binder composite with improved resistance to stresses caused by traffic and climate. The bearing capacity, the water and frost resistance of the strengthened and solidified soil is improved

¹ A clay formed from volcanic ash decomposition and largely composed of the clay mineral montmorillonite [Parker, 1997].

in a sustainable way. If the appropriate clay constituents are present in the soil, shear strength development due to the pozzolanic reaction will be gradual but continuous for long periods of time [Broms, 1984]. The rate of increase is generally rapid during the first 48-72 hours after mixing, then starts to decrease with time but may continue for several years in some instances [Taylor & Arman, 1960]. The shear strength increases linearly with time when plotted at log-log scale [Broms, 1984] or linearly with the logarithm of time [Brandl, 1981; Okamura & Terashi, 1975].

The primary variable that can be altered is lime percentage, since the inherent properties and characteristics of the soil are fixed and the optimal water content is adjusted during construction. Therefore, the major objective of the mixture design process is to establish an appropriate lime content. For the purpose of strength development in the long-term, a wide variety of lime contents could be used successfully. By comparison with historical mixture design of Roman pozzolan-lime mixtures (up to 43% lime), the lime additions that are usually applied in soil solidification (up to ~12%) seem quite low. Mitchell & Dermatas (1992) report on the possibility of less swelling in sulphate-rich soils when increasing the lime content. More lime leads to more cementitious reaction products over time, which results in increased strength. As a material disrupts if the expanding forces become greater than the material's (tensile) strength, more lime might be considered beneficial for the reduction of swelling and heave of problematic soils.

2.5 Chemical aspects associated with the pozzolanic reaction

There may be as many as five mechanisms associated with the addition of lime to clayey materials [UN, 1992]:

- (i) Water absorption: Quicklime undergoes hydration using added water or soil moisture, releasing heat in the process.
- (ii) Cation exchange: Calcium ions from the lime are replaced by exchangeable cations from the soil constituents, including potassium and magnesium. The amount of exchange is a function of the soil's cation exchange capacity.
- (iii) Flocculation and aggregation: Soil particles flocculate and aggregate due to cation exchange and increased electrolyte activity in the pore water. In effect, the grain size distribution is modified.

- (iv) Carbonation: Added lime reacts with atmospheric carbon dioxide to form weak carbonated cements.
- (v) Pozzolanic reaction: This is the dominant reaction in lime stabilisation of soil. The strength of the resulting material is largely a function of the dissolution of clay minerals in the alkaline environment created by the lime and the recombination of clay-derived silicon and aluminium with lime-derived calcium to form hydrated cement minerals.

Water absorption by the hydration of quicklime, and carbonation of free lime, will not be considered in this study, as experiments were only performed with hydrated lime, and mixtures were prepared excluding carbon dioxide.

It is well established in soil science and clay mineralogy, that cation exchange and dispersion/aggregation phenomena are closely interrelated phenomena [e.g. Ho & Handy, 1963; Shainberg & Kemper, 1966; Shainberg & Otoh, 1968; Reddi & Inyang, 2000; Quirk, 2001]. The cation exchange state (distribution of monovalent and bivalent cations between liquid and solid phase) influences the mechanical, hydraulic and swelling properties in clayey soils [Lang, 1989; Madsen & Müller-Vonmoos, 1989; Müller-Vonmoos & Loken, 1989; Weiss, 1989; Quirk, 2001]. The effect of lime additions on zeta potential, viscosity, plastic limit and flocculation/aggregation in montmorillonite dispersions was studied by Ho & Handy (1963) and the effect on the grain size distributions of soils e.g. by Caprez (1984) and Croce & Russo (2003). These properties are related to cation exchange and mainly influence the engineering properties of fresh clay-lime mixtures in the short-term, before the mixtures start to harden.

In contrast, the pozzolanic reaction is a slow process. It is the major process responsible for strength development in pozzolan-lime composites and for improved strength of modern composite cements [Mehta & Monteiro, 1993]. Due to this solidifying action, the reaction of clay minerals and lime is subdivided into the periods before and after substantial solidification occurred [Eades & Grim, 1960]:

The first period is characterised by a fast cation exchange contribution with its influence on the rheological and swelling engineering properties.

The second period is characterised by a slow dissolution/precipitation (pozzolanic) reaction with its longer term influence on engineering properties e.g. porosity, permeability and strength.

It is worth mentioning here that the same distinction is made by civil engineers for soil-lime stabilisation. There is a certain amount of lime necessary in order to reduce the plasticity index to a minimum. This is mainly caused by an increase to the maximum plastic limit and a change of the liquid limit. This dosage is termed the lime fixation point [Bergado et al., 1996] or defined as the minimal lime content [SN 640 503a]. Lime additions equal to the lime fixation point will generally contribute to the improvement¹ in soil workability, but may not result in sufficient strength [Hilt & Davidson, 1960]. Addition of more lime generates no improvement in workability, but mainly contributes to a long-term strength increase through the cementing action of the pozzolanic reaction.

2.5.1 Pozzolanic reaction of clay minerals I: cation exchange, swelling and rheology

Sodium and calcium are two major cations in Portland cement and soil pore solutions (also inter void fluid). Serious problems may arise from both swelling cement through the alkali-aggregate reaction [Prezzi et al., 1997, 1998; Rodrigues et al., 1999a, 1999b, 2001] and swelling agricultural soils [Quirk, 2001], both caused by the action of exchangeable sodium. Sodium-calcium exchange in the presence of lime may therefore be critical with a large influence on the rheological (e.g. yield point²) and engineering properties (e.g. swelling, hydraulic conductivity).

In this study, investigations related to the three phenomena: **sodium-calcium exchange**, **swelling** and **yield point tests**, were performed on a bentonite. Their interrelation is shown and implications, particularly for the construction industry, are discussed. As these phenomena are attributed to quite a range of natural and engineering sciences, short introductions will be given in the following sub-sections.

¹ The German literature on soil stabilisation makes a distinction between soil improvement/stabilisation (“Bodenverbesserung” and “Bodenstabilisierung”) and soil solidification (“Bodenverfestigung” and “Bodenvermörtelung”) [e.g. Hermanns Stengele, 2005].

² The yield point of a supporting liquid is the shear stress, which causes flow to appear. It depends, among other parameters, on the temperature, and for thixotropic fluids, on the thixotropic thickening time. Thixotropic thickening is associated with an increase in the yield point after ending a flow. It is reversible. The yield point is at its minimum at the end of a flow (dynamic yield point) and increases asymptotically to its maximum (static yield point). [Pulsfort & Walz, 2000].

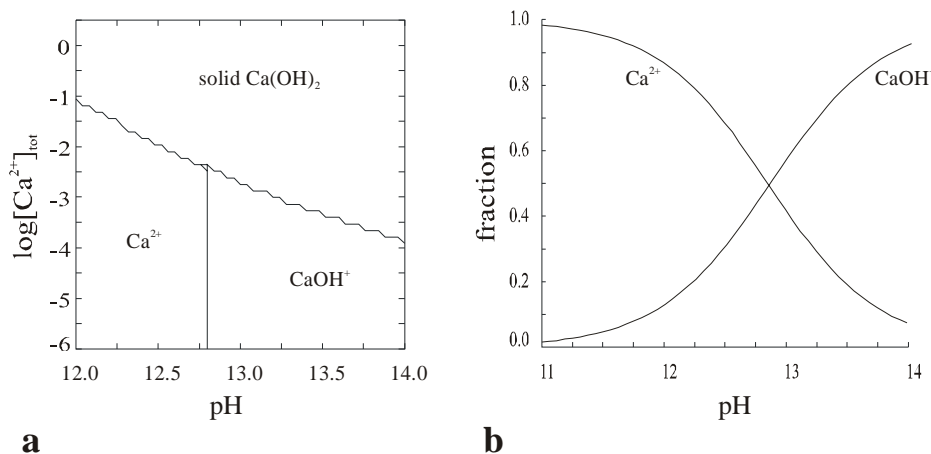
Solution chemistry in the presence of lime

The solubility of $\text{Ca}(\text{OH})_2$ (lime) in water decreases from 1.85 g/l at 0°C to 1.28 g/l at 50°C and to 0.71 g/l at 100°C [Haslam et al., 1924]. At 25°C, the pH value is ~12.5 and the total molar calcium concentration is ~21 mM. The effect of different alkali salt solutions on the solubility of lime was modelled by Duchesne & Reardon (1995), the effect of particle diameter by Johannsen & Rademacher (1999). Due to the hydrolysis of the hydrated calcium ion:



the species CaOH^+ also has to be taken in consideration [Baes & Mesmer, 1976]. At a pH of 12.5 it accounts for ~30% of the total dissolved calcium (fig. 2-2b). An increase of the pH e.g. by the addition of NaOH results in a decreased solubility of lime, decreased total calcium concentration and increased fraction of the species CaOH^+ (fig. 2-2a). At a pH of 12.85 equal to the value of the first hydrolysis constant of Ca^{2+} [Parkhurst & Appelo, 1999], the two soluble species are equally present in solution (fig. 2-2b). The species CaOH^+ has a much higher selectivity constant against Na^+ as does Ca^{2+} [e.g. Tournassat et al., 2004a, 2004b] and is therefore of particular importance to sodium-calcium cation exchange phenomena at a high pH.

Figure 2-2. (a) Predominance area diagram in the system Ca^{2+} - H_2O - $\text{Ca}(\text{OH})_2$ as a function of pH and $[\text{Ca}^{2+}]$ concentration and (b) fractions of soluble calcium-species with pH in this system; calculated with the chemical equilibrium program Medusa [Puigdomenech, 2000].



Cation exchange

One of the basic properties of many clay minerals is the ability to exchange cations located on and between the mineral's layers. The maximum exchangeable amount, termed the cation exchange capacity (CEC), originates from two contributions. One is the permanent negative layer charge. It arises from isomorphous substitutions of cations in the crystal lattice of the clay mineral. It may be calculated as a theoretical structural CEC value from the structural formula. As the name implies, this charge is permanent and independent of the systems' pH. The other contribution originates from the (de-) protonation of surface groups of the clay mineral layers' edges. The edges' protonation state depends on the pH and may range from positive to negative. At a pH of 7, ~20% of the CEC of smectites is located at the edges [Lagaly, 1981].

In a cation exchange reaction, the preference for one cation over another is qualitatively described by a selectivity series [e.g. Jasmund & Lagaly, 1993]. For clay minerals, this series is very similar to the Hofmeister series for cations, which was established from the ions' impact on the coagulation behaviour of a protein mixture [Hofmeister, 1888]. In the absence of specific sorption, one reason for different selectivity is found in the ionic potential of cations, the ratio of cation charge to radius. Since exchangeable cations at surfaces are usually hydrated, it is the ratio of charge to hydrated radius that governs the attraction to the surface. A higher ionic potential of the "naked" cation results in a larger hydration shell, i.e. in a hydrated cation with a lower ionic potential and less attraction to the charged surface.

Swelling of clay minerals

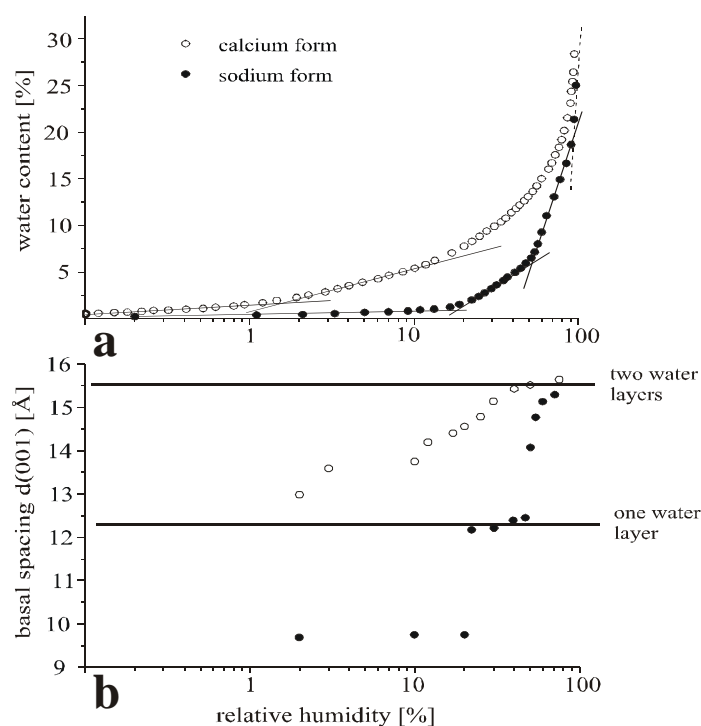
Some clay minerals like montmorillonite are capable of changing their volume in one dimension by de- or adsorption of water layers (fig. 2-3b). The clay mineral's water content is related to the chemical potential of water which is related to a particular relative humidity [Tambach et al., 2004] amongst other factors. The volume change process is either termed swelling, if water is taken up, or shrinkage, if water is released from the mineral. There is much consensus in the literature that the first swelling steps from the dehydrated state onwards, the so-called crystalline swelling, proceed mainly via the hydration of the interlayer cations. The driving force is the cationic hydration energy [Norrish, 1954b].

The enthalpy of hydration (per single charge) for calcium is about twice that of sodium [Marcus, 1985]. This qualitatively explains why calcium montmorillonite at a fixed relative humidity has a greater volume and water content than sodium montmorillonite (fig. 2-3). These homoionic forms show completely different swelling and water uptake curves with increasing humidity (fig. 2-3a).

Water adsorption in the crystalline swelling regime proceeds in a step-wise manner by the inclusion of water layers; it stops somewhere around four water layers corresponding to a surface separation of ~ 10 Å or a basal spacing of ~ 20 Å [Norrish, 1954b]. Each water layer separates the mineral layers by about 2.7 Å to 3 Å, roughly equivalent to the diameter of a water molecule.

In aqueous solution, this crystalline swelling may proceed into the continuous swelling regime, which is mainly an osmotic process driven by concentration gradients [Norrish, 1954a]. Low ionic strength in the bulk solution forces water to enter between the mineral layers and drives them apart. In such solutions, clay mineral layers may be separated by distances of up to some hundreds of Å. This process is independent of cation type [Norrish, 1954a]. For bivalent and higher valent cations however, swelling often stops at the transition from the crystalline to the continuous swelling regime [Norrish, 1954a].

Figure 2-3. Crystalline swelling of the sodium and calcium form of montmorillonite: (a) water content with relative water pressure (relative humidity), (b) basal distance between clay mineral's layers with relative humidity [modified from Plötze & Kahr, 2003].



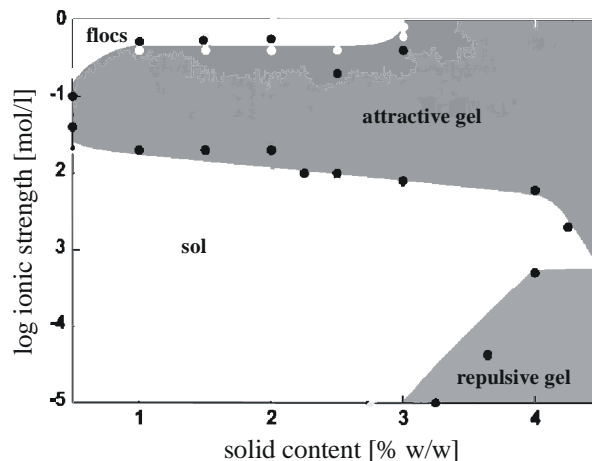
Rheology of montmorillonite dispersions

“Rheology, a branch of mechanics, is the study of those properties of materials which determine their response to mechanical force. The word *rheology* was coined in the 1920's to represent the science of the deformation and flow of matter.” [The Society of Rheology].

Rheology is an interdisciplinary science at the boundary of continuum mechanics and fluid mechanics and investigates both the solid and fluid states of materials and also the transition between the two. When a force is applied to a volume of material, a displacement (deformation) occurs. High deformations lead to a flow of many materials, other materials break in brittle mode. The deformation response might be reversible (elastic deformation) or irreversible (viscous and/or plastic deformation) or a combination of all of them (visco-elasto-plastic deformation).

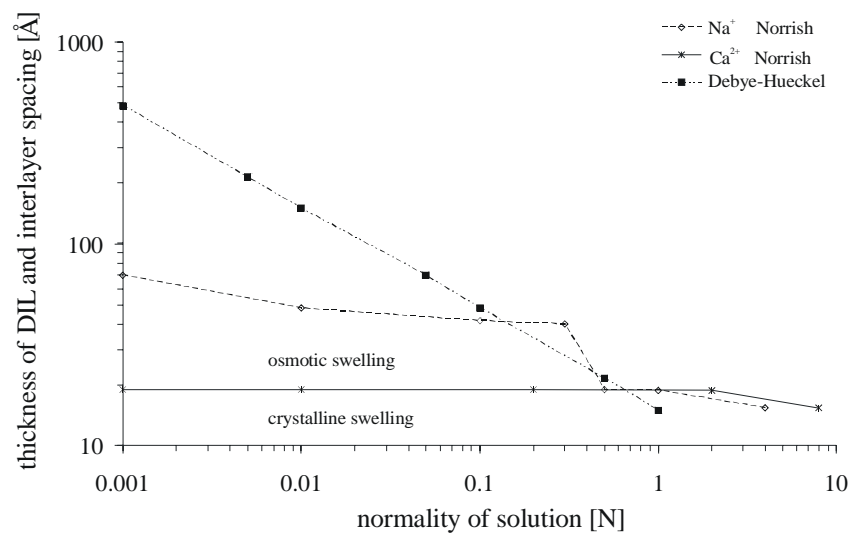
Montmorillonite dispersions are dependent on their solid content viscous or visco-elasto-plastic, thixotropic, gel-like fluids. They may be in the state of a sol (stable colloidal dispersion), may be coagulated (destabilised by salts), flocculated (destabilised by polymers) or thickened in the state of a gel [Abend & Lagaly, 2000]. These different states are separated through phase boundaries indicated by a change in the rheological properties (e.g. yield point). The phase diagram in fig. 2-4, showing the influence of solid content and ionic strength on the state of dispersion, was determined from rheological measurements [Abend & Lagaly, 2000]. Other factors influencing the state of dispersion are pH [Lagaly, 1989], age of dispersion [Karstedt, 1980], temperature, cation exchange [Alther, 1986; Lagaly et al., 1997] and type of bentonite [Huder, 1972].

Figure 2-4. Phase diagram showing the different states of a bentonite dispersion as a function of ionic strength and solid content [modified from Abend & Lagaly, 2000].



Even dilute sodium montmorillonite dispersions are not completely delaminated [Jasmund & Lagaly, 1993], i.e. their individual layers are not fully separated. These primary layers are arranged in so-called tactoids of approximately four to ten layers [Jasmund & Lagaly, 1993]. Each of these tactoids is surrounded by a zone of relatively immobile water, the so-called diffuse ion layer (DIL), which is a result of the permanent negative charge of the clay mineral's layer and the surrounding region of charge-neutralizing hydrated cations. The thickness of the DIL is often approximated via the Debye-Hückel theory and assumed to be five times the reciprocal Debye-Hückel length [Lagaly et al., 1997]. The thickness of the DIL is not equal to the interlayer space between the layers of tactoids. Fig. 2-5 shows both the variation of the DIL (5 times the reciprocal Debye-Hückel length) and the interlayer spacing [Norrish, 1954b] with the normality of solution.

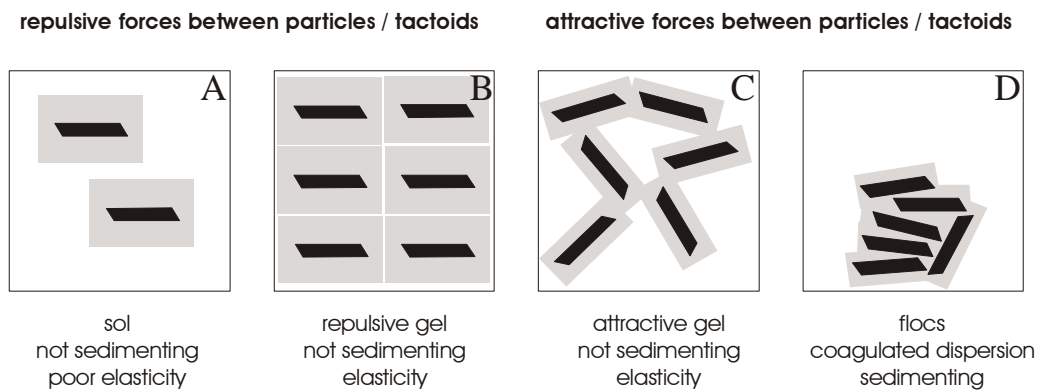
Figure 2-5. Thickness of the diffuse ion layer for monovalent ions approximated as five times the reciprocal Debye-Hückel length [data taken from Lagaly et al., 1997] and measured basal spacing [data taken from Norrish, 1954b], both as a function of the normality of solution.



The tactoids with their surrounding diffuse ion layers and the different states of dispersion are schematically shown in fig. 2-6. The states are characterised by their inter particular forces, either repulsive or attractive ones. At low ionic strength and low solid content, bentonite dispersions are in a stable (not sedimenting), repulsive state with a very low yield point (fig. 2-6a). Increasing the solid content will not or will only slightly change the DIL, but may induce a phase transition to the repulsive gel state; a significant yield point appears (fig. 2-6b). Increasing the ionic strength at constant solid content will decrease the thickness of the DIL. This may lead to the formation of an attractive gel, the inter particular forces become attractive, water is immobilised inside the gel pores (fig. 2-

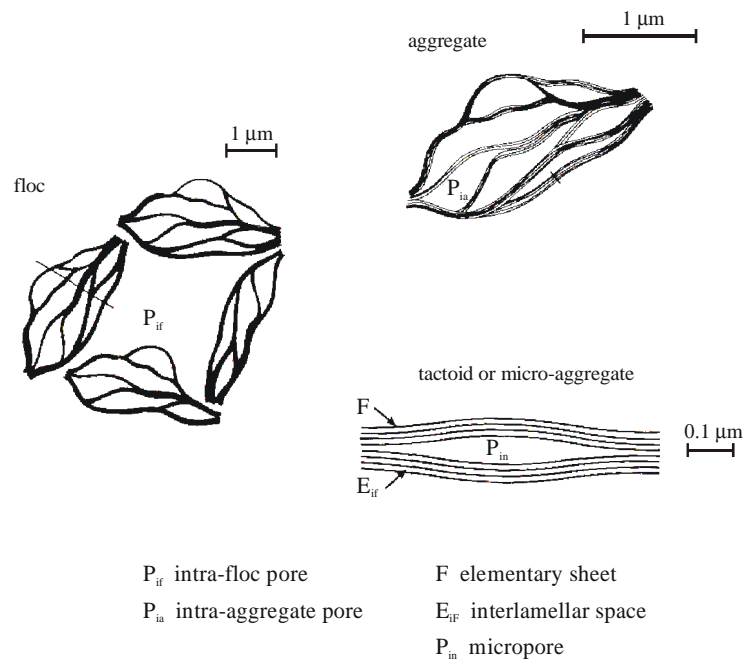
6c). Further increase of the ionic strength leads to coagulation and formation of flocs, the dispersions show sedimentation (fig. 2-6D). A significant yield point as a result of the dispersion's elastic properties is only observed above ~1% bentonite content and transition to a gel-like state above ~3% bentonite content [Abend & Lagaly, 2000]. Dispersions of relevance for the construction industry usually have a bentonite content between 3% and 8% and are therefore typically in the state of a gel.

Figure 2-6. Schematic representation of the four states of a bentonite dispersion; solid content and ionic strength lead to transitions between the states; the influence of solid content is symbolised through the number of tactoids in black, the one of ionic strength through the thickness of the diffuse ion layer in grey surrounding the particles.



The distribution of clay minerals inside aggregates and flocs as shown in fig. 2-7 also influences the distribution and mobility of water inside the different types of pores [Schoonheydt, 1995].

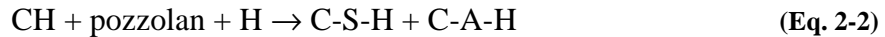
Figure 2-7. Aggregation of elementary clay particles [modified from Touret et al., 1990].



2.5.2 Pozzolanic reaction of clay minerals II: dissolution, precipitation and pore refinement

The pozzolanic reaction

The slow chemical reaction between a pozzolan and calcium hydroxide (lime) is called the pozzolanic reaction [Mehta & Monteiro, 1993] and leads to the formation of calcium-silicate-hydrates and calcium-aluminate-hydrates:



C-S-H is a generic name for any amorphous or poorly crystalline calcium silicate hydrate; the dashes indicate that no particular composition is implied [Taylor, 1997]. C-A-H is used here in the same way, note however, that calcium aluminate hydrates are usually of higher crystallinity and their composition is usually easier to determine than the composition of C-S-H.

“Because pozzolans are low in CaO, this component must be added in **stoichiometric quantity**” [Taylor, 1997]. This CaO is either added as lime or, in a composite cement, provided by the lime formed during cement hydration. The consumption of lime, followed by the precipitation of hydrated cement minerals with a lower density is very efficient in filling up capillary pore space thereby decreasing porosity. This lime consuming process and the associated **pore refinement process** lead to increased strength, impermeability, durability and chemical resistance of pozzolan cements [Mehta & Monteiro, 1993].

Literature on the pozzolanic properties of clay minerals

As mentioned before, mineralogical literature on the pozzolanic properties of clay minerals is rare due to their unfavourable properties in common cement/concrete technology. Although Malhorta & Mehta (1996) still classify clay minerals as non-pozzolanic, it is already inferred from engineering practice that there is some extent of pozzolanic reaction occurring with clay minerals. The presence of at least 10% clay fraction in a soil is required for a successful lime-stabilisation process [e.g. SN 640 500a]. Recent findings by Jackson (2004) even indicate that a non-dispersive smectite cemented with opaline silica was the major reactive mineral component of a pozzolan in ancient Roman cements. There is also evidence that smectitic expandable soils were lime-stabilised by the Romans [Borchardt, 1989].

The first direct X-ray evidence for the pozzolanic reaction of clay minerals, the consumption of lime and formation of cementitious reaction products was established in the 1960's [Eades & Grim, 1960; Hilt & Davidson, 1961; Herzog & Mitchell, 1962, 1963; Glenn & Handy, 1963; Diamond et al., 1963]. Following their microscopic evidence, Diamond et al. (1963) postulated that the pozzolanic reaction involved **progressive dissolution of the clay mineral's edges**, followed by separate **precipitation of the reaction products**.

Major reaction products at ambient temperature were identified as a crystalline calcium aluminate hydrate, possibly C_4AH_{13} [Hilt & Davidson, 1961], an AFm phase as termed today in cement chemistry [Taylor, 1997], and hydrated calcium silicate gel (C-S-H) [Diamond et al., 1963]. At a temperature of 60°C, the phase assemblage had changed to a cubic hydrogarnet phase (C_3AH_6) and a C-S-H of different morphology [Diamond et al., 1963].

The only information regarding the **extent of reaction** is found in Diamond et al. (1963). In general, the reaction extent increased with temperature. For aqueous montmorillonite- and kaolinite-lime mixtures at 60°C, the initial 29% of lime reacted completely after 2 months. The extent of reaction of the kaolinite was estimated to be 28% of the total mixture, no estimate for montmorillonite is given. At 45°C after 2 months, the majority of the initial 20% of clay minerals reacted. The following order of reaction extent was estimated: kaolinite > montmorillonite \cong mica \cong illite > pyrophyllite (Talc did not react and the extent of lime reaction was not estimated). Despite considerable attack, the residual clay minerals retained their crystallinity as evidenced e.g. by the sharpness of the X-ray peaks of the mica and illite polymorphs. After 6 months at 23°C, a 1:1 kaolinite-lime suspension remained considerably unreacted. Reaction extent was not estimated.

Combined dissolution and precipitation at high pH relevant to clay-lime mixtures

In order to understand the rates of change in chemical systems, controls by nucleation of solids, mineral dissolution and growth, aqueous and solid-state diffusion, oxidation-reduction, adsorption, ion-exchange, aqueous complexing, radioactive decay and fluid flow have to be considered [Murphy et al., 1989]. Rate limiting processes for the overall reaction are either the slow steps of processes occurring in sequence or the fast steps of parallel processes. Dissolution or crystal growth at the interface between minerals' sur-

faces and aqueous solutions and the diffusion of reactive species into the aqueous phase to and from the surfaces commonly occur in sequence [Murphy et al., 1989].

As mentioned earlier, the pozzolanic reaction is discerned to be a combined process of dissolution of the lime surfaces and of the clay minerals' edges followed by the precipitation of cement hydrates. From micro structural investigations during cement hydration, it is established that precipitation may occur (i) on the dissolving clinker grains that provide all the chemical species necessary, (ii) in solution away from the surfaces and (iii) on (relatively) inert surfaces of e.g. aggregate grains [Taylor, 1997]. In pure pozzolan-lime mixtures, where part of the chemical species necessary for precipitation are either provided by the lime or the pozzolan, precipitation products have been found on the surfaces of both reactants, the lime and the pozzolan [Biernaki et al., 2001; Williams et al., 2002] and possibly also in solution. It is therefore concluded that diffusion of reactive species and precipitation on or near surfaces and in solution are important processes in clay-lime mixtures (likewise in cement hydration [Gartner et al., 1989]).

The relative importance of diffusion and surface reactions on the overall mass transfer rate at the mineral surface depends on the magnitude of the surface reaction rates and diffusion coefficients (both temperature dependent), the geometry, structure and hydrodynamics of the system, the degree of disequilibrium at the mineral-solution interface and elsewhere in the system [Murphy et al., 1989] and the morphology of the mineral's surface [Jeschke & Dreybrodt, 2002]. Minerals with low dissolution rate constants (typically e.g. silicates at ambient temperature) tend to be in the surface-reaction-dominated regime as the rates for the diffusing aqueous species involved in the mineral's dissolution and growth are greater; i.e. the overall coupled steady-state rate is dominated by the slow surface reaction. In contrast, minerals with high dissolution rate constants tend to be in the diffusion-dominated regime (e.g. calcite or portlandite/lime).

Surface precipitates influence the dissolution rate in such a way that reactive species may have to diffuse through them. The (effective) porosity of the overgrown precipitate, through which diffusion occurs, is thus of major importance for the overall reaction rate, at least for fully covered surfaces. The solution in contact with the overgrown phase is likely to be saturated with respect to this overgrowth. Further dissolution of the substrate can then only occur by diffusion of reactant- and/or product-derived chemical species through the overgrowth, which is likely to be extremely slow [Gartner et al., 1989]. For

coupled surface and diffusion reaction modelling, Murphy et al. (1989) among others therefore introduced a parameter describing the ratio of total interfacial surface area over which the reaction occurs to the cross-sectional surface area perpendicular to diffusional mass transport. “This parameter depends on surface roughness and the porosity of the medium through which diffusion occurs if it affects the quantity of mineral surface that contacts the aqueous phase.” [Murphy et al., 1989].

It has been established by Ritchie & Xu (1990) and Giles et al. (1993) that the **dissolution or slaking** of both quicklime and slaked lime is kinetically controlled at low stirring speeds by the slow diffusion of calcium and hydroxide away from the dissolving surface. At higher stirring speeds, the slow rate-determining step is the dissolution of calcium hydroxide at the surface [Giles et al., 1993]. For reactions of lime with solutions containing carbonate or aluminate, Xu et al. (1997, 1998) found that the reaction products (CaCO_3 or C_3AH_x) deposited at the dissolving surfaces slow down the dissolution reaction of lime. If the aluminate concentration in solution is high enough, the lime particles even become encapsulated by the calcium aluminate hydrate (passivation) and further dissolution ceases [Xu et al., 1997].

Bauer & Berger (1998), among others, investigated the alkaline **dissolution of clay minerals** (kaolinite and montmorillonite). The montmorillonite dissolved at a much lower rate, controlled by the dissolution of the tetrahedral (silicate) sheet. The rate determining step for kaolinite was the dissolution of the octahedral (aluminate) sheet. Berger et al. (2002) however, suggested for feldspar dissolution that a competition occurred between two parallel reactions at the mineral surface, the hydrolysis of the silicon and aluminium units of the tecto- (framework) silicate. The rate determining step might therefore depend on the experimental conditions or even change during the experiments through growth and re-dissolution of new phases [Berger et al., 2002]. It is often observed that natural minerals weather in intimate contact with reaction products. This strongly influences the rate and character of natural weathering [Casey, 1995, and references therein]. Unlike in well-controlled laboratory experiments, where a small amount of mineral is dispersed in a large volume of solution, natural weathering usually occurs at low water to mineral ratios in the porous networks of soils, sediments and rocks. Solute transport by diffusion through precipitates to and from the dissolving surface might thus control the overall dissolution rate both in natural and laboratory systems [Murphy et al., 1989, and ref. therein;

Ritchie & Xu, 1990; Giles et al., 1993]. The solution composition mainly in contact with the precipitate might imply true equilibrium in the system. However, apparent equilibria are in reality often multiple steady states of both irreversible and reversible reactions [Sverdrup & Holmqvist, 1999].

The hydration of Portland cement pastes can provide another example for the influence of mineral precipitates on the dissolution reaction. Three periods of micro-structural development in cement pastes are usually distinguished, an early, middle and a late period, with divisions at 3 and 24 hours of hydration time [Taylor, 1985; Scrivener, 1989; Taylor, 1997]: In the middle period of hydration after ~4 h, the dissolving clinker grains are completely covered by cracked shells of C-S-H, which show after ~12 h a thickness of 0.5 - 1 μm . These shells are separated from the clinker grains through spaces up to 0.5 μm wide and are still permeable to migrating aqueous species. Precipitation occurs inside these spaces, in the pore solution but also on the surfaces of inert grains. From ~18 h onwards but basically in the late period of hydration, these spaces become progressively filled with the so-called inner product C-S-H. The shells may be now thicker than 8 μm , restricting the diffusion of dissolved species and substantially slowing down the hydration reaction. In contrast to the through-solution processes (dissolution, aqueous diffusion and precipitation from solution), further hydration was suggested to occur very slowly by a topochemical mechanism due to the lack of a true liquid phase in contact with the dissolving surfaces [Taylor, 1985].

3 Analytical methods, materials and sample preparation/handling

3.1 Standard analytical methods

All mineralogical data given in this study are referred to the ignited mass. Calcium hydroxide content is e.g. given as percent CaO in the ignited mixture. This is very common in cement chemistry, as the mass of the ignited mixture is a constant reference point in systems of low water to solid ratios. The mass of the dissolved species is negligible compared to the mass of the solids in such systems when no chemical species are removed. The main process in cementitious systems is the uptake of water into the solid mass. The amount of metal oxides (equal to the ignited mass) is therefore regarded as constant before and after the reaction.

3.1.1 Loss-on-ignition

Loss-on-ignition (LOI)

$$\text{LOI} = \frac{m_{\text{volatiles}}}{m_{\text{initial}}} 100 \quad [\%] \quad (\text{Eq. 3-1})$$

is conventionally determined by heating several grams of the sample (m_{initial}) in the muffle furnace up to a specified temperature in order to remove all the volatile components ($m_{\text{volatiles}}$) desired (e.g. up to 1000°C). This method was not applicable in this study due the high sample mass necessary. Loss-on-ignition was determined by thermal analysis (TA), either in a gas flow of air or, in the case of carbon dioxide sensitive samples, in a gas flow of nitrogen. Results in table 3-1 justify this approach.

Table 3-1. Comparison of LOIs determined at 1000°C either by standard method or by thermal analysis (TA).

	LOI conventional [%]	LOI from TA [%]	relative deviation [%]
China Clay	13.8 (2)	13.1	5.1
Illite MC	10.2 (4)	9.8	3.9
Volclay	13.7	13.8	0.7
Volclay <20µm	13.90 (17)	14.6	5.0

3.1.2 Inductively coupled plasma atomic emission spectroscopy

The equilibrium aqueous composition is indicative of minerals present in a system. Inductively coupled plasma atomic emission spectroscopy (ICP-AES) was used to analyse major elements in the extracted supernatants. The aqueous samples were prediluted 1:5 to 1:10 in order to prevent precipitation of dissolved silica and then acidified by adding 2 Vol.% of concentrated nitric acid. ICP-AES measurements were carried out with the model Spectro Ciros Vision (Spectro Analytical Instrument, Kleve, Germany) at the Swiss Federal Institute of Aquatic Science and Technology (EAWAG).

3.1.3 Wavelength dispersive X-ray fluorescence

In order to characterise the clay minerals studied, the chemical composition of the clay materials was determined by wavelength dispersive X-ray fluorescence (XRF) spectroscopy. Finely ground materials (< 30 µm) were dried over night in the oven at 105°C, then, after cooling in the exsiccator, transferred in previously annealed porcelain crucibles. Calcination for 30 min at 1070°C was performed in the muffle furnace and materials cooled again in the exsiccator. 1 g of calcined material was mixed with 5 g of di-lithium tetraborate (necessary for calibration to the internal standard Li), transferred into a platinum crucible, melted for 30 min at 1150°C and then poured into a casting dish to produce the glass bead. The glass beads were measured for major elements with the instrument PW 1404 (Philips) at the Swiss Federal Laboratories of Materials Testing and Research (EMPA).

3.1.4 Cation exchange capacity and exchangeable cations

Cation exchange is one of the basic properties of clay minerals. The cation exchange capacity (CEC) was determined according to the ammonium-acetate method [Mackenzie, 1951]. The determination is based on the replacement of the exchangeable cations by

NH_4^+ at pH 7 with a 1 M ammonium-acetate (purum p.a.) solution, transformation of sorbed NH_4^+ to NH_3 with a 1 M sodium hydroxide solution, distillation of the NH_3 (Distillation Unit 323, Büchi, Switzerland) and determination of the captured NH_3 (in boric acid) through titration with sulfuric acid.

The exchange of interlayer cations against NH_4^+ was performed by overhead agitation for 24 h and for a second 24 h after renewal of the solution. Several washing procedures were applied in order to remove excess salts and solutions. Each sample was determined in duplicate.

Exchangeable cations were determined in the supernatant and all the washing solutions kept after each of the two replacement steps. A method described in Emmerich (2000) was slightly modified. The solutions containing the exchanged cations were dried at 60°C until no water was left and some of the excess ammonium removed. The solid remains were redissolved with concentrated HNO_3 (1:1 with water). Solution composition was measured with ICP-AES against a standard series of a multi component standard.

3.1.5 X-ray diffraction

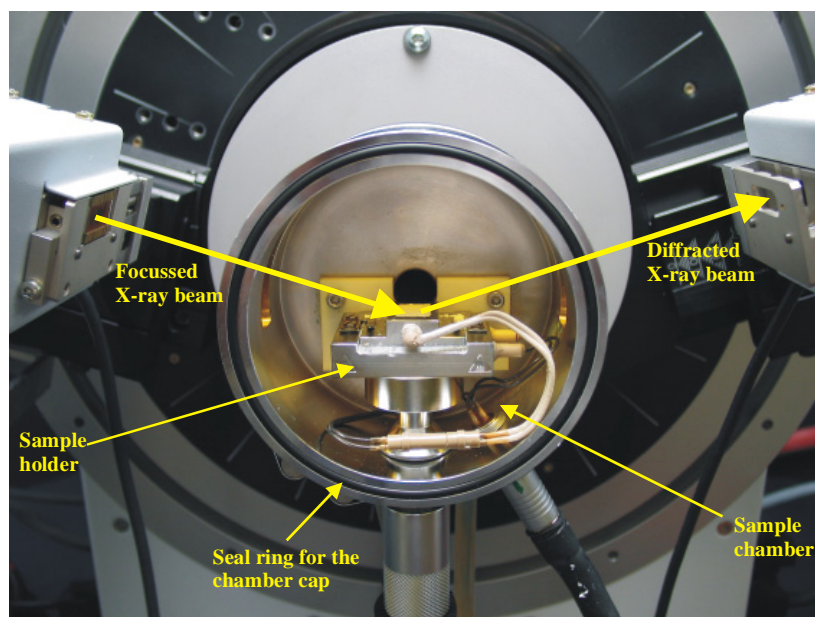
In general

The mineralogical composition of the sample material was characterised by X-ray diffraction (XRD) techniques. This is based on the fact that the crystalline fraction of the sample material interferes with the X-rays resulting in a characteristic diffraction pattern. This pattern (diffracted intensity with diffracting angle) is recorded by the detector system. By comparison with reference data, the qualitative composition of the sample material is determined.

X-ray diffraction (XRD) analyses were performed mainly on powders with a Bragg-Brentano diffractometer (Bruker AXS D8, Cu-K α radiation, automatic divergence and antiscattering slit, graphite monochromator). The X-ray tube was operated at a voltage of 40 kV and a current of 40 mA. Variable counting statistics were applied, however applied step width W was between 0.02° and 0.04° 2 θ and step counting time T between 2 and 9 s. For patterns intended for use in Rietveld refinement (quantitative analysis), profile intensities of around 2500 counts per second were aimed at.

At controlled humidity and temperature

Figure 3-1. XRD sample chamber (without the closure unit) for experiments at controlled humidity and temperature.



In-situ XRD measurements under controlled relative humidity (RH) were performed in order to investigate the different crystalline swelling behaviour of montmorillonites with various adsorbed sodium to calcium ratios. They were run at constant temperature between 25°C and 27°C in the sample chamber TTK450 (Anton Paar) shown in fig. 3-1. The RH was controlled by mixing wet and dry pressurised air with a humidity controller (Sycos H) and automatically controlled by a program designed in LabView (National Instruments).

Quantitative XRD analysis

Quantitative X-ray diffraction analysis of the mineral content is described in detail in Chapter 4.

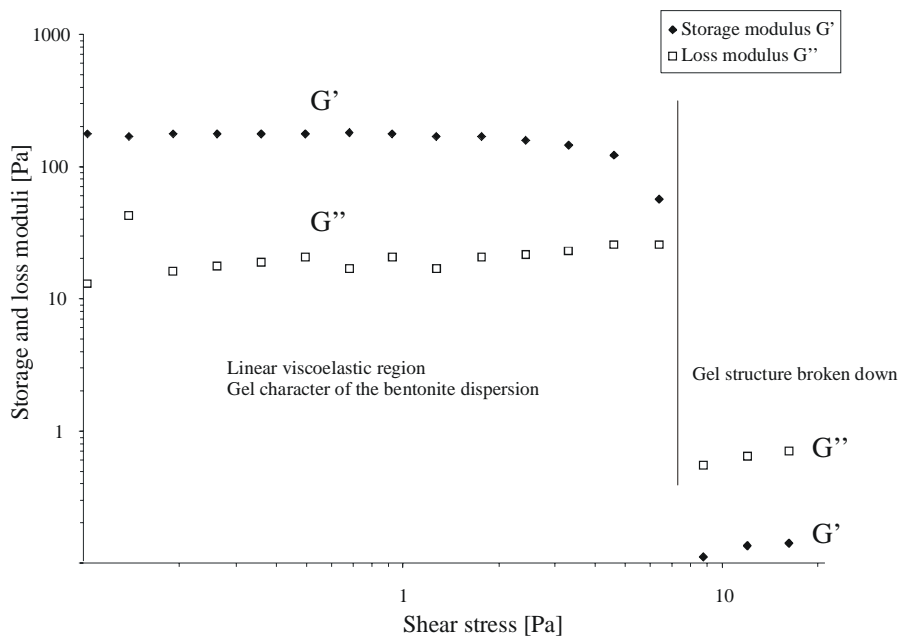
3.1.6 Rheological measurements

Bentonite dispersions are shear-thinning fluids, i.e. the viscosity of the dispersion decreases with increasing shear stress, the fluid becomes thinner. This is because bentonite dispersions show an internal structure (spatial arrangement of clay mineral layers inside the dispersion) that is progressively destroyed by an increase in shear stress. The yield point is the shear stress which causes flow to appear. It depends among other param-

eters on the temperature and for thixotropic fluids on the thixotropic thickening time [Pulsfort & Walz, 2000]. Thixotropic thickening is caused by the reconstitution of the dispersion's internal structure. This is associated with an increase in the yield point after ending the enforced flow. Shear thinning and thixotropic thickening of bentonite dispersions are reversible processes. The yield point at the end of a flow process is at its minimum (dynamic yield point) and increases asymptotically to its maximum (static yield point) [Pulsfort & Walz, 2000].

The yield point was measured with a rotational rheometer (Physica MCR 300) as the "Cross-Over Point" determined in an amplitude sweep test: This test is performed in oscillatory motion at variable controlled shear stress (CSS) but constant angular frequency in order to determine the boundary of the linear viscoelastic region. The elastic part of the deformation is characterised by the storage modulus G' (measure of reversibly stored deformation energy), the viscous part by the loss modulus G'' (measure of irreversibly lost deformation energy). The Cross-Over Point (COP) is determined as the transition from the gel state ($G' > G''$) to the fluid or sol state ($G'' > G'$). This transition appears when deformations caused by increasing the shear stress become greater than a limiting value: the dispersion's internal structure breaks down.

Figure 3-2. Determination of the Cross-Over Point of a bentonite dispersion with 100g/l bentonite: Storage and loss moduli of a bentonite dispersion with shear stress.



Oscillatory measurements were performed in amplitude sweep tests with controlled shear stress at a constant angular frequency $\omega = 10 \text{ s}^{-1}$. Bentonite concentration in the dispersion was 100g/l. The dispersion is filled between the two plates of the rheometer. The plate/plate distance was 0.1 mm (~ five times the maximum grain size of 20 μm). Evaluation of the COP was visually estimated using plots such as the one shown in fig. 3-2. It has to be noticed that the value of this COP is only valid at $\omega = 10 \text{ s}^{-1}$. The effect of different angular frequencies was not tested. However, this angular frequency is typically used by operators in the industry [Mezger, 2000].

3.1.7 Extraction of remaining clay minerals

A method for the removal of CaCO_3 and CaSO_4 in clays (Bodine & Fernald, 1973; Köster et al., 1973) was adapted in order to dissolve any remaining CH and newly formed cement hydration products and to extract the remaining clay mineral fraction. Dissolution of C-S-H phases was tested on freeze-dried C-S-H with a C/S ratio of 0.7 and shown to be complete (less than 0.5% solid remains). The dissolution of calcium aluminate hydrates was checked by the disappearance of their basal reflections in diffractograms of the extracted clay minerals. The results were recalculated with the LOI of the materials and expressed as a percentage of volatile free clay mineral per ignited mass. The material recovery is given in Table 3-2 for China Clay and Volclay as an average of three and four determinations.

Table 3-2. Initial mass before and percentage of material recovery after extraction.

	initial mass [g]	material recovery [%]
China Clay	4.5 - 5.3	95.7 \pm 0.3
Volclay	4.5 - 5.1	93.7 \pm 0.6

Approximately 5 g of reacted clay-lime mixture were dispersed in 400 ml of a 0.2 M Na-EDTA solution (EDTA tetrasodium tetrahydrate) and agitated overhead for 24 h. After renewal of the EDTA solution, a second extraction step was applied for another 24 h, followed by three washing steps. The highly dispersed state of the extracted sodium bentonite made it necessary to convert the extracted sodium bentonite back to its calcium form (4% CaCl_2 solution). After the washing steps, material recovery was otherwise below 70%.

3.1.8 (Environmental) Scanning electron microscopy (ESEM and SEM)

Electron microscopic investigations are based on the interactions of a focused electron beam with a sample surface. These interactions lead to emission of secondary electrons (SE) and back scattered electrons (BSE) from the surface. The electron beam scans the sample surface and the locally emitted electrons (SE, BSE) are detected. The SE are used to generate a picture of the sample surface. Additionally, local chemical variations in the sample surface are obtained by the detection of the BSE. The interaction of the electron beam with the sample surfaces produces also X-rays with an energy spectrum characteristic of the (sub)surface's chemical composition. This energy dispersive X-ray analysis (EDX) is used for the quantitative measurement of the chemical composition of small sub-surface regions (several μm^3 with modern electron microscopes).

Investigations of the samples were performed on an Environmental Scanning Electron Microscope (ESEM), Philips ESEM XL 30 FEG.

In the so-called ESEM-modus, the sample chamber is operated in contrast to conventional electron microscopes (high vacuum) under low vacuum and water vapor atmosphere (~ 1 Torr). One advantage of these operating conditions is that samples need not to be sputtered with gold or carbon in order to improve the electrical conductivity of the sample surface and to prevent excessive charging of the surface. Discharge of the sample surface is partially accomplished by the water vapour atmosphere. The possibility of the investigation of e.g. humid materials without pre-drying is the most important advantage of the ESEM-modus.

3.1.9 Mercury intrusion porosimetry

Pore size distributions and porosities of the samples were determined with a mercury intrusion porosimeter (Pascal 140 and 440, CE Instruments). Such measurements are based on the intrusion of mercury into the open pore system of a sample and on the non-wetting liquid property of mercury with a lot of solids. Mercury penetrates through the open pores of a solid sample under the effect of pressure. Cylindrical pores with diameter d filled at an specific pressure are inversely related to this pressure p by the Washburn-equation [Washburn, 1921]:

$$d = \frac{-4\sigma \cos\theta}{p} \quad (\text{Eq. 3-2})$$

with the surface tension σ (480 mN/m) and the wetting angle of contact θ (with purified mercury, assumed to be 130° for clay minerals and cement [Winslow & Shapiro, 1959; Diamond, 1970]).

Measurements are performed in a volume calibrated glass vessel. Due to the high porosity (55% to 75%) of the samples studied, only ~ 0.1 g of sample could be used for each measurement. The freeze-dried material was weighed to a precision of ± 0.1 mg inside a dilatometer and evacuated for ~ 15 min to about 0.01 bar in the macropore unit (Pascal 140, CE Instruments). Mercury was then added to a marked level on the capillary tube. The pressure was raised continuously from vacuum to about 370 kPa. The dilatometer was then transferred to the micropore unit of the porosimeter (Pascal 440, CE Instruments). The pressure was increased stepwise to 400 MPa using a special pressure transmission oil. Penetration of mercury in the pores was followed by measuring the electric capacity along the capillary tube. The resulting volume values were corrected for the compressibility of mercury determined in a similar experiment with mercury only. Pores with a radius down to 2 nm were measured over the applied pressure range.

3.2 Thermal gravimetry with evolved gas analysis

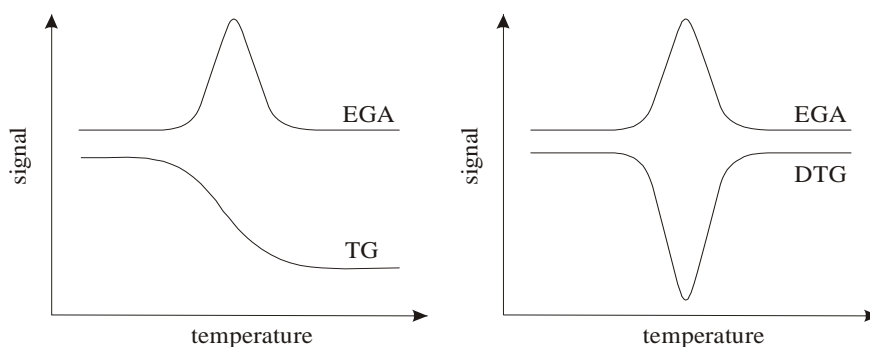
Thermal analysis summarises a group of methods which determine physico-chemical properties of pure substances but also of mixtures by heat treatment. In this study, only thermogravimetric (TG) measurements at a constant heating rate with simultaneous evolved gas analysis (EGA) were performed. The first derivative of the TG curves (DTG) leads to better resolution of the peak data. Thermal gravimetry with evolved gas analysis was performed on a thermal balance (Mettler TGA/SDTA 851e) coupled through a capillary to a quadrupole mass spectrometer (Balzers ThermoStar). Between 20 to 100 mg of finely ground material was heated in a platinum crucible at a rate of $10^\circ\text{C min}^{-1}$ and a gas flow (air or nitrogen) of 50 ml min^{-1} . The evolved gas was analysed for water and carbon dioxide by their most abundant fragments of the two components, CO_2^+ ($m/e = 44$) and H_2O^+ ($m/e = 18$).

3.2.1 Evaluation model for quantification of TG-EGA data

For substances or mixtures of substances that show a well-resolved mass loss peak due to the decomposition and emission of volatile components, the analogy of mass loss data and

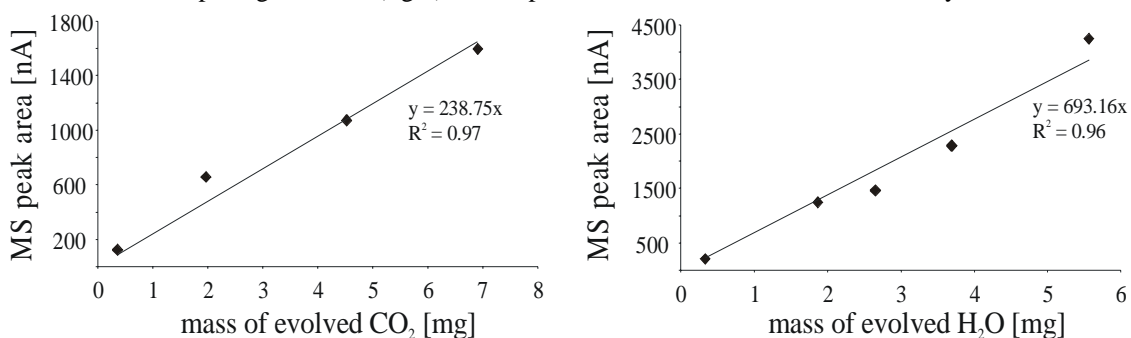
simultaneous EGA data is obvious from fig. 3-3. The schematic figure shows part of a TG mass loss curve and an associated EGA signal from the mass spectrometer and the relationship between the first derivative of the TG curve and the EGA signal.

Figure 3-3. Schematic representation of a mass loss and the associated signal from the mass spectrometer due to an evolved volatile component.



If (i) mass transport time of the evolved gases is negligible (no dead time), (ii) no adsorption phenomena occur in the capillary, (iii) the baseline is perfectly defined and (iv) no other interferences occur, the EGA signal is directly related to the first derivative of the TG data, the DTG curve. The ratio of EGA signal to DTG signal is then just a constant, termed here the effective sensitivity of the mass spectrometer. Effective only, because in such types of measurements, it is not known, which fraction of the evolved gas is actually transferred from the oven to the capillary¹. Thus, the mass of gas transferred to the mass spectrometer is not equal to the mass lost during decomposition.

Figure 3-4. Calibration lines for the carbon dioxide evolving from decomposing calcite (left) and for the water from decomposing kaolinite (right); the slope of the lines is the effective sensitivity.



The linearity of the ratio of EGA peak area to differential mass loss is given in fig. 3-4 as determined by the decomposition of pure calcite and pure kaolinite. Calcite mass loss was

¹ The oven is an open system. Expansion of the gas inside the oven is free. Only part of the evolved gas is transferred through the capillary right above the heated sample to the mass spectrometer.

determined between 600°C and 750°C and kaolinite mass loss due to evolved hydroxyl water between 400°C and 700°C. It is concluded that mass loss in a specified temperature range is proportional to the EGA signal and that mass transfer rate of the evolved gas to the capillary is thus independent of the amount evolved. Assuming that the effective sensitivities (the slope of the lines in fig. 3-4) are independent of operation temperature between 25 and 1000°C, then the ratio of the effective sensitivities of two gas components is again a constant. This constant is the so-called ionization factor, which must be known if quantification is desired.

For mixtures of substances emitting only water and carbon dioxide upon heating, the associated mass losses can be quantified using the approach described above. At each temperature/time¹ step, the sum of the two EGA signals, each multiplied with an appropriate constant, must match the differential mass loss:

$$-\frac{\Delta m(T)}{\Delta T} = k_{CO_2} I_{CO_2}(T) + k_{H_2O} I_{H_2O}(T), \quad (\text{Eq. 3-3})$$

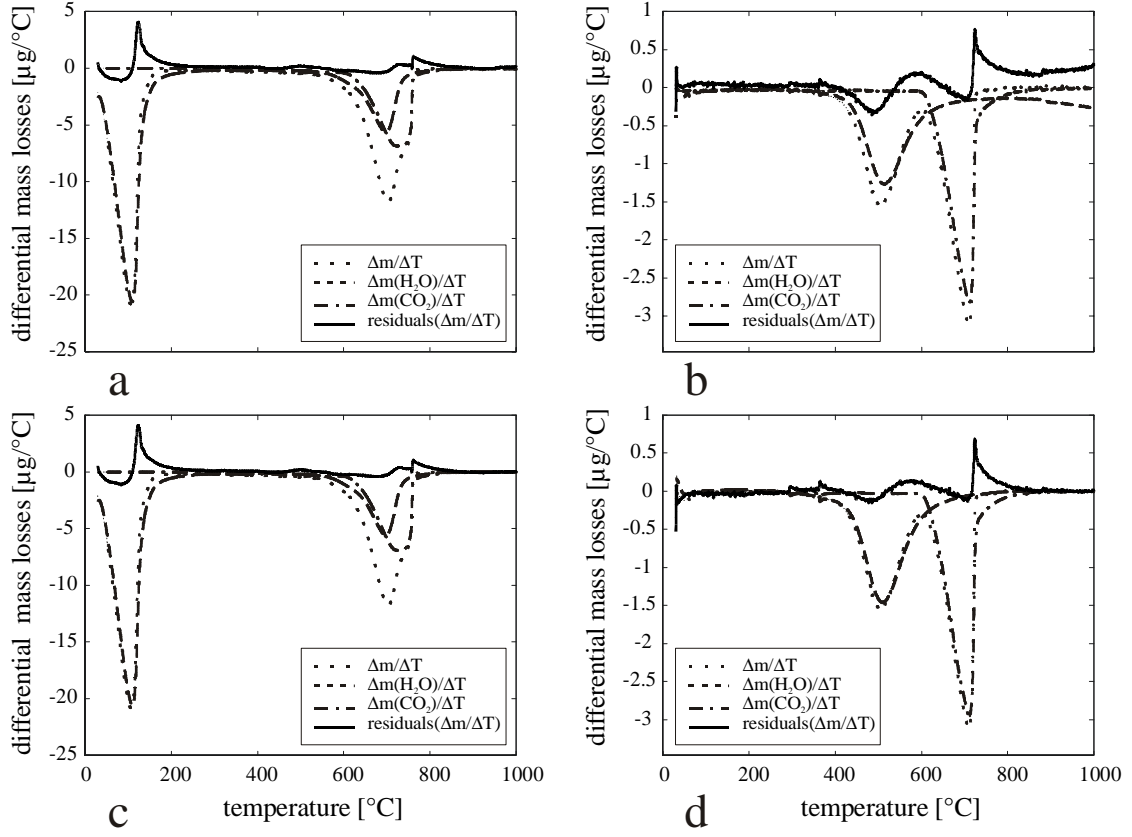
with k_i the reciprocal effective sensitivity [mg nA^{-1}] of the i -th component and I_i the mass spectrometer signal [nA] for this gas components. This equation is an overdetermined equation system (there are two variables and the number of equations is equal to the number of recorded time steps, usually more than 1000) and might be solved using matrix left division.

The solution of several TG-EGA data sets revealed that the primitive model (eq. 3-3) was insufficient in order to match the TG and EGA data. Typical results are shown in fig. 3-5A and B for mixtures of clay minerals with calcite. A major problem is the tailing of the EGA data, which is probably attributed to sorption effects in the capillary. The inclusion of a physical attenuation model as an analogue for linear sorption did not improve results substantially. The best results were obtained by assuming that the reciprocal effective sensitivity k_i of each gas component is a linear function of time according to the following equation:

$$k_i = a_i T + k_i^0 \quad (\text{Eq. 3-4})$$

¹ Time and temperature are equivalent in thermal analysis with a constant heating rate.

Figure 3-5. Two mixtures of clay and calcite analyzed by their evolved gases from decomposition; Volclay with calcite (a) fitted with the primitive model and (c) with the temperature dependent model; China Clay with calcite (b) fitted with the primitive model and (d) with the temperature dependent model.



A physical meaning can be attributed to this temperature dependency. Increase of the temperature inside the oven will lead to a dilution of the atmosphere as the gas inside the oven is allowed to expand freely. A specific mass loss and emission of a gas component causes an increase in the partial pressure of this component with increasing temperature. The same mass loss at 100°C and 1000°C leads to a stronger EGA signal at 1000°C. Inserting eq. 3-4 into eq. 3-3 leads to:

$$-\frac{\Delta m(T)}{\Delta T} = a_{CO_2} T I_{CO_2}(T) + a_{H_2O} T I_{H_2O}(T) + k_{CO_2}^0 I_{CO_2}(T) + k_{H_2O}^0 I_{H_2O}(T) \quad (\text{Eq. 3-5})$$

which was solved using matrix left division:

$$\begin{bmatrix} a_{CO_2} \\ a_{H_2O} \\ k_{CO_2}^0 \\ k_{H_2O}^0 \end{bmatrix} = \begin{bmatrix} I_{CO_2} & I_{H_2O} & I_{CO_2} & I_{H_2O} \end{bmatrix} \setminus \left(-\frac{\Delta m(T)}{\Delta T} \right) \quad (\text{Eq. 3-6})$$

In some cases, physical meaningful solutions were only obtained when constraining the parameters to reasonable values (e.g. positive values). Prior to any solution procedure, basal lines have been subtracted using polynomials of different degree. Fig. 3-5 compares the results of the primitive model (eq. 3-3) and the temperature dependent model (eq. 3-5). The data match judged by the mean square value of the residuals was for the latter model always better, however visual observation of fig. 3-5 still reveals problems from the tailing of the EGA data. Some results of the quantification procedure with this model are given in Table 3-3 for mixtures of clay and calcite. Fitting the predicted calcite contents is very effective for significant deviations from zero. However, for low contents the relative error increases drastically. Therefore, the results given by this method for the usually low calcite contents in this study (< 2%) are only regarded to be semi-quantitative.

Table 3-3. Comparison of contents of added calcite with the fitted values.

sample	added calcite [%]	fitted calcite^a [%]	relative deviation [%]
China Clay and calcite	22.6	22.4	0.1
Volclay and calcite	9.2	9.4	2.2
Volclay and calcite	4.5	5.2	15.6

^aCO₂ mass loss times the molar mass ratio $M(\text{CaCO}_3)/M(\text{CO}_2) = 2.27$

Nevertheless, the potential of this method is judged to be high. There is no restriction in the number of gas components. Much better results are expected if both a model for automatic determination of the EGA base line and a model of non-linear sorption (e.g. by inverse modelling of the EGA data) be included. If one a perfect match of the DTG and EGA data is achieved, quantification with a high accuracy and precision is expected. Problems arise if chemical reactions occur as e.g. the combustion of organic matter: Chemical species responsible for the mass loss and detected species are not of the same stoichiometry. For combustion of organic matter, the mass loss is attributed mainly to carbon loss, but with full combustion, carbon dioxide is detected.

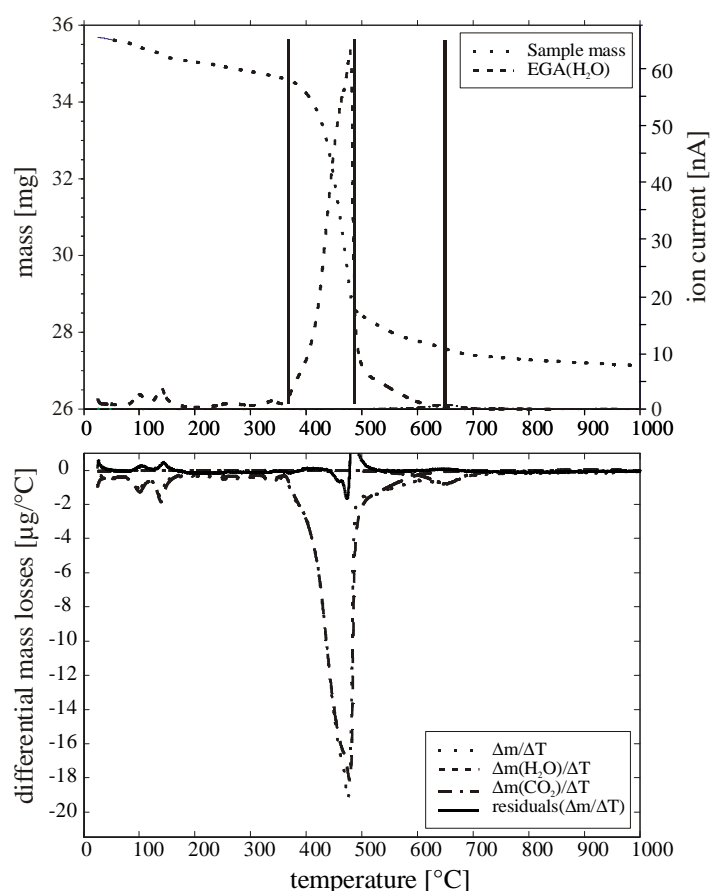
3.2.2 Determination of portlandite and clay minerals by their evolved crystal or hydroxyl water

The goal of determining clay mineral consumption in the reacted clay-lime mixtures with quantitative X-ray diffraction analysis was not achieved (cf. chapter 4.). Therefore, thermal analysis had to give supplementary information on clay mineral consumption in order to check the plausibility of results obtained by the extraction and XRD techniques. The

results of the chemical extraction procedure for the remaining clay minerals were used as a first estimate. Together with the XRD data on the consumption of calcium hydroxide, the extraction results gave an average mass ratio for the two reacted minerals.

Peak fitting of thermal analysis patterns is very complicated due to superposition of various different effects and processes [Emmerich, 2000]. Estimation of the water evolved from decomposing portlandite and kaolinite in reacted mixtures was therefore performed as follows and is exemplified by the China Clay-lime mixture shown in fig. 3-6.

Figure 3-6. TA data for a 7 month reacted China Clay-lime-water mixture (15 g/70 g/100 g); calcite content 1.5%. Simulation of used mineral fractions per total ignited mass ($\text{CaO}/\text{oxide}_{\text{clay}} = 1.4$) gives a consumed content of 12.0% for lime and 8.6% for the clay. The solid lines in the upper figure indicate the cut-offs used as a first estimate for the determination of lime water and China Clay hydroxyl water.



This figure shows the strong degree of overlap of water evolving from portlandite and kaolinite decomposition. The total amount of evolved water per ignited mass was determined from the onset portlandite decomposition ($\sim 370^\circ\text{C}$) to the end of kaolinite decomposition ($\sim 650^\circ\text{C}$). A cut was set arbitrarily at the kink of the TG data (here at $\sim 490^\circ\text{C}$). The amount of water evolved below this kink temperature was multiplied with the factor of 3.12 (molar mass ratio of CaO and water) to yield per cent CaO per ignited mass, the

water evolved above was multiplied with the factor of 7.41 (inverse hydroxyl water content per ignited mass) to yield per cent metal oxides from kaolinite. As the degree of overlap of the two peaks was not known, fractions of the clays' hydroxyl water were transferred between the two compartments until the desired mass ratio was reached. For all the China Clay-lime mixtures analysed, $15 \pm 2\%$ of the kaolinite's hydroxyl water had to be transferred to the lime water in order to match the aimed mass ratio (inferred from the extraction and XRD techniques). This seems justified as the investigated clay-lime mixtures contained high lime contents. Lime decomposition of pure lime shows a large tailing to temperatures greater than 500°C (cf. fig. 3-14). The same procedure was applied to the other reacted clay-lime mixtures.

3.3 Calculation of results

3.3.1 Calculation of consumed contents of clays and lime

All results are expressed as volatile free oxides per ignited mass. The consumption of clay minerals and CH is then just calculated by subtraction of their contents before and after reaction. Reacted fractions are calculated as the ratio of consumption and initial mineral content in the mixture (in percent).

Estimation of errors

For the extraction method, it was demonstrated that up to 7% of the initial clay material (Table 3-2) may be lost during the different washing/centrifugation steps. Clay material consumption was calculated by subtraction of the initial contents as well as those determined after reaction. Due to the small amounts of clay consumption the relative error may result in a up to 30% overestimation of clay consumption by this method.

The remaining CH content in reacted clay-lime mixtures was determined by XRD with the internal standard method. The relative error in quantitative XRD analysis is estimated to 5% [Klug & Alexander, 1974]. The consumption of CH was determined by the subtraction of initial contents as well as those determined after reaction. In mixtures with high initial CH content of e.g. 60%, the absolute error for the determined consumption may be as high as 3%. Taking into account that the difference between initial CH contents and those measured after reaction was only about 10%, the relative error of this method is also high.

3.3.2 Standard deviation and standard error of the mean

Errors of repeated measurements x_i are given as the standard error of the mean calculated from the standard deviation:

$$\sigma = \sqrt{\frac{\sum_{i=1}^N (x_i - M)^2}{N - 1}} \quad (\text{Eq. 3-7})$$

$$\sigma_M = \frac{\sigma}{\sqrt{N}} \quad (\text{Eq. 3-8})$$

with M the mean of the sample, N the sample size, σ the standard deviation (unbiased estimate), σ_M the standard error of the mean.

3.4 Materials and their characterisation

Selection criteria for the three clays were as follows:

- (i) High clay mineral content.
- (ii) Fineness to prevent grinding of reacted freeze-dried materials (clay minerals and cement hydrates are susceptible to grinding).
- (iii) Frequently occurring clay minerals in natural soils and technical barrier systems.

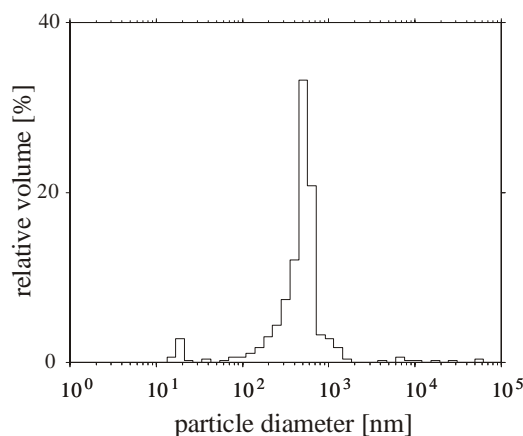
Cation exchange experiments were performed with bentonite fractions freed of soluble salts by dialysis. In this way, remaining salts did not interfere with the analysis of exchangeable cations.

Pozzolanic tests were performed with the more or less raw clay materials. No major purification steps and also no extraction techniques were applied for carbonate or amorphous phases. The three clays were regarded as homogenous as indicated from X-ray diffraction. No difference in different subsamples could be detected. The chemical compositions, as measured in previous studies as well as in this study, showed no significant differences. Major purification and enrichment steps were set aside because of the amount of material needed for the pozzolanic tests (more than 300 g of each clay used in this study) and the great deal of work and time associated with clay mineralogical purification of even small amounts of just several grams.

3.4.1 Kaolin 'China Clay'

The kaolin 'China Clay' originates from Cornwall, England. The particle size distribution given in fig. 3-7 was estimated by mercury intrusion porosimetry (MIP). The China Clay's median particle size is ~500 nm when determined by MIP [Kahr & Plötze, 2000]. Cation exchange capacity is 5 meq/100g.

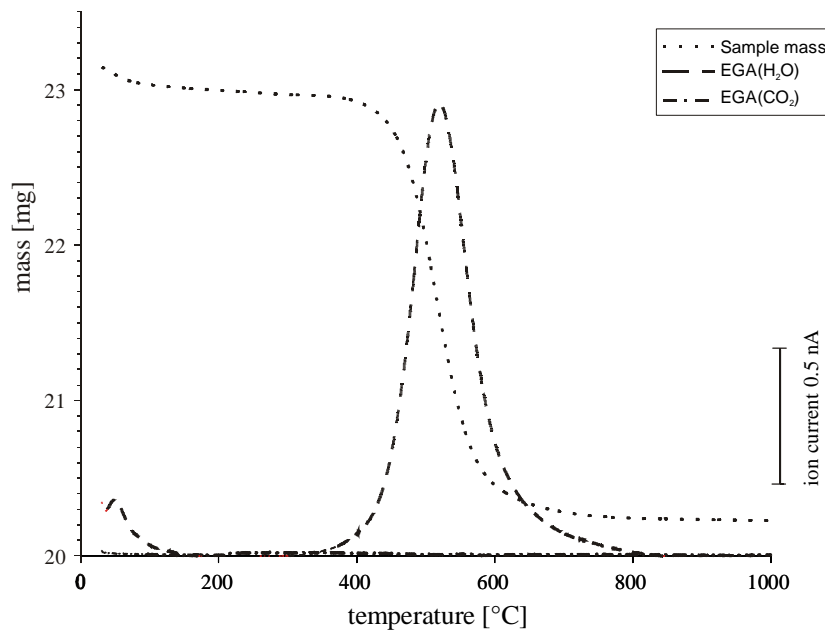
Figure 3-7. Particle size distribution of the China Clay calculated from mercury intrusion porosimetry.



Mineral composition was determined from the combination of chemical analysis, thermal analysis and X-ray diffraction. The average chemical analysis of 4 determinations of the raw material is shown in Appendix I and compared to an analysis of Köster [in Jasmund & Lagaly 1993] and a theoretical analysis of pure kaolinite with the structural formula $\text{Al}_2[\text{Si}_2\text{O}_5(\text{OH})_4]$.

The chemical composition of the raw sample is very close to an ideal kaolinite, especially the loss on ignition, which is only due to evolved water (fig. 3-8). Thermal analysis of the raw material (fig. 3-8) indicates some water evolving between 30 to 200°C, which is attributed to interlayer or surface water of accessory phases (e.g. illite). The main mass loss between 400°C and 800°C is due to crystal structure breakdown and loss of the hydroxyl water (dehydroxylation) of the kaolinite. The mineral contents given by Köster indicate muscovite as the only hydrous mineral besides kaolinite. Köster determined the kaolinite content in the raw sample to 86.4 %. Assuming a K_2O content of 8% in an average illite (cf. illite analyses given in Jasmund & Lagaly (1993) and references therein), 87.5% kaolinite are calculated from the chemical analysis in Appendix I. This is in agreement with Rietveld analysis of the diffraction pattern which indicated 88% kaolinite, 4% microcline, 7% muscovite/illite and minor (~1%) quartz.

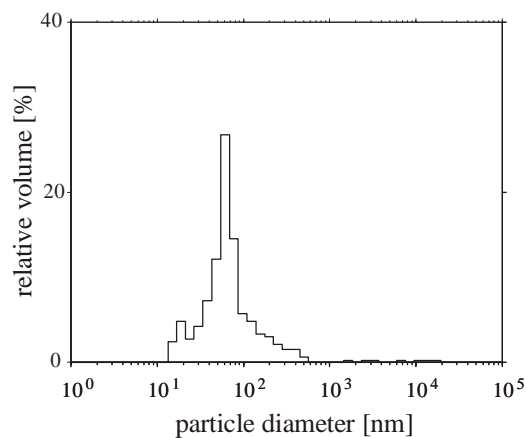
Figure 3-8. TG-MS data of the kaolin China Clay; the first water peak of the illite corresponds to ~1 % water loss.



3.4.2 Illitic clay from Massif Central (Le Puy)

The illitic clay is from Massif Central (MC), France. It was known from previous analyses [Müller Vonmoos et al., 1991], that the primary particles are extremely fine, however they are mainly found in a highly agglomerated state. 500 g of the raw material were therefore dispersed in deionised water using ultrasonic treatment, followed by wet-sieving through 20 μm and freeze-drying. All of the dispersed material passed the 20 μm sieve after this treatment. The particle size distribution of the dispersed, dry material is given in fig. 3-9 as estimated by mercury intrusion porosimetry (MIP). The illite MC median particle size by MIP is ~60 nm. Cation exchange capacity is 27 meq/100g.

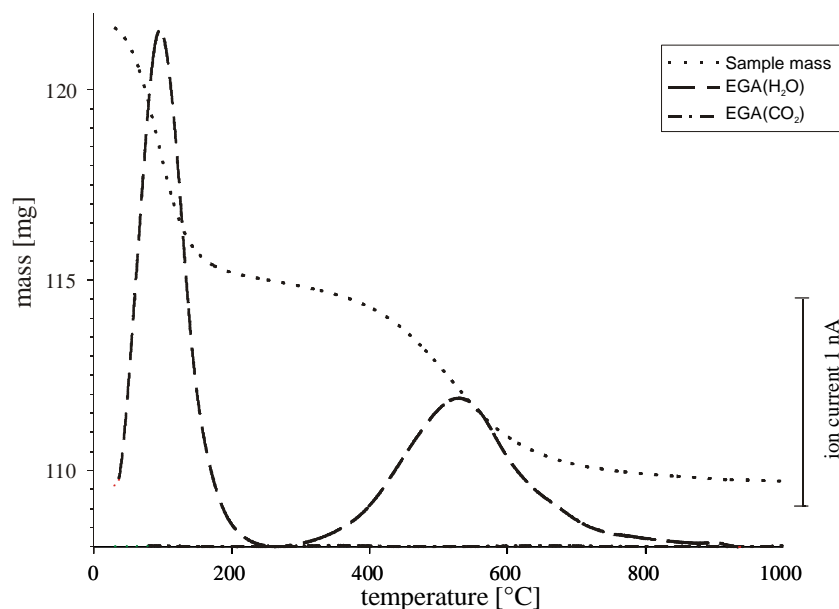
Figure 3-9. Particle size distribution of the illite MC calculated from mercury intrusion porosimetry.



Mineral composition was determined from the combination of chemical analysis, thermal analysis (fig. 3-10) and X-ray diffraction. The average chemical analysis of three determinations of this material is shown in Appendix I and compared to an analysis of the $< 0.2 \mu\text{m}$ fraction reported by Müller Vonmoos et al. (1991).

Based on the Al_2O_3 content of the analysis of Müller Vonmoos et al. (1991) and of the raw material used in this study, only $\sim 70\%$ of illite in the clay is calculated, whereas based on the K_2O content it seems to be almost pure illite (cf. illite analyses given in Jasmund & Lagaly (1993) and references therein). Rietveld analysis of the diffraction pattern has given 87% illite and 13% potassium feldspar. A broad asymmetric basal peak at around 10 \AA indicates a significant content of expandable clay minerals.

Figure 3-10. TG-MS data of the illitic clay.



3.4.3 Bentonite Volclay

The bentonite Volclay is from Wyoming, USA. 40 g of a sodium exchanged $< 2 \mu\text{m}$ fraction of the Volclay were produced by sedimentation and ion exchange with 2 M NaCl solution (three times), followed by dialysis (until electrical conductivity stayed below $10 \mu\text{S}$) and freeze-drying. This fraction was used for the cation exchange experiments. X-ray diffraction revealed residual quartz ($\sim 5\%$) in this fraction.

500 g of the raw material was dry-sieved through $20 \mu\text{m}$. This fraction was used for the pozzolanic tests. 40 g of this fraction were converted to the calcium form and salt remains removed by dialysis. The particle size distribution of the $< 20 \mu\text{m}$ fraction given in fig. 3-

11 was estimated by mercury intrusion porosimetry (MIP). The bentonite's median particle size by MIP is ~150 nm. However, the distribution is extremely broad compared to the other clays, possibly due to the aggregated state of the material. Cation exchange capacity of the <20 μm fraction is 85 meq/100g.

Figure 3-11. Particle size distribution of the bentonite Volclay calculated from mercury intrusion porosimetry.

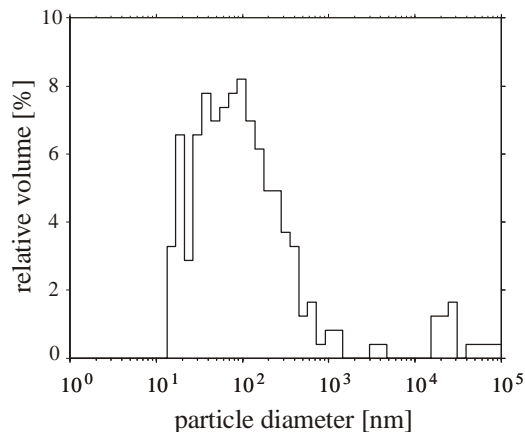
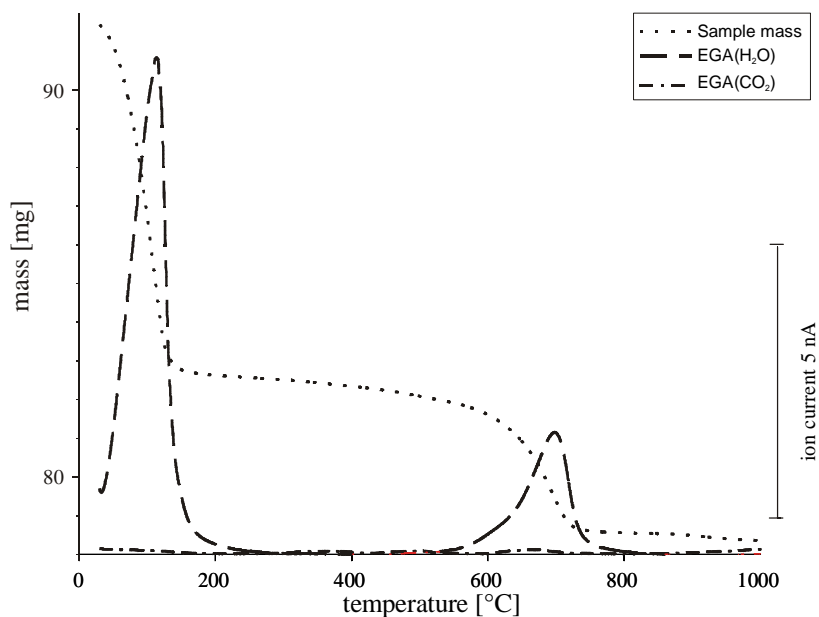


Figure 3-12. TG-MS data of the < 20 μm sieve fraction of the bentonite Volclay.



Mineral composition was determined from the combination of chemical analysis, thermal analysis (fig. 3-12) and X-ray diffraction. The average chemical analyses of the raw material and the <20 μm sieve fraction are given in Appendix I and compared to a chemical analysis performed by Mermut & Cano (2001) on the SWy-2 Source Clay, which is a comparable Wyoming bentonite. Loss on ignition of the material was determined at

750°C, as thermal analysis indicated no significant mass loss above this temperature and alkali ion losses due to evaporation were detected to be significant at 1070°C.

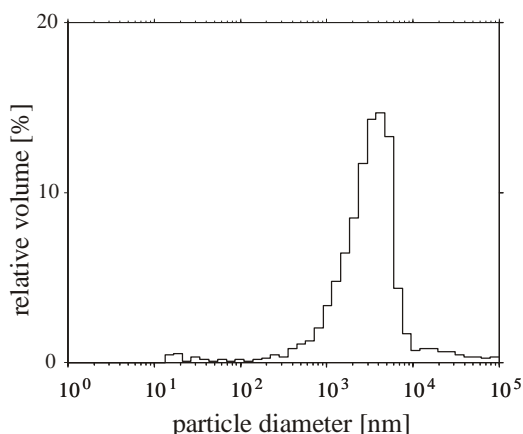
Quartz content in the <20 µm fraction determined by the standard addition method based on peak area determinations and also by Rietveld analysis is 5.6 % [Müller et al., 2002]. Additional phases are gypsum (~1%), calcite (~0.5%), magnetite (~0.5%), plagioclase (~5%) and 87% montmorillonite.

3.4.4 Decarbonated water

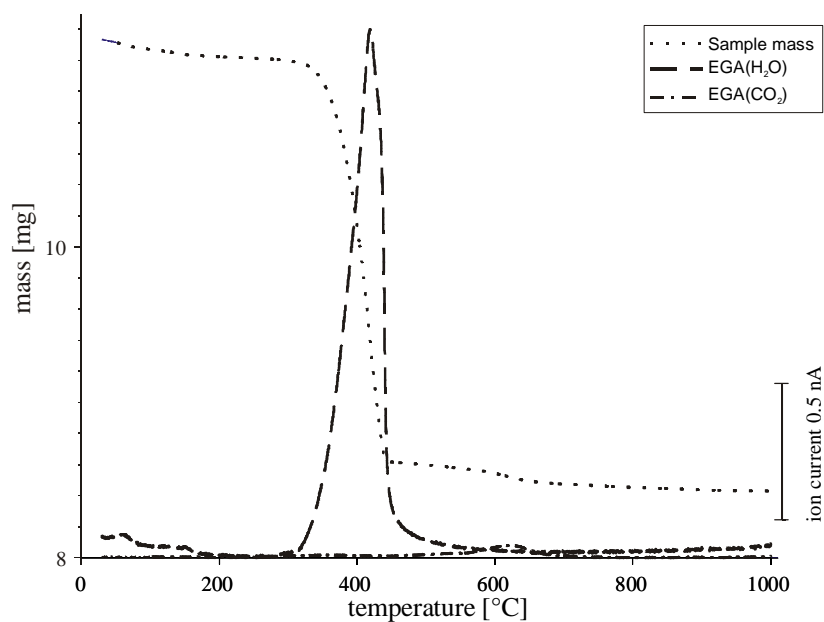
Milli-Q water (Millipore, USA) was boiled until two third of the initial volume was vaporised in order to remove carbon dioxide. The hot water was transferred into bottles and then into the glove box. This water was used for all the mixtures prepared.

3.4.5 Calcium hydroxide

Figure 3-13. Particle size distribution of the calcium hydroxide calculated from mercury intrusion porosimetry.



Calcium hydroxide (CH) was prepared from the hydration of calcium oxide over humid nitrogen in an exsiccator in the glove box. The nitrogen was humidified with decarbonated water. Completion of the hydration process was confirmed by X-ray diffraction and thermal analysis (fig. 3-14). Minor amounts of calcite (1.5%) could be detected by both methods. The particle size distribution of the calcium hydroxide given in fig. 3-13 was estimated by mercury intrusion porosimetry (MIP). The median particle size by MIP is ~4 µm.

Figure 3-14. TG-MS data of portlandite; the small loss of CO₂ corresponds to ~1.5% of calcite.

3.4.6 Other chemicals

All other chemicals used (e.g. sodium chloride and sodium perchlorate) were prepared from Fluka “supra-pur” grade.

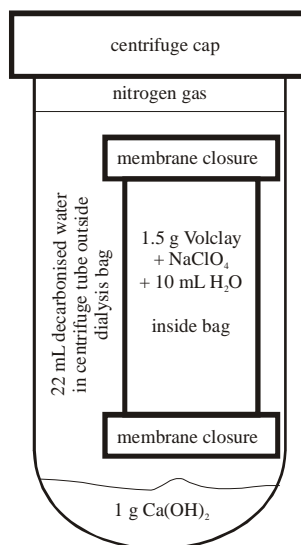
3.5 Sample preparation and handling

All materials and mixtures sensitive to carbon dioxide were prepared and handled in the glove box and mixed with decarbonated water in order to keep carbon dioxide away from the suspensions. The glove box was purged with nitrogen evaporated from a dewar with 300 l liquid nitrogen which lasted for about three months.

3.5.1 Pozzolan reaction of clay minerals I

Preparation of samples for the cation exchange experiment

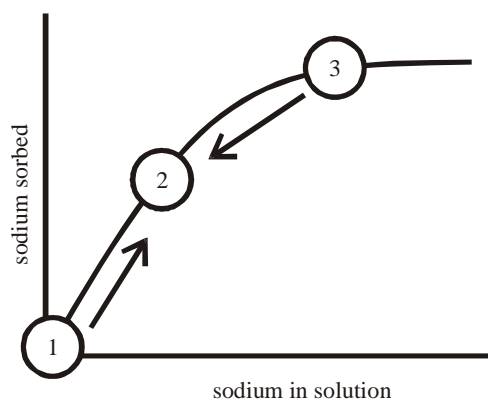
Bentonite samples with different Na/Ca ratios were produced in Ca(OH)₂ buffered solutions by addition of NaClO₄. The bentonite and the Ca(OH)₂ were separated by a dialysis bag (Spectrum Spectra/Por 1, regenerated cellulose membrane tubing, molecular mass cut-off 6000-8000) to prevent mixing of the solids (fig. 3-15). 1.5 g of bentonite and the desired amount of NaClO₄ were transferred together with 10 ml of decarbonated water into the dialysis bag. The closed bag was put into the centrifuge tube which was filled with 1 g of Ca(OH)₂ and 22 ml decarbonated water.

Figure 3-15. Schematic picture of the experimental setup for the cation exchange experiment.

After approximately 90 h of equilibration, suspensions inside and outside the dialysis bag were centrifuged separately and the contact solutions analysed by ICP-AES. Bentonite samples were washed 5 times with ethanol (98%) to prevent carbonation of the solids and disturbance of the adsorbed sodium amount. One washing step with a small water to solid ratio (2 parts of decarbonated water to 1 part of solids by volume) was necessary in order to remove ethanol, which disturbed the freeze drying process. Both, metal concentrations in solution and adsorbed were measured. The results of the cation exchange experiment are therefore termed “direct determination” in chapter 5. The results from the rheological measurements on the cation exchange state are termed “indirect determinations”, as only the metal concentrations in aqueous solution were determined. Adsorbed concentrations are calculated by mass balance from the measured aqueous solutions.

Preparation of the dispersions for rheological measurements

The calcium exchanged, wet sieved <20 μ m size fraction was dialyzed and freeze-dried. The dispersions were prepared for each experiment series by mixing 2 g of calcium-bentonite, 0.1 g of calcium hydroxide and 20 g of decarbonated water. The dispersions were twice dispersed with a 5 min ultrasonic treatment. First, when the pure bentonite dispersion was prepared and second after both additives were added. The first additive was mixed into each dispersion by shaking thoroughly. Two different steps were distinguished for the addition of calcium hydroxide and NaCl. Thereby, the equilibrium position was approached from two different sides.

Figure 3-16. Schematic adsorption isotherm showing the two different preparation steps.

- (i) If NaCl was added first to the calcium bentonite dispersion, a 60 h equilibration step followed, before the calcium hydroxide was added. The agitated dispersions were given an additional 12 h equilibration step. The cation exchange state changes from point 3 to point 2 (fig. 3-16).
- (ii) If calcium hydroxide was added first to the calcium bentonite dispersion, NaCl was added 5 h later, and then allowed to equilibrate for 40 h. The cation exchange state changes from point 1 to point 2 (fig. 3-16).

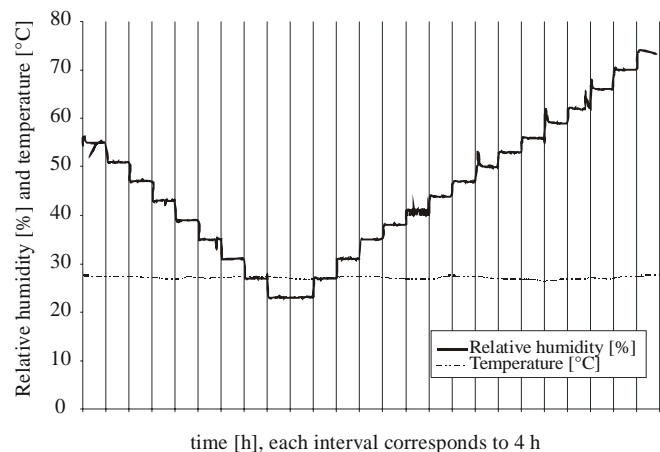
Fig. 3-16 shows the assumed effect of the two steps. Point 1 in Fig. 3-16 is the initial Ca-Volclay. After addition of NaCl and equilibration for 24 h in the first step, point 3 will be achieved on the isotherm. Addition of calcium hydroxide will result, because of the increase of calcium in solution, in an desorption of sodium which ends at point 2, the equilibrium amount of adsorbed sodium. In the second step, the system is assumed to go directly from point 1 to 2 without going over point 3 (cf. Fig. 3-16).

Preparation and handling of the samples for the swelling curves

The ethanol washed, freeze-dried powders of the cation exchange experiment were used for the XRD measurements of the swelling curves. Preliminary swelling measurements have, on one hand, shown that it is more favourable to perform the desorption measurements prior to adsorption measurements: Expansion from the one- to the two-layer hydrate was found to be hindered sometimes if adsorption was performed first. On the other hand, the interlayer spacing did not always behave in a reproducible way for repeated measurements in humid air because samples were not equally carbonated. This effect was ascribed to progressive carbonation in the humid air flow. Calcium hydroxide species at the edges of the clay minerals (cf. results of cation exchange experiment) probably led to the Couture effect, to the blocking and cementing of individual clay mineral

layers to non-expandable ones [Couture, 1985]. These hydroxide-species will become progressively carbonated in humid air leading to an increased fraction of expandable clay mineral layers (evidenced by an increase in the basal spacing). Therefore, prior to the swelling measurements, the individual samples were carbonated for several weeks under a continuous flow of moist carbon dioxide (~50 ml/h). The swelling measurements were then conducted with the carbonated samples after an additional one week equilibration at 72% RH and room temperature. The samples were mounted in the sample holder, followed by desorption and adsorption measurements at constant relative humidity and constant temperature between 25°C and 27°C. Intervals of 3% RH were applied between each individual measurement (fig. 3-17). Prior to each measurement, the sample was equilibrated for one and a half hours in the chamber. A typical course of the RH during an desorption/adsorption experiment is shown in fig. 3-17. The diffraction pattern was recorded between 1.5° and 30° 2theta with a step width of 0.04° and a step counting time of 9s.

Figure 3-17. Automatic control of relative humidity and temperature during a desorption and adsorption measurement in the humidity chamber.



3.5.2 Pozzolanic reaction of clay minerals II

In general, the initial composition of each prepared clay-lime-water mixture is given as amounts in grams of the raw materials. 15/70/100 refers to a clay-lime mixture with 15 g of clay mineral, 70 g of lime and 100 g of water. All other mineralogical data (e.g. initial composition or consumption, both in percent) are given as the mineral's metal oxides per ignited mass (cf. beginning of section 3.1).

Preparation of mixtures for the pozzolanic tests

Inside the glove box, CH and clays were filled in the desired proportion into the centrifuge tubes and dry-mixed in the closed tubes by shaking. Then, decarbonated water was added, the tube closed again and the final mixtures shaken. Tubes were removed from the glove box, put in an overhead agitation unit and run at ~6 rounds per minute for the desired time of several months. The influence of clay mineral to lime ratio, water to solid ratio and reaction time was investigated in various preparations. After the desired reaction time of up to seven months, solids were separated from the contact solutions by centrifugation. Supernatant solutions were decanted in the Glove Box, and further hydration in the solids was stopped by freeze-drying.

Clay mineral and calcium hydroxide consumption were determined by a combination of X-ray diffraction, thermoanalytical methods and chemical extraction.

Preparation of specimen for porosity measurements

The pozzolanic reaction is not only a cementing, strength giving process, but also a pore refinement process as termed by Mehta & Monteiro (1993). In order to show the decrease of total porosity, clay-lime specimens have been prepared and put in stainless steel containers, stored at 100% relative humidity. After freeze-drying of the specimen, the total porosity and the pore size distributions were measured with mercury intrusion porosimetry. Four clay-lime mixtures have been prepared with the following criteria: Firstly, the initial mixtures were desired to be in a pasty state in order to pour them in the specimen holders. Secondly, the four mixtures were desired to have approximately the same initial porosity. The initial porosity was calculated (assumption: added water equals pores) on the basis of literature data on minerals' densities and volumes (Table 3-4) to be close to 75%. Porosity changes are calculated as the total water porosity with the assumption of zero air void content. According to the Powers-Brownyard model, the total water porosity for a water saturated Portland cement paste is the sum of the capillary water and gel water porosities [Powers & Brownyard, 1948; Taylor, 1997]. In cement chemistry, it is estimated through the so-called evaporable water, measured by the weight loss during freeze-drying.

Table 3-4. Molar volumes calculated from the mineral densities and their molar masses

	density [g cm ⁻³]	molar mass [g mol ⁻¹]	molar volume [cm ³ mol ⁻¹]
dry Volclay	2.70	370	137
~20 Å Volclay ^a	1.84	518 ^b	282 ^c
Chinaclay	2.70	258	96
Illite MC	2.70	402	149
CH	2.24	74	33
C _x SH ₄ ^d	1.90	227	119
C ₄ AH ₁₉ (AFm) ^d	1.80	669	371
water	1.00	18	18

^a the basal distance in cementitious systems is assumed to be 20 Å; compare Lagaly (1993)

^b at 20 Å basal distance the water content is ~40% (Kraehenbuehl et al. 1987), 40% of the molar mass of Volclay gives the mass of the water, corresponding to ~8.2 moles of water in the structure

^c the volume per formula unit is calculated for a typical base plane (5.2 Å times 4.5 Å) of a monoclinic structure of montmorillonite times the basal distance of 20 Å assuming orthogonal axes; multiplied with Avogadro's constant $N_A = 6.02 \cdot 10^{23} \text{ mol}^{-1}$ leads to the molar volume

^d TAYLOR (1997)

4 Quantitative X-ray diffraction and calibration of internal standard method

Shortly after the discovery of X-rays by Wilhelm Conrad Röntgen in 1895, Hull (1919) pointed out that X-ray diffraction of powder samples would also offer the opportunity for quantitative analyses of crystalline phases in mixtures. He stated “that every crystalline substance gives a pattern; that the same substance always gives the same pattern; and that in a mixture of substances each produces its pattern independently of the others, so that the photograph obtained with a mixture is the superimposed sum of the photographs that would be obtained by exposing each of the components separately for the same length of time. This law applies quantitatively to the intensities of the lines, as well as to their positions, so that the method is capable of development as a quantitative analysis.”

4.1 Introduction to the internal standard method

Since Hull's statements, various XRD methods for quantitative mineral analysis have been developed. Problems may arise from mass absorption¹, microabsorption², particle size and preferred orientation effects. Various XRD methods for quantitative mineral analysis were developed and designed to overcome these problems [summaries in Klug & Alexander, 1974; Snyder & Bish, 1989]. External standard methods determine or calculate the mass absorption coefficient of the matrix from e.g. chemical analysis. The internal standard method is aimed at the elimination of mass absorption effects of the matrix [Snyder & Bish, 1989]. The reference intensity ratio method is a more general approach

¹ A strong X-ray absorbing phase in a matrix, which is less absorbing, results in a deeper penetration of the X-rays into the sample and a relatively higher intensity of this phase and thus an overestimation of this stronger absorbing phase [Allmann, 2003].

² “Microabsorption is an effect that causes two or more phases in a mixture to contribute diffraction intensities that are related to both their relative proportions and their mass absorption coefficients; it occurs in coarse powders; and causes the underestimation of the highly absorbing constituents;” [Bish & Reynolds, 1989].

of this method. The absorption diffraction method may be applied if analyte and matrix have identical mass absorption coefficient and the method of standard additions (also spiking method) is known from analytical chemistry.

The internal standard method is based on the addition of a known weight fraction of internal standard. The ratio of the measured diffraction line intensities I of the two crystalline phases, the standard st and the analyte a in a mixture is proportional to their weight fractions X in the mixture, the influence of matrix absorption is cancelled out:

$$\frac{I_a}{I_{st}} = K \frac{X_a}{X_{st}}, \quad (\text{Eq. 4-1})$$

with the proportionality constant K . This relation holds true irrespective of the number of other phases in a mixture. The weight fraction of an unknown can be calculated from the known addition (arbitrarily selected) of an internal standard and the measured intensity ratio of the two phases [Snyder & Bish, 1989].

Intensity information for a phase might be taken from the height or area of individual lines or a group of lines or from the whole diffracted intensity. The extraction of line height or area involves intensive manipulation of the XRD pattern as e.g. background subtraction and fitting of individual profile lines. Conventional internal standard methods all have the need of determining a calibration line in order to determine the constant K in eq. 4-1. With full-profile fitting methods, the full information of the pattern is used. A synthetic pattern is calculated and fitted by a least-square formalism to the measured pattern. The need of extracting reproducible intensity information (difficult for complex patterns) is automated and problems due to e.g. line overlap and preferred orientation are minimised [Snyder & Bish, 1989]. The synthetic pattern might be calculated from two approaches: either from crystal structure data or from a superposition of observed standard diffraction patterns [Snyder & Bish, 1989]. In the first case, the calculation of the synthetic pattern is based on the Rietveld method for crystal structure refinement [Rietveld, 1969]. The major work with the conventional Rietveld method is still the determination of both background curves and well-adjustable mathematical model profile functions for the diffraction lines [Allmann, 2003].

It was already suggested by Klug & Alexander (1974) however, that the shape of a diffraction profile may be ascribed to and calculated from some few physical values without

the use of physically meaningless profile model functions. These physical values or so-called fundamental parameters are the intensity distribution of the X-ray tube, the device-dependent values (geometry and size of the diffractometer's units) and the phase-specific values as absorption, crystal structure, mean crystallite size and crystallite microstrain [Allmann, 2003]. Analytical models for the description of these phase-specific values are well-established. Besides the numerical stability of this approach, advantages are e.g. the possibility of refining device-dependent values and the intrinsic description of asymmetric line profiles. This approach combined with the internal-standard method eliminates the influence of the X-ray tube and device-dependent contributions. The remaining intensities are then only attributable to refineable crystal properties (crystal structure, size and strain). For perfect crystals described by well-characterised structure models, determination of a calibration line according to eq. 4-1 may be principally neglected. Exceptions are due to inadequate description of real crystals¹ and the lack of real structure models. The use of fast detector systems and of stable refinement codes based on this fundamental parameter approach offers today the possibility of fast automatic routine quantitative mineral analysis.

4.2 Determination of portlandite content

4.2.1 Internal standard

In general, an internal standard should be of high purity, of a suitable crystallinity to give sharp diffraction lines and of a grain morphology not very susceptible to preferred orientation. Analyte and standard should have similar mass absorption coefficients in order to minimise microabsorption effects. The internal standard's diffraction lines have to be strong and near the strong lines of the analyte and have to show no superposition with lines of the analyte [Klug & Alexander, 1974].

In this study, three minerals were tested as internal standard for portlandite quantification, a calcite (Fluka), a rhodochrosite (CERAC) and a microcrystalline diamond (Rudolf Spring AG). The reddish-brown rhodochrosite and the black diamond powders addition-

¹ "The intensity of X-ray radiation diffracted by typical powder samples is traditionally interpreted using the theory of X-ray diffraction for *ideally imperfect* crystals that have numerous lattice imperfections and small mosaic blocks (as opposed to *ideally perfect* crystals). However in some cases the intensities measured from *real* crystals are measurably less than would be predicted for ideally imperfect crystals. This effect is described by the term extinction;" [Bish & Reynolds, 1989].

ally showed the advantage that the mixing progress of the internal standard could be controlled through visual inspection. However, it was observed that the rhodochrosite powder showed microabsorption effects. This was evidenced from the dependency of the quantification results on the applied parameter for microabsorption (Brindley correction in the Rietveld program BGMN®). The artificial diamond powder was also not appropriate, as the line profiles could not be fitted sufficiently well with available structure models, probably due to the presence of stacking faults and inadequate description of the atomic displacement factors in some of the structures in the ICSD [Gao & Peng, 1999].

It was then decided to use the calcite powder although it showed preferred orientation effects. A second disadvantage is that quantification with calcite as the internal standard could possibly interfere with calcite already present in the (cementitious) mixtures. It was necessary to verify by TG-EGA for each sample that its calcite content was negligible.

4.2.2 Calibration line for portlandite quantification

All the calculations were performed with the windows version of BGMN® (BGMNwin level 1.6.1 [Bergman et al., 1998]). A number of refinements were run on measurements of samples of known composition in order to test for the sensitivity of the quantification result on parameter and variable selection. Portlandite (CH) and calcite and diluents were mixed in different proportions and then measured, fractions are given always in per cent by weight. As only portlandite and calcite were fitted to the measured pattern, the sum of the two fractions always equalled 100%. Calibration was performed as if the weight fraction of CH was not known. The weight fraction of CH in the sample with added standard ($w_{\text{unknown,CH}}$) is calculated from the known fraction of internal standard in the sample ($w_{\text{target,st}}$) and the fitted weight fractions of CH ($w_{\text{fitted,CH}}$) and internal standard ($w_{\text{fitted,st}}$):

$$\frac{w_{\text{unknown,CH}}}{w_{\text{target,st}}} = \frac{w_{\text{fitted,CH}}}{w_{\text{fitted,st}}} \Leftrightarrow w_{\text{unknown,CH}} = w_{\text{fitted,CH}} \frac{w_{\text{target,st}}}{w_{\text{fitted,st}}} \quad (\text{Eq. 4-2})$$

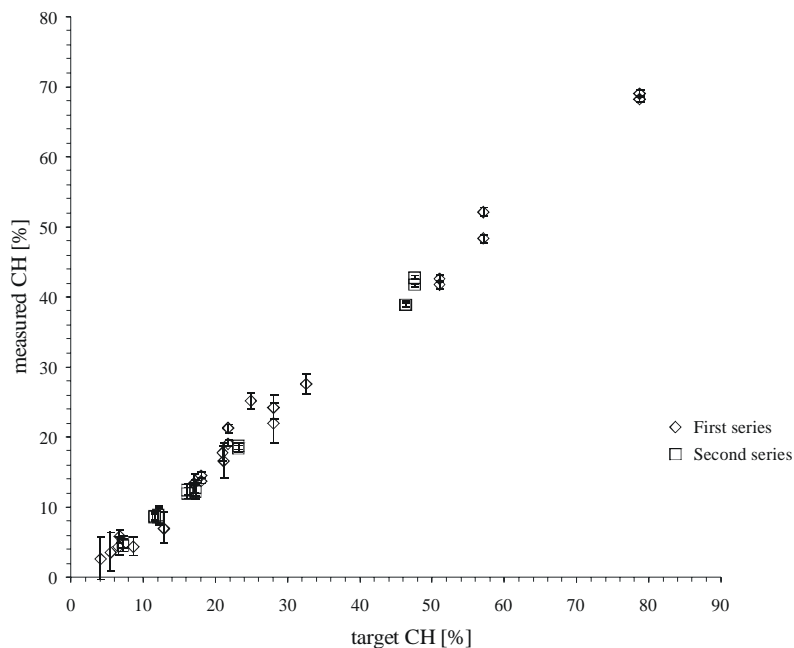
and was then tested against the known added portlandite contents.

Although preferred orientation is typical for calcite and was evidenced in this study also, quantification results did not change significantly when using different spherical harmonics up to the 6th order to correct for preferred orientation. The effect on quantification of portlandite by using different profile functions (lorentzian and/or squared lorentzian), or different orders of the background model, or different grain sizes for the Brindley micro-

absorption correction was negligible. The variable for the description of strain was not used as it also showed no significant improvement in describing the profiles. The desired 1:1 relationship between the added and measured portlandite contents was not reached. Portlandite content was systematically underestimated by about 5 - 15%.

A number of more complex structure models was run in order to improve the quantification result. Two portlandites were fitted and refined independently but the quantification result showed no substantial improvement. Other structure models used were two-sub-phase models with different crystallinity or with slightly different cell dimensions for each subphase and also a triclinic portlandite structure (cf. section 4.5). The best results with respect to a desired 1:1 relationship were obtained for a structure model with two independent crystallite sizes (the slope of the calibration line increased to 0.95). However one crystallite size always showed very high values ($> 1 \mu\text{m}$) which seemed not realistic. Sometimes, unexplained effects occurred, which resulted in an overestimation of portlandite content. The model was therefore disregarded.

Figure 4-1. Calibration line for the measured portlandite content versus the actual content; error bars correspond to the $1\text{-}\sigma$ estimated standard deviation, as calculated by the program BGMN.



Matching the desired 1:1 relationship was not achieved. Therefore the calibration line parameters had to be determined. The linear relationship between known target and measured CH contents is shown in fig. 4-1 (slope of 0.91 and y-axis intercept of -1.5%). It was determined on various samples, which were diluted with a third phase (clays or C-S-H).

Refinement of a portlandite structure model (ICSD 15471) against a calcite structure model (ICSD 100676) yielded the values that were recalculated according to eq. 4-2. The calibration line contains two series of samples. The first one was determined in a nitrogen filled chamber. Counting statistics were unfavourable because of the low intensity emitted by the X-ray tube, which was at the end of its lifetime. However, the second series (cf. Table 4-1) was recorded with much improved counting statistics (average of at least 1000 to 2000 counts per second) and did not show significant variation of the previously determined points. So reproducible quantification results are also obtainable for fast scans with low intensity [cf. Hill & Madsen, 1987].

Table 4-1. Second series of mixtures prepared for the calibration of portlandite quantification with XRD

CH to calcite ratio	CH [mg]	calcite [mg]	diluent Volclay [mg]
~0.4	185.5	484.9	1880.0
	290.0	783.4	1364.2
~0.8	397.3	526.6	1491.0
	500.7	615.3	998.2
~1.5	1012.7	675.9	400.5
	302.5	239.2	1931.5
~2.0	1025.8	525.5	616.0
	422.6	198.9	1792.5

4.2.3 Calculation of results in the reacted samples

In reacted samples, results for the portlandite content in the mixture with standard (w_{CH}) were corrected with the calibration line parameters ($w_{\text{unknown,CH}}$ from eq. 4-2):

$$w_{\text{CH}} = (w_{\text{unknown,CH}} + 1.5)/0.91 \quad (\text{Eq. 4-3})$$

Because the original mixture is diluted by the internal standard addition, the final result, the measured portlandite content $w_{\text{CH,final}}$ is calculated as follows:

$$w_{\text{CH,final}} = w_{\text{CH}} \frac{100}{(100 - w_{\text{target,st}})} \quad (\text{Eq. 4-4})$$

In order to express the portlandite content as percent CaO per ignited mass w_{CaO} , the $w_{\text{CH,final}}$ were recalculated with the LOI and the molar mass ratio of CaO M_{CaO} and $\text{Ca}(\text{OH})_2$ M_{CH} :

$$w_{\text{CaO}} = w_{\text{CH,final}} \frac{100}{(100 - \text{LOI})} \frac{M_{\text{CaO}}}{M_{\text{CH}}} = 0.757 w_{\text{CH,final}} \frac{100}{(100 - \text{LOI})} \quad (\text{Eq. 4-5})$$

4.2.4 Summary

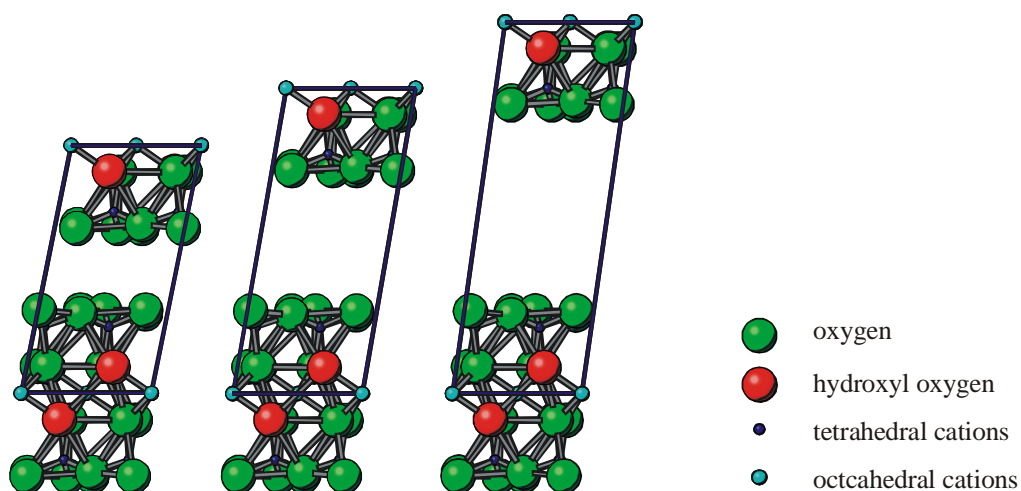
- In this study, the effect of using different degrees of preferred orientation, background polynomial order, various types of line profile functions was not very pronounced. It is indicated that the deviation from a desired 1:1 calibration line is a result of an inadequate description of the real structures of the minerals.
- The internal standard should be very well characterised in terms of imperfections. In this study, constraints have been put on the crystallite size of the internal standard (160 - 200 nm). This prevents the determination of unrealistic crystallite sizes and line broadening in complicated samples (e.g. superposition of the strongest line of calcite onto high amorphous background or broad lines of montmorillonite or C-S-H).

In order to use the internal standard method together with the fundamental parameter approach without calibration, much more work on the real structures of minerals is necessary. Real structure models should only contain as few additional parameters as possible.

4.3 Flexible structure models

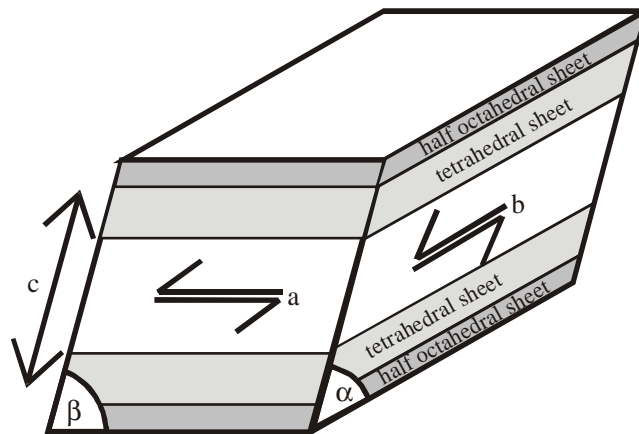
Development of a suitable model for the real structures of layered crystal structures (clay minerals and portlandite e.g.) was essential. In particular, it should be flexible in the sense that adjacent layers may be translated in any direction parallel to the layers without changing the geometrical arrangement of atoms inside the individual layers (atomic distances and angles between atoms must stay the same). Additionally, the ability of expanding interlayer space without changing the geometrical arrangement inside the solid layer (fig. 4-2) was of significant interest given prospective advantages.

Figure 4-2. The original montmorillonite structure of Tsipursky & Drits (1984) and the expanded ones in bc projection, with basal distances of 9.85 Å (left), 12.4 Å (middle) and 15.2 Å (right).



A first approach was performed in two dimensions by allowing for a variation of unit cell parameters c and β and thus translation of mineral layers in direction of crystallographic axis \mathbf{a} and/or expansion of interlayer space. This was deduced trigonometrically and applied to the expansion of a montmorillonite structure by Tzipursky & Drits (1984). Such expanded structures (fig. 4-2) were successfully used for Rietveld refinement [Müller et al., 2002] and for the simulation of cations and water molecules inside the interlayer space [Müller et al., 2004a,b]. It was then decided to allow also for a translation of mineral layers in direction of axis \mathbf{b} through variation of the angle α (fig. 4-3). This extended approach is based on coordinate system transformation from the triclinic coordinate system to the cartesian system and back again to another triclinic system, without changing the location of the origin. As cartesian atomic coordinates are held fixed, the interatomic distances and angles stay constant. However, by changing the triclinic system, atomic environments across the interlayer space will change.

Figure 4-3. Schematic representation of a flexible structure model for a triclinic 2:1 layer clay mineral. In this example, the unit cell is defined (as commonly) such as the lower and upper half part of an individual solid layer may slide over each other with the interlayer as the sliding plane.



A schematic unit cell with oblique axes in a triclinic crystallographic system is shown in fig. 4-3. The coordinates in such a system can be transformed to orthogonal cartesian coordinates in several ways depending on the chosen orientation of the oblique system with respect to the cartesian one [e.g. Cowtan, 2005]. Triclinic fractional coordinates \mathbf{x} :

$$\mathbf{x} = \begin{bmatrix} x \\ y \\ z \end{bmatrix} \quad (\text{Eq. 4-6})$$

and cartesian coordinates \mathbf{X} :

$$\mathbf{X} = \begin{bmatrix} X \\ Y \\ Z \end{bmatrix} \quad (\text{Eq. 4-7})$$

are generally transformed back and forth with the following notation:

$$\mathbf{X} = \mathbf{M}^{-1} \mathbf{x} \quad (\text{Eq. 4-8})$$

and

$$\mathbf{x} = \mathbf{M} \mathbf{X} \quad (\text{Eq. 4-9})$$

where \mathbf{M} is the deorthogonalisation matrix and its inverse \mathbf{M}^{-1} the orthogonalisation matrix. With the two coordinate systems having the same origin, the orthogonalisation matrix is:

$$\mathbf{M}^{-1} = \begin{bmatrix} a \cos \gamma & c \cos \beta \\ 0 & \frac{c(\cos \alpha - \cos \beta \cos \gamma)}{\sin \gamma} \\ 0 & 0 & \frac{V}{ab \sin \gamma} \end{bmatrix} \quad (\text{Eq. 4-10})$$

and the deorthogonalisation matrix is:

$$\mathbf{M} = \begin{bmatrix} \frac{1}{a} - \frac{1 \cos \gamma}{a \sin \gamma} \left(\frac{bc \cos \gamma (\cos \alpha - \cos \beta \cos \gamma)}{\sin \gamma} - bc \cos \beta \sin \gamma \right) \frac{1}{V} \\ 0 & \frac{1}{b \sin \gamma} & -\frac{ac(\cos \alpha - \cos \beta \cos \gamma)}{V \sin \gamma} \\ 0 & 0 & \frac{ab \sin \gamma}{V} \end{bmatrix} \quad (\text{Eq. 4-11})$$

with V the volume of the unit cell:

$$V = abc \sqrt{1 - \cos^2 \alpha - \cos^2 \beta - \cos^2 \gamma + 2 \cos \alpha \cos \beta \cos \gamma} \quad (\text{Eq. 4-12})$$

These formulas hold for the following conventions:

- cartesian axis \mathbf{A} is collinear with crystallographic axis \mathbf{a} ,
- cartesian axis \mathbf{B} is collinear with $(\mathbf{a} \times \mathbf{b}) \times \mathbf{A}$,
- cartesian axis \mathbf{C} is collinear with $(\mathbf{a} \times \mathbf{b})$.

With these equations, via back and forth transformation, formulas were obtained for the recalculation of crystal coordinates dependent upon the changing cell parameters during the refinement process. For the new triclinic coordinates \mathbf{x} , a shift is calculated as a function of the initial triclinic coordinates \mathbf{x}_i , the initial cell parameters $a_i, b_i, c_i, \alpha_i, \beta_i, \gamma_i$ and the new cell parameters¹ c, α, β . The resulting formulas are shown below (eq. 4-13 to eq. 4-19):

$$x = x_i + z_i x_{shift} \quad (\text{Eq. 4-13})$$

$$y = y_i + z_i y_{shift} \quad (\text{Eq. 4-14})$$

$$z = z_i z_{shift} \quad (\text{Eq. 4-15})$$

with

$$x_{shift} = \frac{c_i}{a_i f \sin^2 \gamma_i} (f_i \cos \alpha \cos \gamma_i - f_i \cos \beta + f \cos \beta_i - f \cos \alpha_i \cos \gamma_i) \quad (\text{Eq. 4-16})$$

$$y_{shift} = \frac{c_i}{b_i f \sin^2 \gamma_i} (f_i \cos \beta \cos \gamma_i - f_i \cos \alpha + f \cos \alpha_i - f \cos \beta_i \cos \gamma_i) \quad (\text{Eq. 4-17})$$

$$z_{shift} = \frac{c_i f_i}{c f} \quad (\text{Eq. 4-18})$$

with

$$f = \frac{V}{abc} \quad (\text{Eq. 4-19})$$

The x_{shift} and y_{shift} are independent of the new cell dimensions, however they depend on the new cell angles.

The principle and some results of including these equations in the Rietveld refinement process will be demonstrated in the following sections.

¹ New triclinic coordinates were not calculated for changing a, b, γ as these are the parameters defining the geometry inside the solid layer and this was not intended to be changed.

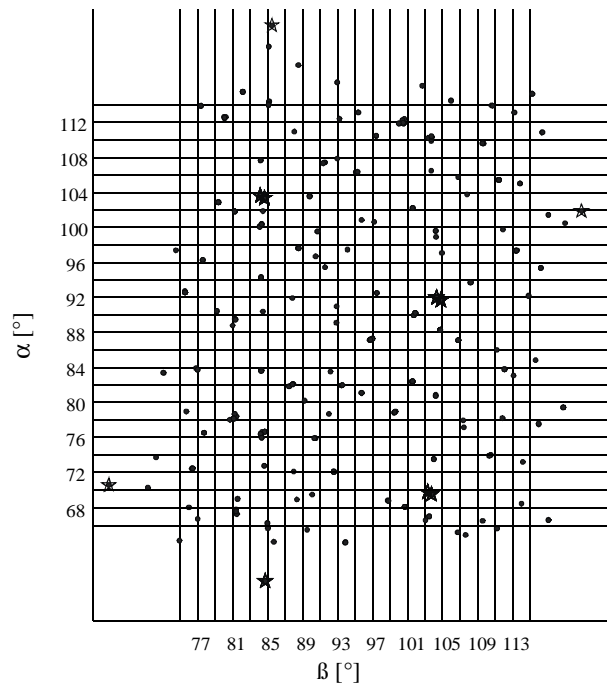
4.4 Flexible structure model of triclinic kaolinite

The kaolinite structure model refined by Bish & Von Dreele in 1989 (ICSD 063192) was used in this study. The flexible structure approach was implemented into this model. For the resulting flexible structure, all combinations of starting values for the crystallographic angles α and β from 66° to 114° and 75° to 115° (in 2° steps) were introduced into the structure file and refined on the kaolin China Clay. Starting value for the cell dimension c were adjusted in order to match the basal spacing $d(001)$ of the original structure. This was done with the following equation derived from eq. 4-18 with $z_{shift} = 1$:

$$c = \frac{c f_i}{f} \quad (\text{Eq. 4-20})$$

Fig. 4-4 shows the starting values for α and β at the grid points, the refined angles are shown as dots, whereas the stars indicate the refined angles of the best fits judged by the R_{wp} values (< 0.7 of the mean R_{wp}). For an explanation of numerical criteria used to judge a Rietveld refinement see e.g. Hill & Madsen (1987) or Young (1993).

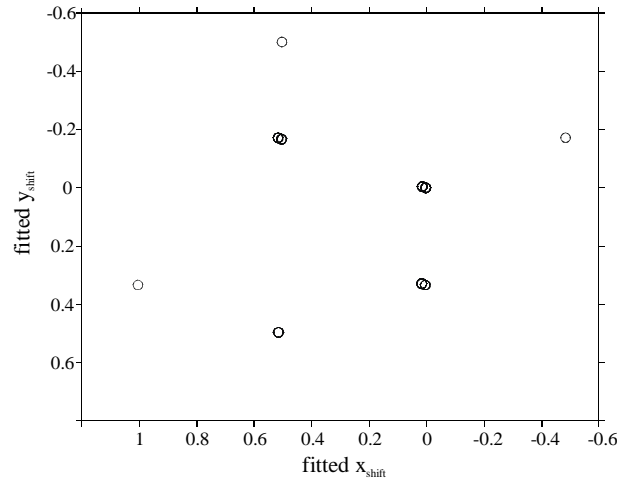
Figure 4-4. Starting crystallographic angles α and β and fitted ones (dots), the stars indicate the fits with the best R_{wp} values < 0.7 of the mean R_{wp}



If only these best fits are plotted as their associated shifts in crystallographic **a** and **b** direction, one observes only the following shifts (fig. 4-5): $(0,0)$, $(0,1/3)$, $(1/2,1/2)$, $(1/2,-1/6)$.

These shifts can be further reduced by applying the centering vector $(1/2, 1/2)$ of the original structure in spacegroup C1. Only the shift with $+b/3$ remains. Because $-b/3$ is also a very common stacking fault in kaolinites, the unit cells and associated diffraction patterns corresponding to crystals with only perfect $\pm b/3$ shifts have been calculated.

Figure 4-5. Shifts in the crystallographic **a** and **b** direction calculated from the fitted unit cell parameters.

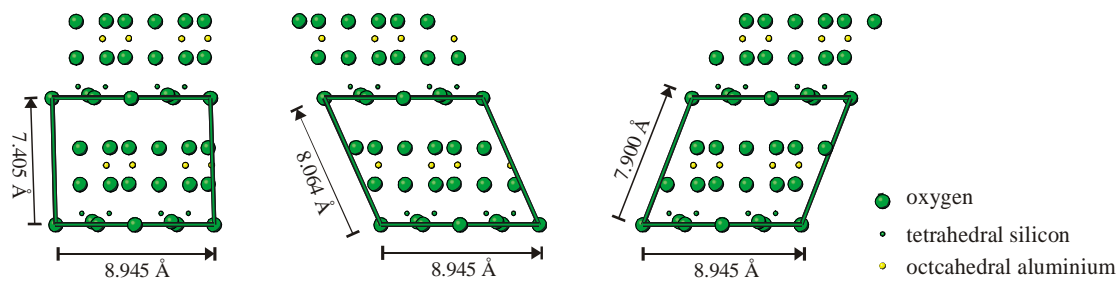


The associated cell parameters were calculated with eq. 4-16 to eq. 4-19 and $x_{shift} = 0$, $y_{shift} = \pm 1/3$ and $z_{shift} = 1$ and are shown in Table 4-2. Projections onto the **ac** plane of the original structure and the two translationally disordered structures are shown in fig. 4-6 (note the geometrically undisturbed environment of the atoms). Simulated diffraction patterns of the three kaolinite structures for Bragg-Brentano geometry and a variable slit [Kraus & Nolze, 2000] are shown in Appendix II.

Table 4-2. Unit cell parameters for the original kaolinite structure and the $-b/3$ and $+b/3$ translationally disordered ones.

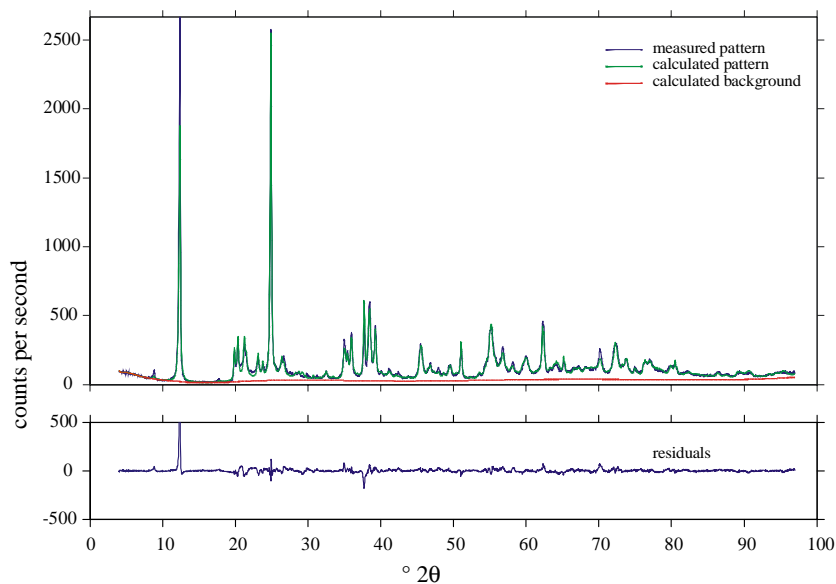
Interlayer shift	(0,0)	(0,-1/3)	(0,+1/3)
a [Å]	5.155	5.155	5.155
b [Å]	8.945	8.945	8.945
c [Å]	7.405	8.064	7.900
α [°]	91.7	113.4	69.5
β [°]	104.9	103.7	103.9
γ [°]	89.8	89.8	89.8

Figure 4-6. The original kaolinite structure in bc projection and the $-b/3$ and $+b/3$ translationally disordered ones.



One observes clear differences in the 3 diffraction patterns, the clearest ones for the $-b/3$ kaolinite. The basal spacing is constant as evidenced by the 001 line. The absolute intensity of this line is also constant, whereas the intensity distribution but also the position of the other lines is modified. It has to be emphasised here, that these flexible structure models correspond to ideal structures with $\pm b/3$ shifts. In order to simulate stacking faults with such shifts, a passable approach could be the formulation of a combined model which contains the three crystal structures as sub-phases. The Rietveld refinement plot where these three crystal structure were fitted independently (just a superposition of patterns) is shown in fig. 4-7. The fit looks almost perfect except for the 001 line, which is more intense than the 002 line (the reason for this is not known). The R_{wp} value of this fit is substantially improved ($R_{wp} = 13.6\%$) compared to the one with only the original model ($R_{wp} = 18.0\%$). Total refined kaolinite content was 94% with about an equal contribution of the original kaolinite structure (47%) and the $+b/3$ structure (44%) and only 3% of the $-b/3$ structure.

Figure 4-7. Rietveld refinement plot of the raw China Clay.



4.5 Flexible structure model of triclinic portlandite

The same approach as for the original triclinic kaolinite was used for portlandite. The structure of portlandite was refined in the hexagonal spacegroup $P\bar{3}m1$ [e.g. Petch, 1961]. This structure was transformed from initial spacegroup over spacegroup $C2/m$ into $P\bar{1}$ to the final spacegroup $P1$ and the formulas implemented as derived in the previous section. Again various combinations of starting values for the crystallographic angles α and β were refined. The best fits corresponded always to a full ($x_{shift} = 1$ and/or $y_{shift} = 1$) translational shift, as was expected.

Fig. 4-8 compares the Rietveld refinement plots of flexible structure models for a portlandite with isotropic crystallite size, with anisotropic crystallite size and of the hexagonal structure (judge by the difference patterns of each refinement plot). It is indicated from these refinements that the formulation of a flexible structure model may improve the fitting of individual lines (e.g. the fitting of the 001 line in the upper plot). But it has to be emphasised again that further improvements may be possible by formulating sub-phase models from these flexible models.

Additionally, there are some findings that the refined small deviations of the crystallographic angles α , β and γ from their ideal value of 90° have some physical meaning. Chaix-Pluchery et al. (1987) stated from the analysis of the powder diffraction line broadening of single crystals at room temperature, that “strong lattice distortions take place in the stacking of the hexagonal layers or, more precisely, that there is a distribution of d_{001} spacings” and also a slight rotation of individual mosaic blocks around the c -axis. The flexible structure model might be an adequate average structure model of reduced symmetry to mimic crystal imperfections (e.g. contributions from stacking faults, subphases with slightly differing cell dimensions). Stanjek & Schneider (2000) used a similar approach in order to analyse anisotropic line broadening in an ideally cubic mineral.

Figure 4-8. Three different structure models refined on the same profile. top: triclinic portlandite with isotropic crystallite size ($R_{wp} = 24.8\%$); middle: triclinic portlandite with anisotropic crystallite size ($R_{wp} = 22.7\%$); bottom: hexagonal portlandite with anisotropic crystallite size ($R_{wp} = 23.2\%$).

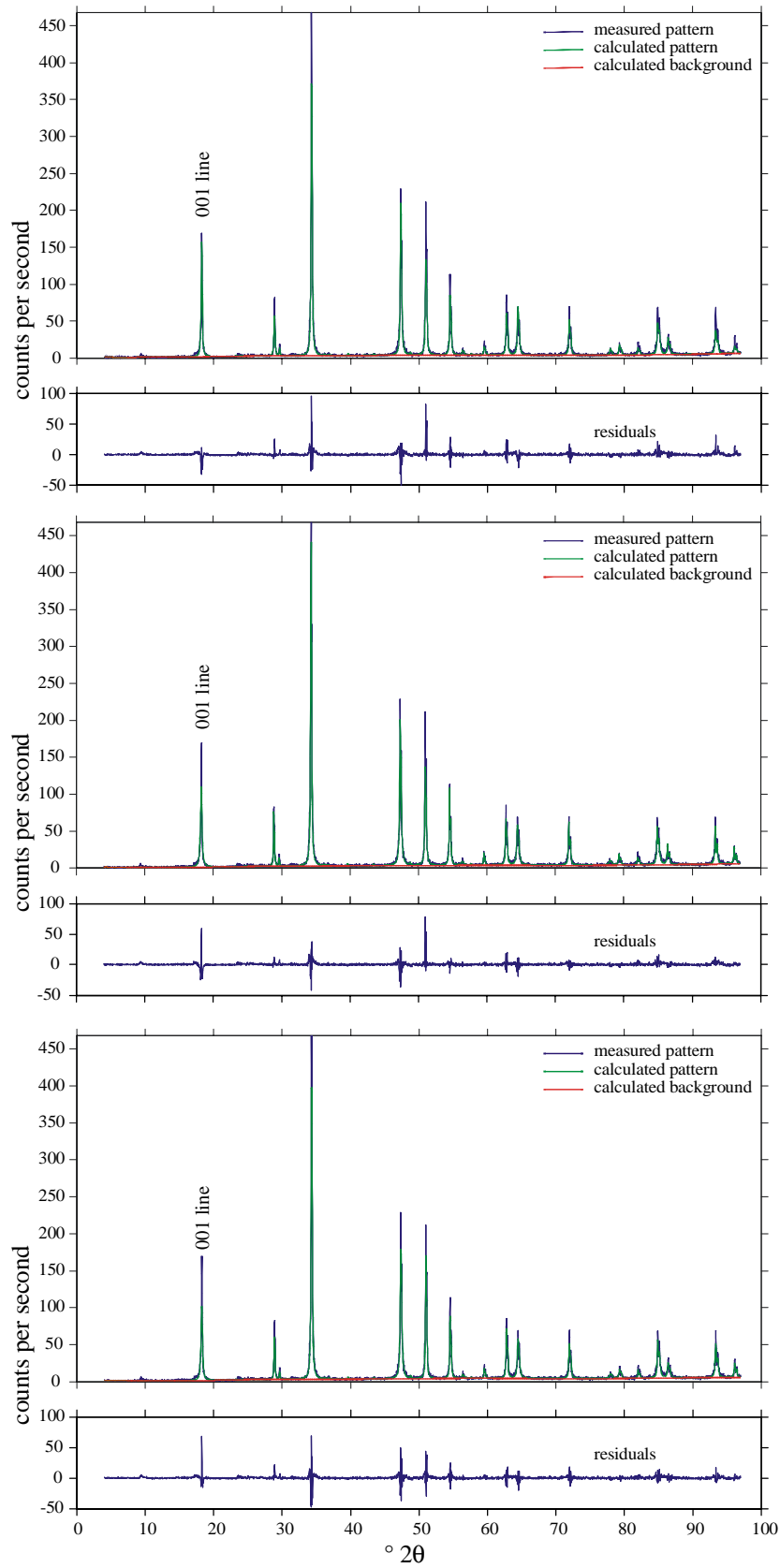
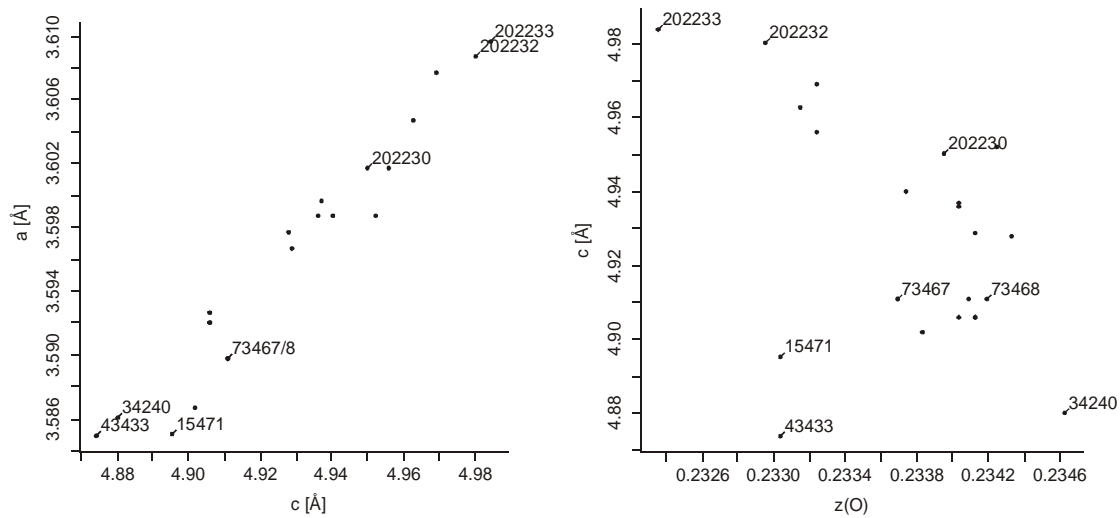


Figure 4-9. Portlandites from the ICSD (some numbers identified at the data points); left: cell dimensions a versus c ; right: cell dimension c as a function of z coordinate of oxygen atom.



The number of refineable parameters increases significantly when transferring a structure model from the hexagonal system to the triclinic system. Calculation time may then increase to impracticable values for routine quantification analysis. However, it is known from the literature [e.g. Chaix-Pluchery et al., 1987; ICSD, 2001] that cell parameters of the portlandite structure are strongly correlated as is shown in fig. 4-9. Table 4-3 summarises the linear regression relationships obtained for these data sets and additionally the ones obtained by plotting the displacement factors TDS of the calcium and oxygen atoms versus the cell dimension c . Implementing such relationships as constraints in a flexible model of low symmetry strongly reduces the number of refineable parameters, thereby decreasing calculation effort again.

Table 4-3. Linear relationships obtained by analysing crystal structure data of the portlandites in the ICSD

parameter (as function of)	linear equation	R^2
$c(a)$ [nm]	$c = 3.9288a - 0.9197$	0.9373
$z(c)$ [nm]	$z = -0.1465c + 0.306$	0.5971
TDS ^a (c) [nm ²]	TDS(Ca) = $1.3494c - 0.654$	0.7035
	TDS(O) = $1.3023c - 0.631$	0.7291

^aisotropic thermal displacement factor of the atoms

4.6 Flexible structure models applied to swelling montmorillonite

The swelling measurements in this study were conducted in a relative humidity range, where the mineral is known to consist of interstratified layers of one- and two-layer hydrates. There is no experimental evidence for intermediate basal spacings between the one- and two-layer hydrate, i.e. there is supposed to be no such thing as a one and half layer hydrate. Measured intermediate basal spacings are a result of interstratified¹ layers of different hydration states [Brindley & Brown, 1980; Moore & Reynolds, 1997] which gives rise to a non-rational series of basal reflections (the 00l lines occur as a non-integral series). X-ray diffractograms of such interstratified samples may be modelled using statistical approaches used e.g. in Newmod [Reynolds & Reynolds, 2005]. Such models then give the percentage of interstratified layers for each type and the degree of order.

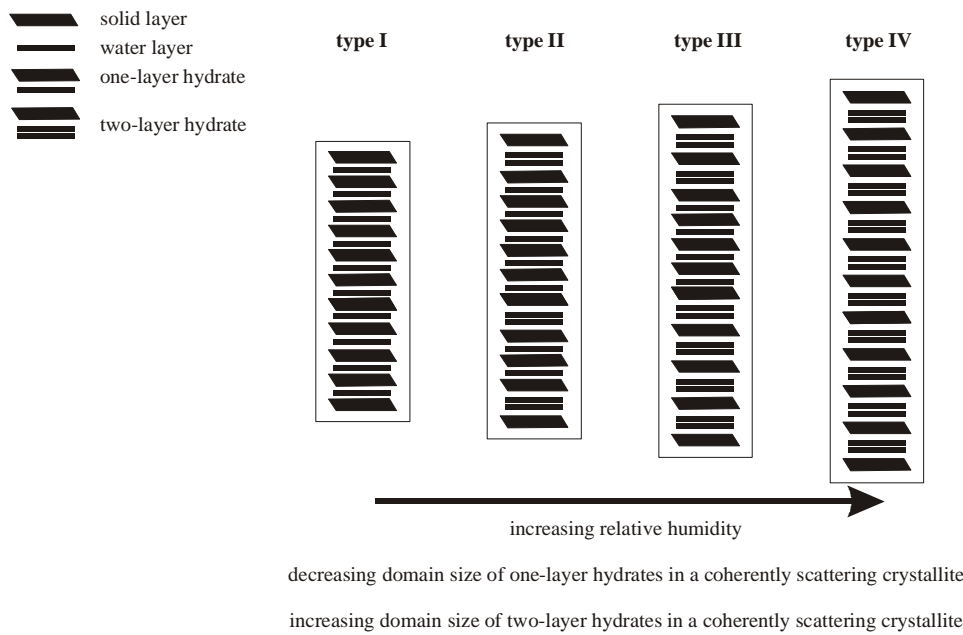
Uncertainties and errors of measuring d-spacings by the line position maximum may become very large when measuring in the low 2 θ region, i.e. line maximum and line position do not coincide any more [Allmann, 2003]. Line decomposition provides a better measure of peak position, width and intensity than manual stripping or “eye-ball” methods. The accuracy/precision of d-values in this region is also influenced by the flatness of the specimen, by a zero shift of the X-ray tube, by sample height position and penetration depth of the X-rays into the sample. All four factors may be changing through the course of such swelling measurements as the mineral volume and thus the packing density and/or sample height increase. Such changing conditions are taken into account using a fundamental parameter approach where the three factors can be refined. For the use of this approach, one needs crystal structure models describing the intensity distribution and line positions of the profiles.

A new approach was undertaken in this study, using fundamental parameters together with two incomplete structure models for montmorillonite [Müller & Plötze, 2005]. The crystal structure data were taken from the intermediate montmorillonite model of Tsipursky & Drits (1984), which was transformed to spacegroup C1. Interlayer contents were left empty. This is justifiable as Allmann (2003) states that a starting model for Rietveld

¹ The terms interlayering, mixed-layer and interstratification all describe phyllosilicate structures in which two or more layer types are stacked vertically to the layer planes.

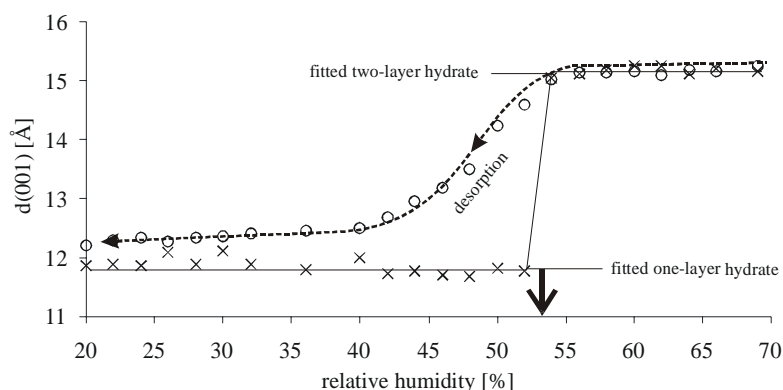
refinement must be correct, but may be incomplete in terms of missing atoms. These incomplete structure models were set up as flexible models. Only the cell parameters c , α and β were refined, cell dimensions of the solid layer were kept constant (a , b and γ), i.e. the models were freely expandable in terms of the basal spacing without changing the geometry inside the solid layer. Also refined in the 2θ range of 4° to 30° were zero shift, sample height, penetration depth, anisotropic crystallite size and a background polynomial of the 5th degree, ending up with a small set of refineable parameters.

Figure 4-10. Schematic picture of the average development of an interstratified sample of one- and two-layer hydrates of montmorillonite with increasing humidity



There is another basic assumption of this approach, besides that of using incomplete structure models. This is the perception that a montmorillonite powder at a given relative humidity consists of different types of crystallites (Fig. 4-10). There may be purely one-layer hydrated crystallites (type I) coexisting with interstratified ones (type II and III) coexisting with purely two-layer hydrated ones (type IV). This is justified as it is known that montmorillonites are heterogeneous in terms of e.g. their charge density and crystallite size, both of which influence the swelling state. So either one of the two models is assumed to represent either a discrete crystallite of a one- or a two-layer hydrate. The remaining model is used as an, admittedly primitive, place holder of an interstratified layer structure (type II and III).

Figure 4-11. Basal spacing with relative humidity of the pristine Volclay material in desorption; open circles: desorption measurements of an at 75 % RH pre-equilibrated sample, crosses: basal spacing of either one of the flexible structure models supposed to represent discrete one- or two-layer hydrate crystallites; the arrow indicates the extracted transition point discussed in the text.



The goal of this new procedure was to define the transition point on the relative humidity scale, where the main fraction of crystallites is either composed of one-layer hydrate or two-layer hydrate. Fig. 4-11 shows an example of a swelling curve measured in desorption (more a shrinkage curve) on the pristine Volclay material. The two horizontal lines at $\sim 12 \text{ \AA}$ and $\sim 15 \text{ \AA}$ are the fitted basal spacings of one of the two structure models. The jump from the one- to the two-layer hydrate is clearly indicated at $\sim 53\%$ relative humidity (RH). Figures 4-12 and 4-13 provide examples of some results of this refinement procedure on a sample of almost pure sodium montmorillonite ($< 2 \mu\text{m}$) from the cation exchange experiment. Fig. 4-12 shows the development of the basal spacings of the two structure models but also the development of their fractions with relative humidity. Remarkable effects include the constant fraction of quartz ($\sim 5\%$) and the smooth change in the fractions of the two montmorillonite models. It is also indicated that the transition point in terms of the basal spacing ($\sim 50\%$ RH) does not coincide with the one from the associated fractions ($\sim 60\%$ RH). The development of fitted basal spacings was more smooth in all the measured samples compared to the development of the fractions. Therefore, fitted basal spacing was used as the indicator of the transition, as it allowed easier visual determination.

Figure 4-12. Top: Basal spacing of the two flexible structure models with relative humidity; bottom: Fractions of quartz (crosses) and of the two flexible structure models with relative humidity.

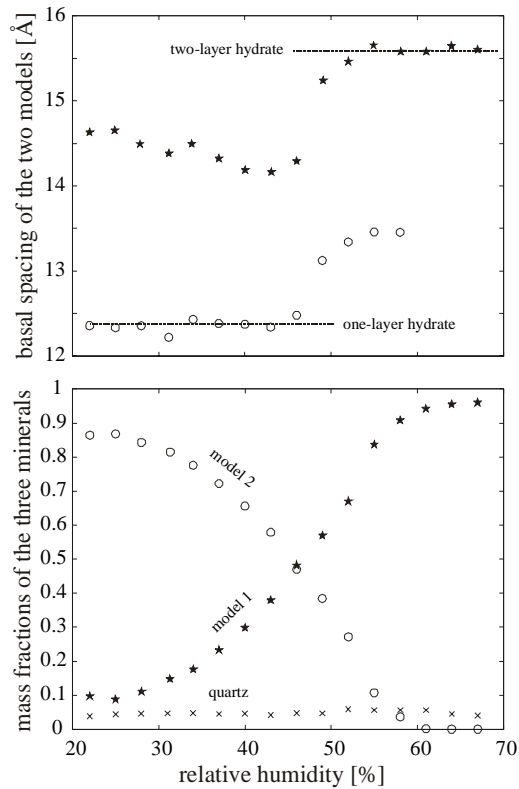
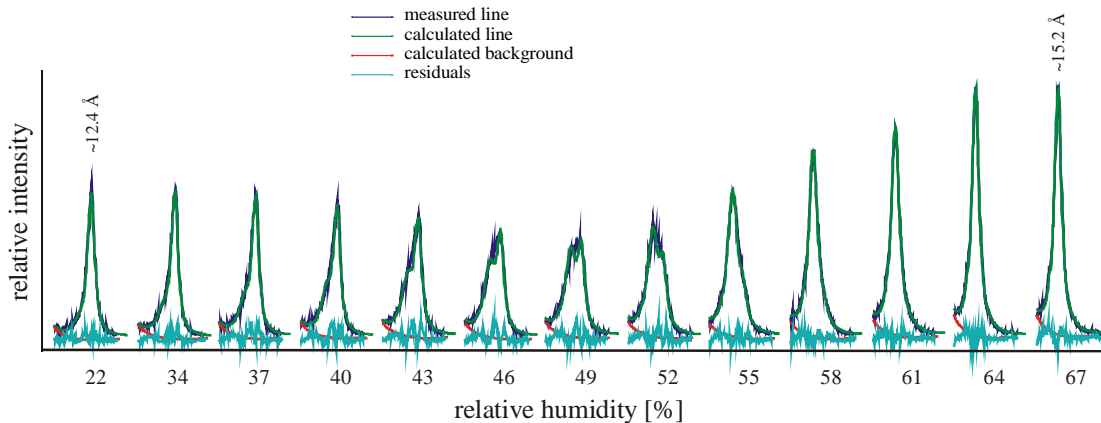


Fig. 4-13 shows the development of fitted 001 line profiles of the sample in fig. 4-12. It is clearly indicated how the profile shape becomes asymmetric and symmetric again during the additional inclusion of a water layer between the mineral's layers. With increasing RH, the line profile at ~ 12.4 Å develops an additional component at its left-hand side (> 12.4 Å). This component starts to grow, until it is the main component at $\sim 58\%$ RH. The profile becomes more and more symmetric with a maximum at ~ 15.4 Å.

Figure 4-13. Development of the basal spacing of a sodium montmorillonite with relative humidity; measured data in dark blue, baseline in red, fitted data in green and the residuals in light blue.



4.6.1 Summary

Flexible structure models combined with the fundamental parameter approach may be successfully applied for the description of one-dimensional swelling effects in minerals. The first results look promising, but further systematic work has to be done in order to justify this approach (e.g. reproducibility, comparison with other methods, significance of the results obtained).

For the purpose of quantification, the use of such models should be the object of further research. Flexible structure models might be an appropriate and simple approximation of imperfections in crystals. The inclusion of flexible structure models into sub-phase models is expected to improve obtainable quantitative results substantially. The use of crystallographic constraints might improve the unambiguousness of refinement results [Baerlocher, 1993] and also minimise computational effort.

5 Pozzolanic reaction of clay minerals I: cation exchange, swelling and rheology

5.1 Results and discussion

5.1.1 Cation exchange

Direct determination of cation exchange state

Appendix III shows the sodium and calcium concentrations after 4 days inside and outside the dialysis membrane. The mean of the concentrations inside and outside has in most cases a standard error of below 10%, therefore the diffusion process was regarded as completed. A pH of 12.7 ± 0.2 during the experiment was calculated from ion charge balance. Calcium concentrations tend to rise with increasing ionic strength (Appendix III) due to the diverse ion effect. Addition of sodium (NaClO_4) leads to an increased CH solubility [Duchesne & Reardon, 1995].

Figure 5-1. Double logarithmic plot of the sodium isotherm at constant calcium concentration but variable ionic strength.

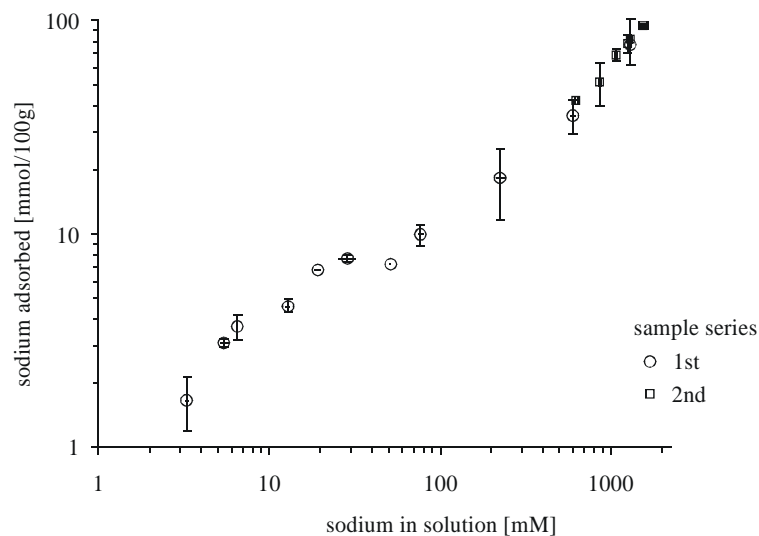


Fig. 5-1 shows, for two independent series, the measured concentrations of sodium in solution versus those on the ion exchanger in a double-logarithmic isotherm plot, both with their standard errors. The isotherm is plotted according to the work of Vulava (1998), who showed the equivalence of plotting cation exchange isotherms with the bound and solution concentrations expressed as (i) ratios or (ii) absolute concentrations. A slope of less than one for such a sodium exchange isotherm was also observed by Vulava. The kink and plateau at an amount of adsorbed sodium of ~ 8 mmol/100g (fig. 5-1) might be a result of different sites for adsorption (edge and interlayer sites), as this is exactly the same number of edge sites determined by Tournassat et al. (2004b) after modelling their titration data on montmorillonite (MX80). It is also indicated from the isotherm that very high sodium concentrations of > 1000 mM are needed in order to stabilise a sodium bentonite. This is partly due to the high solubility of CH, but also due to the aqueous speciation of calcium at a pH of 12.7. More than 40% of the total dissolved calcium exists as the complex CaOH^+ at this pH (fig. 2-2). This complex was proposed to have a much higher selectivity against Na^+ than does Ca^{2+} [Tournassat et al., 2004b], comparable to CaCl^+ , which was investigated by Sposito et al. (1983a, b).

Figure 5-2. Correlation between sorbed sodium and calcium amounts on the bentonite samples.

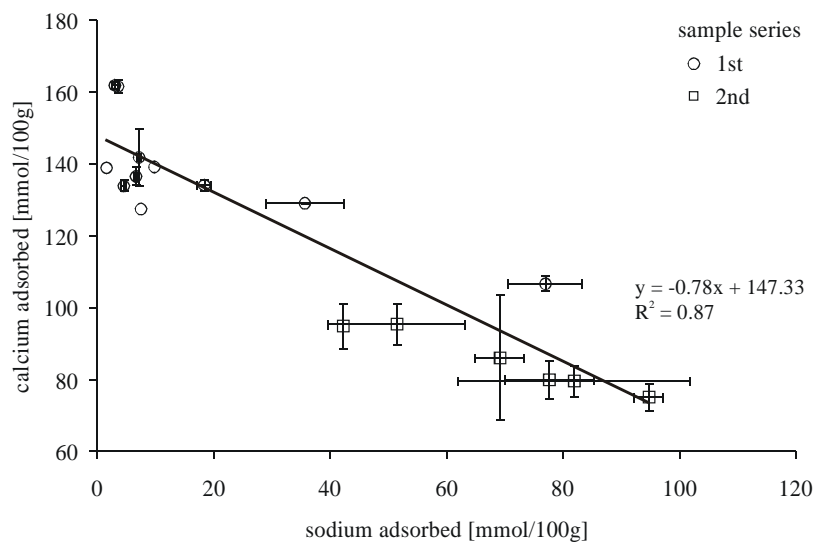


Fig. 5-2 shows the correlation between sorbed sodium and calcium amounts of the bentonite samples. The sums of the sorbed molar amounts of sodium and calcium in each individual sample are constant at 154 ± 3 mmol/100 g ($n = 17$). This value is quite similar to that found by Tournassat et al. (2004a) on a MX80 montmorillonite fully exchanged with calcium at a pH between 11 and 12. They concluded that the measured sorbed

amount of calcium at a pH > 9 is mainly due to sorption of CaOH^+ ionic pairs and to some extent due to the precipitation of a tobermorite-like phase.

Table 5-1. Crystalline Ca-phases and equivalent amounts of calcium

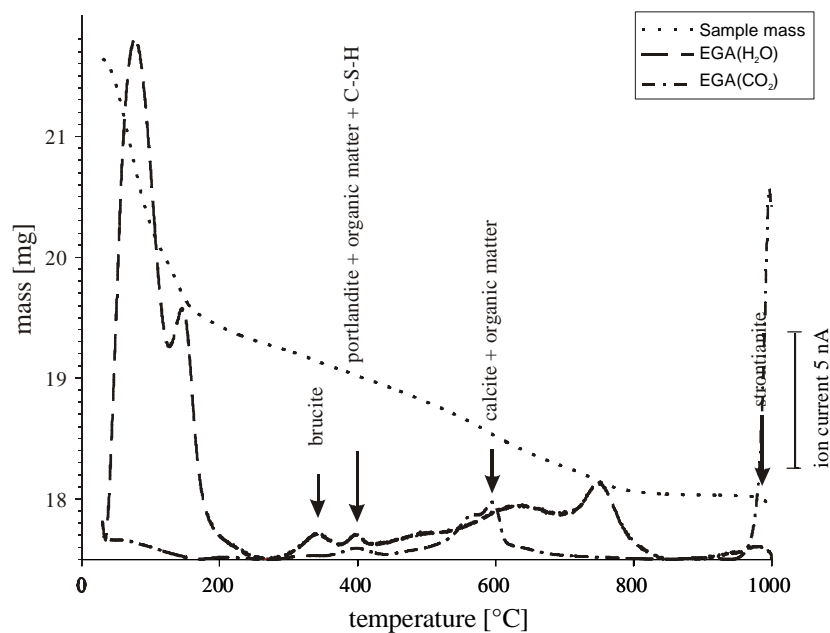
Method	Crystalline phase	Ca [mmol/100g]
exchangeable cations	2 ± 0.2 mmol Si ⁺ /100 g	4 ^b
TG-EGA	$1.9 \pm 0.2\%$ $\text{Ca}(\text{OH})_2$ (n = 11)	26
TG-EGA	$1.4 \pm 0.2\%$ CaCO_3 (n = 11)	14

^a Attributed to C-S-H.

^b Assuming a maximum C/S ratio of 2 in a C-S-H phase [Taylor, 1997].

Indications of such a phase and additional crystalline phases are gained from the results on the exchangeable cations but also from TG-EGA measurements. Table 5-1 lists the method from which the concentrations of the crystalline phases were estimated and also the equivalent amount of calcium per 100g of ignited bentonite. Small amounts of brucite ($\text{Mg}(\text{OH})_2$) and strontianite (SrCO_3) were also indicated (Mg and Sr from dissolved montmorillonite and lime), the carbonate phases being the results of residual carbonate contents of the starting material but also of carbonation during sample handling (for an example see fig. 5-3).

Figure 5-3. TG-MS curve under nitrogen of the sample with sorbed sodium (7 mmol/100g) and calcium (142 mmol/100g).



Subtracting all the calcium equivalent to these crystalline phases (44 mmol/100 g in Table 5-1) from the sum of adsorbed sodium and calcium (154 mmol/100 g), results in a value of ~110 mmol sodium plus calcium per 100 g of ignited mineral. After correcting this value with the hydroxyl content of the bentonite (5.1 % determined from TG-MS of the starting material) and providing that all of the calcium is adsorbed as CaOH^+ , an estimate for the CEC at a pH of 12.7 is ~105 meq/100 g. After subtraction of the structural CEC value of 74 meq/100g¹, an estimate for the pH dependent part of the CEC of 31 meq/100g is obtained at a pH of 12.7.

Comparing the total mass losses between 220°C and 500°C of the starting material with 0.9% to those of the exchanged bentonites with $3.9 \pm 0.2\%$, it is clear that the difference of 3% is only partially attributable to portlandite decomposition (cf. fig. 5-3). The remaining mass loss of 2-2.5% must be due to evolved water, as there is no carbonate decomposing in this region and other volatiles can be excluded. Minerals expected to appear in the system studied (clay minerals, calcium silicate/aluminate hydrates) lose their adsorbed water below 220°C [Jasmund & Lagaly, 1993, Taylor, 1997]. Therefore, this water loss most probably originates from hydroxide species of calcium (and magnesium due to brucite) adsorbed at the clay mineral's surface, releasing their hydroxyl water over a wide temperature range.

In spite of uncertainties regarding the determination of the structural CEC (Tournassat et al. (2004b) estimated a 10% error), it is concluded from the results presented, that adsorbed calcium is mainly in the form of CaOH^+ and edge sites amount to 8-30 meq/100g, corresponding to 11 or 40% of the structural CEC. Estimates in the literature for the proportion of edge charge to the structural CEC range from low values of 20% at a pH of ~12 [Tournassat et al., 2004b] to high values of 25% at a pH of 7 [Jasmund & Lagaly, 1993]. Differences in edge charge contribution at a given pH are also a result of different crystallite sizes resulting in different specific edge surface areas.

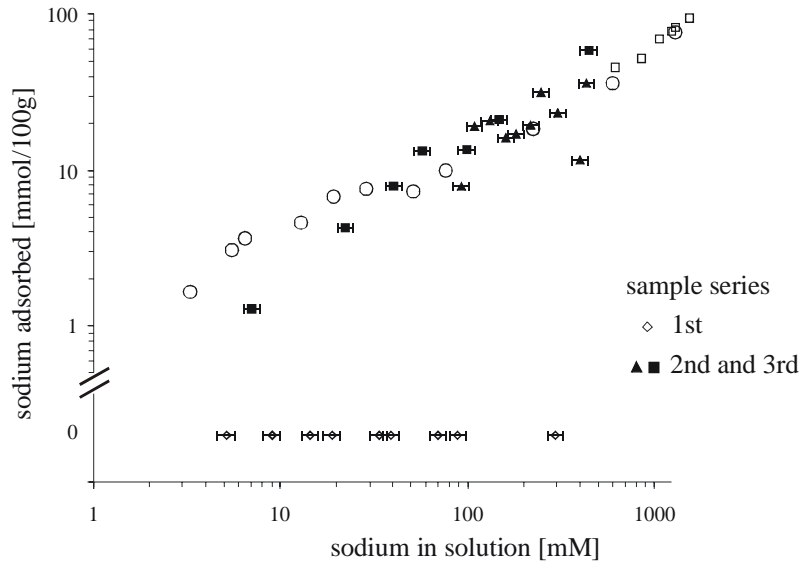
Indirect determination of cation exchange state

Additional support for the importance of the species CaOH^+ in the cation exchange experiments at high pH is given by the dispersions used for the rheological experiments. Only

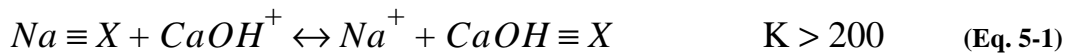
¹ Determined from the structural formula for the SWy-2 bentonite [Mamy & Gaultier, 1976]

the aqueous compositions of calcium and sodium were determined, the adsorbed amounts of sodium are calculated by mass balance. Two different preparation techniques for the bentonite dispersions were applied (see section 3.5.1 and fig. 3-16).

Figure 5-4. Indirect adsorption data from measured solution values in addition with the direct data from Fig. 5-1 (without error bars); note: first sample series adsorbed sodium below detection limit.



The indirect adsorption data in fig. 5-4 show that the two techniques resulted in completely different cation exchange states. This difference in exchange behaviour could be explained by the following reaction for Na^+ - CaOH^+ cation exchange, which was previously proposed as the main exchange reaction at high pH [Tournassat et al., 2004a, b]:



with $\equiv X$ symbolizing a surface site to which the cation is bound. The estimate for the selectivity constant K is taken from Tournassat et al. (2004b).

For the first sample series, CH was added prior to the addition of NaCl, resulting in a pure CaOH^+ montmorillonite, which had to desorb CaOH^+ in order to adsorb Na^+ . This process did not take place in the 40 hours of equilibration time, as is evidenced by the adsorbed sodium, which was below the detection limit. For the second and third sample series, NaCl was added prior to the addition of CH, presumably resulting in a pure Na^+ montmorillonite, which had to desorb Na^+ in order to adsorb CaOH^+ . After only 12 hours, these sample data matched the equilibrium data obtained after 90 hours.

Chemical equilibria are dynamic in nature, i.e. both the forward and reverse reaction proceed even at equilibrium at distinct rates [Atkins, 1994]. Therefore the equilibrium constant gives information about the relative reaction rates of the forward and reverse reaction. It can be deduced that the forward reaction (Na^+ exchange by CaOH^+) of the exchange equilibrium (eq. 5-1) is at least 200 times faster than the reverse reaction (CaOH^+ exchange by Na^+). Assuming pure reversible cation exchange with an appropriate time for equilibration, the end point of the two different types of experiments should be the same. This was not observed and may be explained by the kinetic effect described due to the equilibrium approach from two different sides.

An alternative explanation is that sorbed calcium might be irreversibly bound at specific (edge) surface sites. There have been interpretations in the literature that calcium hydroxide is deposited on clay minerals' surfaces in a fast reaction [Diamond & Kinter, 1965]. Such a surface coating might be hard to remove by cation exchange with sodium. However, the good correlation and the fact that the sum of the amounts of sorbed sodium plus calcium was about constant (fig. 5-2) still points to some interrelation between the two alternatives, adsorption and surface coating/precipitation.

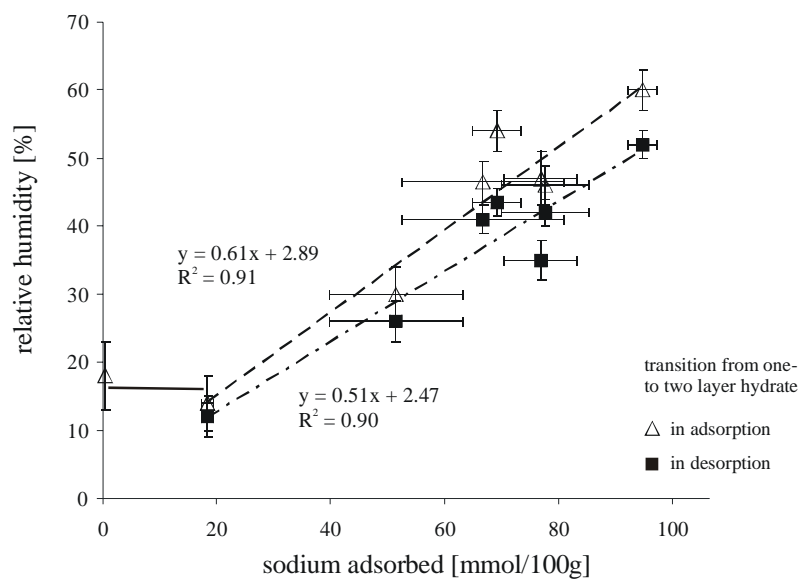
5.1.2 Swelling measurements at controlled relative humidity

The ethanol washed freeze-dried bentonites from the cation exchange experiment were carbonated in humid air (cf. section on page 49) and then subjected to swelling experiments in order to investigate their swelling behaviour as a function of their adsorbed amount of sodium. Swelling measurements were performed at $26^\circ \pm 1^\circ\text{C}$ and in controlled relative humidity. The method for extracting the transition point from the one- to the two-layer hydrate is described in section 4.6.

Fig. 5-5 shows the transition point as a function of the sorbed sodium amount of the bentonite. The transition in adsorption appears at higher relative humidities than in desorption, as is typically observed for sorption hysteresis of clay minerals. Linear regression down to the value at $\sim 20\text{mmol}/100\text{g}$ yields a high correlation ($R^2 = 0.91$ and 0.90) for both the ad- and desorption data. However, pure calcium montmorillonite has the same transition point as a montmorillonite with $\sim 20\text{mmol}/100\text{g}$ of adsorbed sodium. This might be explained in terms of "demixing" of adsorbed cation species [Shainberg & Kemper, 1966; Shainberg & Otoh, 1968]. These authors proposed for Na-Ca exchange that calcium shows a marked preference for inner tactoid surfaces. According to this proposal, sodium

is first sorbed on the outer surface of calcium montmorillonite tactoids. At an exchangeable sodium percentage (ESP¹) of 10% to 20%, calcium starts to be exchanged by sodium from the interlayers and the tactoids break open. The break-up of tactoids was fully accomplished at an ESP value of ~50 %. This is in agreement with the swelling measurements in this study: at an amount of adsorbed sodium of ~20 mmol/100g, corresponding to an ESP value of ~20% of the estimated total CEC, the swelling behaviour differs from a pure calcium montmorillonite and starts to resemble sodium montmorillonite-like behaviour.

Figure 5-5. Transition from one- to two layer hydrate depending on the relative humidity as a function of the adsorbed amount of sodium.



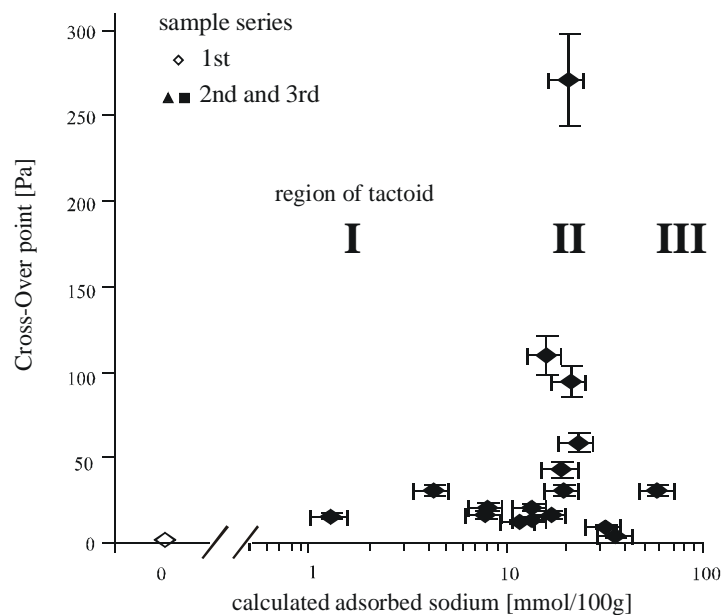
5.1.3 Rheology

The dispersions for the rheological measurements have been prepared in two different ways as explained before (section on page 48). These preparation techniques resulted in an unequal cation exchange state, adsorption of sodium was shown to be hindered. The unequal cation exchange state is also observed by the rheological data in fig. 5-6. The figure shows the Cross-Over Point (COP) or yield point (cf. section 3.1.6) against the calculated amounts of adsorbed sodium. All the COPs of the first sample series, where adsorption of sodium was hindered, are very low and show no significant variation, irre-

¹ Conventionally in soil sciences, the amount of adsorbed sodium is given by the ESP value with $ESP = 100 \cdot Na \equiv X/CEC$. It is the proportion to which the adsorption complex of a soil is occupied by sodium. The total CEC at a pH of 12.7 was estimated in the previous section to 105 meq/100g. Therefore, an ESP value of 20% is roughly equal to 20 meq/100g.

spective of sodium addition, on average 2.2 ± 0.2 Pa. The COPs of the second and third sample series, with more than 1 mmol of adsorbed sodium per 100g of bentonite, are significantly greater with 40.8 ± 13.7 Pa and show a pronounced discontinuity at ~ 20 mmol and COPs up to 271 Pa.

Figure 5-6. Cross-over points as a function of the calculated amounts of adsorbed sodium; note: first sample series adsorbed sodium below detection limit. The three tactoid regions refer to the schematic picture at the end of this chapter.



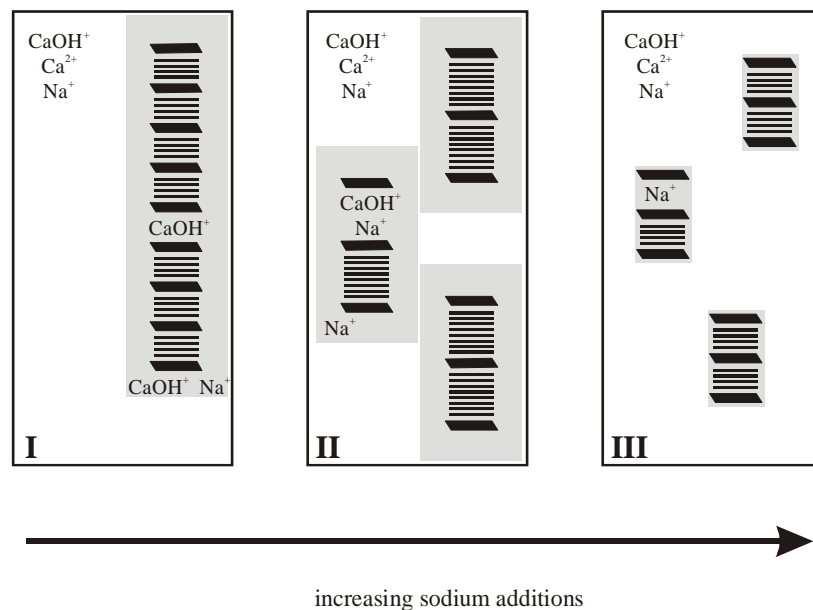
Such a discontinuity is often observed in conjunction with the critical coagulation concentration of added salts [Penner, 1998]. However, this does not seem the appropriate explanation here. Critical salt concentrations of Wyoming montmorillonite dispersions for NaCl lie in the range of 300 to 400 mM, whereas sodium montmorillonite dispersions already start to coagulate after addition of less than 1 mM calcium [Jasmund & Lagaly, 1993]. Calcium concentrations in the presence of portlandite are high at a pH of 12.5 (> 20 mM). It can therefore be concluded that dispersions in a cementitious environment are already in a coagulated state, independent of the applied sodium concentration.

However, an explanation might be given in terms of the different dispersion behaviour of calcium and sodium montmorillonite. It has been established that tactoids in calcium montmorillonite dispersions keep a constant basal spacing of ~ 20 Å up to calcium concentrations of more than 1 N [Norrish, 1954a, b]. This is in contrast to pure sodium montmorillonite dispersions, in which the basal spacing inside tactoids is known to depend on both the sodium concentration and the solid content. A basal spacing of more

than 20 Å is found in dispersions with less than ~500 mM sodium [Norrish, 1954a, b; Norrish & Quirk, 1954] and water to solid ratios > 1 [Hight et al., 1962]. The swelling measurements in the previous section implied that up to an ESP value of ~20% (corresponding with an aqueous sodium concentration of ~200 mM), the montmorillonite behaved like a pure calcium montmorillonite. Putting together this evidence results in a range between 200 and 500 mM sodium where all or some crystallites should be able to swell beyond the 20 Å limit. This drastically changes the state of the dispersion by increasing the solid (tactoid) volume through the consumption of “free” water for the swelling process, thus decreasing the volume of “free” water. This volume effect is probably intensified by a sudden increase of the external surface area at an ESP of 20%. Schramm & Kwak (1982) showed that the number of primary layers in tactoids of calcium montmorillonite suspensions suddenly decreases by a factor of 3 to 4 upon sodium exchange of ~20% and then remains constant. The break-up of tactoids exposes new basal surfaces to the solution, thus increasing the external surface area and immobilizing additional “free” water volume in the diffuse ion layer.

The evolution of tactoids with increasing sodium additions is schematically shown in fig. 5-7. The associated solid volume effects are responsible for the discontinuity of the yield point (fig. 5-6).

Figure 5-7. Schematic picture of the evolution of tactoids in dispersions with constant solid content (number of primary layers), constant calcium (solubility of CH) but varying sodium concentrations; the grey shaded area symbolises the diffuse ion layer.



Tactoid I: Small additions of sodium to a montmorillonite dispersion containing CaOH^+ and Ca^{2+} lead to cation exchange only on external surfaces, the basal spacing is constant at $\sim 20 \text{ \AA}$ (symbolised by four water layers).

Tactoid II: Further addition of sodium leads to cation exchange also from interlayer surfaces, resulting on the one hand in the break-up of tactoids, thereby increasing the external surface area and consequently the amount of water bound in the diffuse ion layer, on the other hand in an expansion of interlayer volume (basal spacing $> 20 \text{ \AA}$), thereby decreasing the volume of “free” water. As a result, the Cross-Over Point is about one order of magnitude higher compared to dispersions with tactoids I and III.

Tactoid III: At high sodium additions ($> 500 \text{ mM}$) the basal spacing collapses again to $\sim 20 \text{ \AA}$. The diffuse ion layer shrinks to minimal values. The volume occupied by the solid and the diffuse ion layer is even lower than in dispersions with tactoids I.

5.2 Conclusions

The results of the multidisciplinary approach to the problem of sodium-calcium exchange in cementitious systems and related swelling and rheological behaviour are summarised as follows:

- (i) The major adsorbed calcium species is most likely CaOH^+ and precipitated $\text{Ca}(\text{OH})_2$.
- (ii) The kinetics of the $\text{CaOH}^+ - \text{Na}^+$ exchange or the coating of the surfaces by a calcium hydroxide layer prevented adsorption of sodium even after 40 hours, whereas desorption to an assumed equilibrium value was already accomplished after 12 hours. It is thus impossible to increase the amount of adsorbed sodium in a reasonable amount of time relevant to practical applications by solely adding sodium.
- (iii) Exchange capacity of the montmorillonite edges amounts to 8 - 30 meq/100g at a pH of 12.7, the first value was deduced from the sodium exchange isotherm, the second one from the total amount of sorbed calcium plus sodium after correcting for crystalline phases.
- (iv) The different exchange behaviour of edge and outer surface sites on the one hand, and interlamellar surface sites on the other hand, greatly influences the swelling and rheological behaviour, as evidenced by the discontinuity of the yield point at an exchangeable sodium percentage of $\sim 20\%$.
- (v) Crystalline swelling behaviour is continuously changing from calcium to sodium montmorillonite as soon as sodium is contained in the interlayers (demixing model).

6 Pozzolanic reaction of clay minerals II: dissolution, precipitation and pore refinement

6.1 Results and discussion

The three clays were dry-mixed with calcium hydroxide/lime (CH) in a glove-box prior to adding CO₂-free water. The final shaken mixtures were agitated overarm at ~6 RPM for the desired reaction time of ~1.5, 3, 4, 5 and 6 months. The influence of water to solid ratio (w/s) between 1.3 and 12.5 (100 g of water with 78 g or 8 g of solids respectively) was investigated, as was the influence of mixing ratio of the two solids.

6.1.1 Comparison of initial and after reaction extracted clays

First of all, the initial and extracted clays were compared by their thermal analysis data (fig. 6-1) and by their X-ray diffractograms (fig. 6-2). If there were no changes, the patterns (both XRD and DTG) for each material before and after reaction should look the same with respect to the peak ratios. In order to judge these peak ratios, the patterns are aligned vertically and scaled in arbitrary units. On a quantitative basis, each material before and after reaction was also compared by its hydroxyl water content which is indicative of the amount of main clay mineral inside the clay material. These hydroxyl water contents show no significant variation before and after reaction (Table 6-1).

Table 6-1. Hydroxyl water content [%] referred to the ignited mass

	China Clay	Illite MC	Volclay
before reaction	13.5 ± 0.1	4.6 ± 0.1	4.0 ± 0.1
after reaction (extract)	13.3 ± 0.1	4.7 ± 0.1	3.9 ± 0.1

However, the DTG data in fig. 6-1 and the XRD data in fig. 6-2 show small changes. Differences in peak temperature of the DTG data may arise from different initial sample weight and packing density [Emmerich, 2000]. These conditions could not be fixed in the measurements presented. This resulted from the different appearance of the raw powders before and the freeze-dried powders after reaction. Freeze dried powders were mostly in

a fluffier state which favoured a looser packing density and less sample weight. For the illite (fig. 6-1a), and especially for the montmorillonite (fig. 6-1c), the difference in peak area of the adsorbed water lost below 200°C is caused by variable drying states, which were also not fixed as all analyses were referred to the ignited mass. The TA data of the extracted Volclay (fig. 6-1c) implies small remains of hydroxide species (due to incomplete extraction), which decompose between 300 and 500°C. Nevertheless, the changes observed are small and not significant with respect to the clay content of the materials before and after.

Figure 6-1. Comparison of thermal gravimetry patterns of initial and after reaction extracted clays: (a) illite MC, (b) China Clay and (c) Volclay. Y-axis: differential mass loss in arbitrary units.

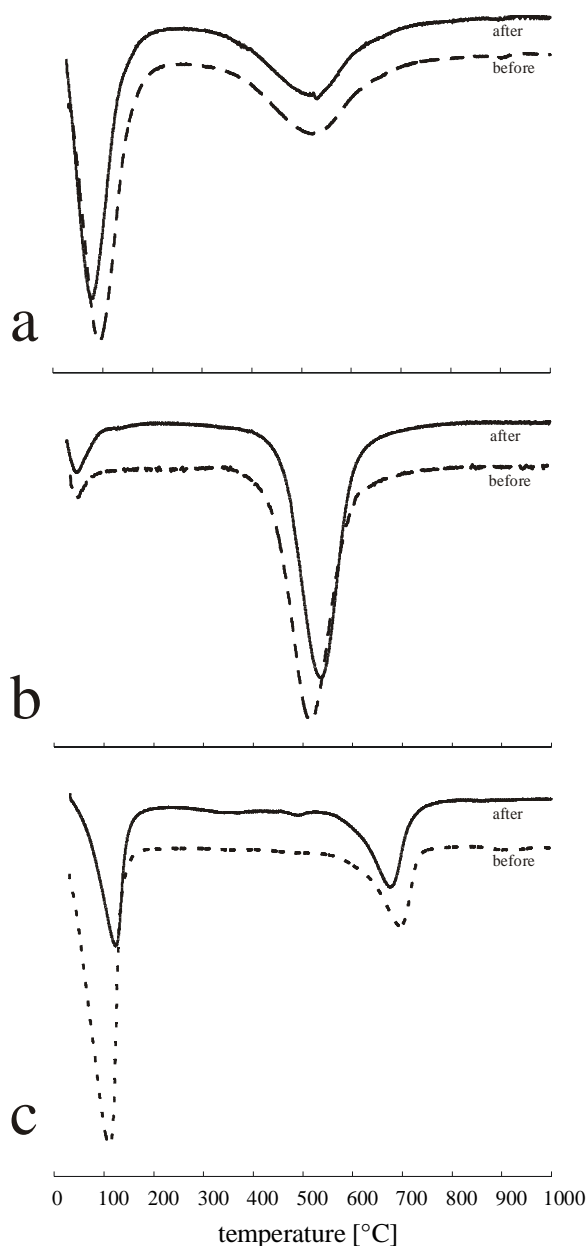
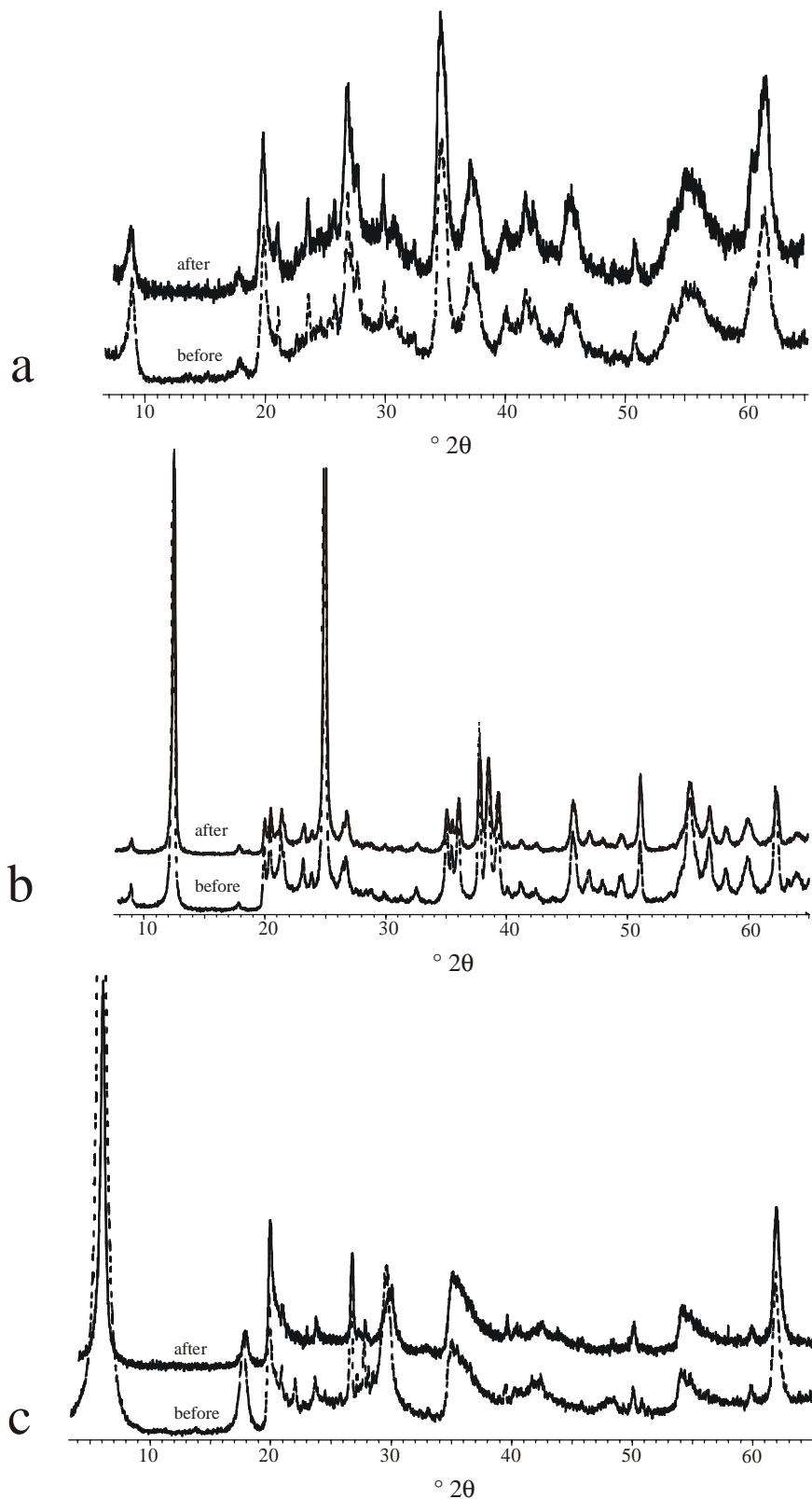


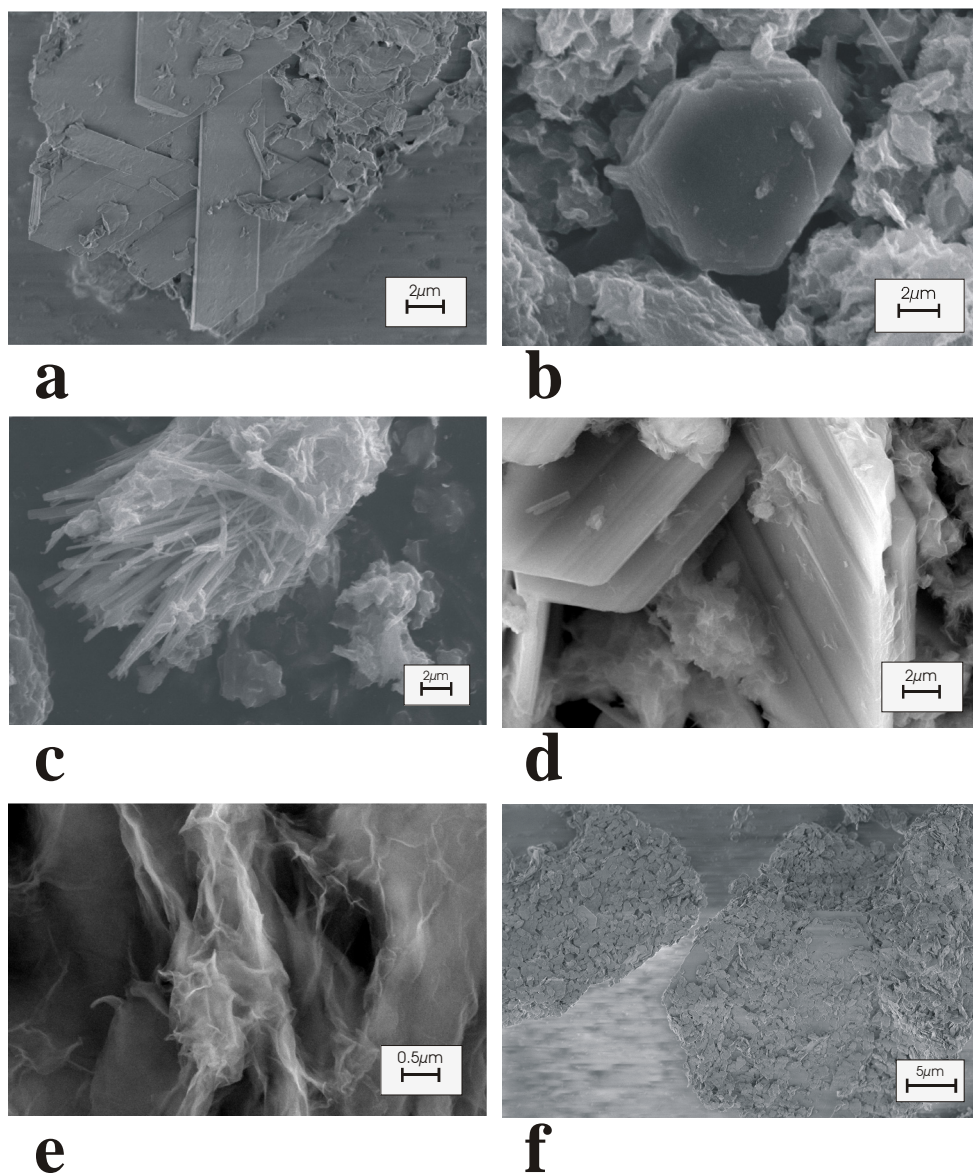
Figure 6-2. Comparison of X-ray diffraction patterns of initial and after reaction extracted clays: (a) illite MC, (b) China Clay and (c) Volclay. Y-axis: X-ray intensity in arbitrary units.



Variations in peak ratio of the XRD patterns are also small and may be attributed to e.g. preferred orientation effects. For the montmorillonite, peak shifts and variable peak height

of the basal reflections below 10° and at around 30° arise again from different drying states (fig. 6-2c). It is concluded that no selective dissolution of impurities in the reacted clay-lime mixture occurred (hydroxyl water content would be significantly elevated if only the impurities in the clays dissolved) and that the clay minerals in the clays were at least equally dissolved. In the following section, it will be therefore assumed that the whole clay material loss is due to clay mineral dissolution. This is justified because the main clay mineral constituted the major phase by at least 87% in the three clays examined.

Figure 6-3. Major reaction products after three months for reacted Volclay-lime mixtures at a water to solid ratio of 13, (a) lath-shaped AFm phase, (b) platy hexagonal AFm phase, (c) bundle of ettringite needles, (d) AFm and C-S-H phases intergrown, (e) foil-shaped C-S-H phase and (f) huge hexagonal AFm phase in an aggregate of a China Clay-lime mixture at a water to solid ratio of 2.



6.1.2 Reaction products

Major reaction products in all of the samples were so-called AFm and C-S-H phases, as abbreviated in cement chemistry. The AFm phases are hydrated calcium aluminate phases with a layer structure derived from portlandite. Ideal crystals show platy hexagonal or lath-shaped morphology (fig. 6-3a, b, d and f). Their permanent positive layer charge results in anion exchange properties and associated swelling properties [Aruja, 1960, 1961; Dosch, 1967; Pöllmann, 1991; Francois et al., 1998; Rapin et al., 1999a, 1999b, 2000, 2001; Renaudin & Francois, 1999]. The general formula is $C_4(A,F)X_2H_x$ or $[Ca_4(Al,Fe)_2(OH)_{12}] \cdot 2X \cdot xH_2O$ where X denotes one formula unit of a singly charged anion [Taylor, 1997]. The Ca/Al ratio in the solid layers is fixed at 2, which has been verified for the AFm phases in this study by energy dispersive X-ray spectroscopy in the (E)SEM. C-S-H is the abbreviation for hydrated calcium silicates of varying structure and composition. Its chemical and structural nature is still subject to scientific debates; its nanostructure is most probably related to the layer structures of tobermorite and/or jennite depending on the C/S ratio in the C-S-H [Taylor, 1997; Merlino et al., 1999; Bonaccorsi et al., 2004]. Fig. 6-3E shows an example of a C-S-H phase in crumpled foil morphology. Ettringite appeared only in the Volclay-lime mixtures as a third major phase. Ettringite is termed the AFt phase or trisulphate phase in cement chemistry [Taylor, 1997]. The appearance of ettringite is a result of the minor sulfate (due to gypsum) content in the Volclay. Fig. 6-3c shows an example of this phase in typical needle-like morphology.

AFm and C-S-H phases are detected also from XRD and TA, whereas ettringite can only be determined from visual observation by SEM/ESEM. X-ray evidence is given in fig. 6-4 for AFm and C-S-H in clay-lime mixtures, which have reacted for 3 months at a water to solid ratio by weight of 2. According to Taylor (1997), AFm phases usually show the first and second order of the basal lines (001 and 002) and sometimes lines at 2.89 Å and 1.67 Å. C-S-H may show reflections at 12.5 Å, 3.04 Å, 2.80 Å and 1.85 Å. Fig. 6-4 shows the XRD patterns of the clays before and after a reaction of 3 months with added portlandite (CH). Remaining CH is indicated and also the lines of the reaction products, C-S-H and AFm.

Figure 6-4. X-ray diffractograms of the three initial clays and clay-lime mixtures (39/13/100) reacted for 3 months: (a) illite MC, (b) China Clay and (c) Volclay. Y-axis: X-ray intensity in arbitrary units.

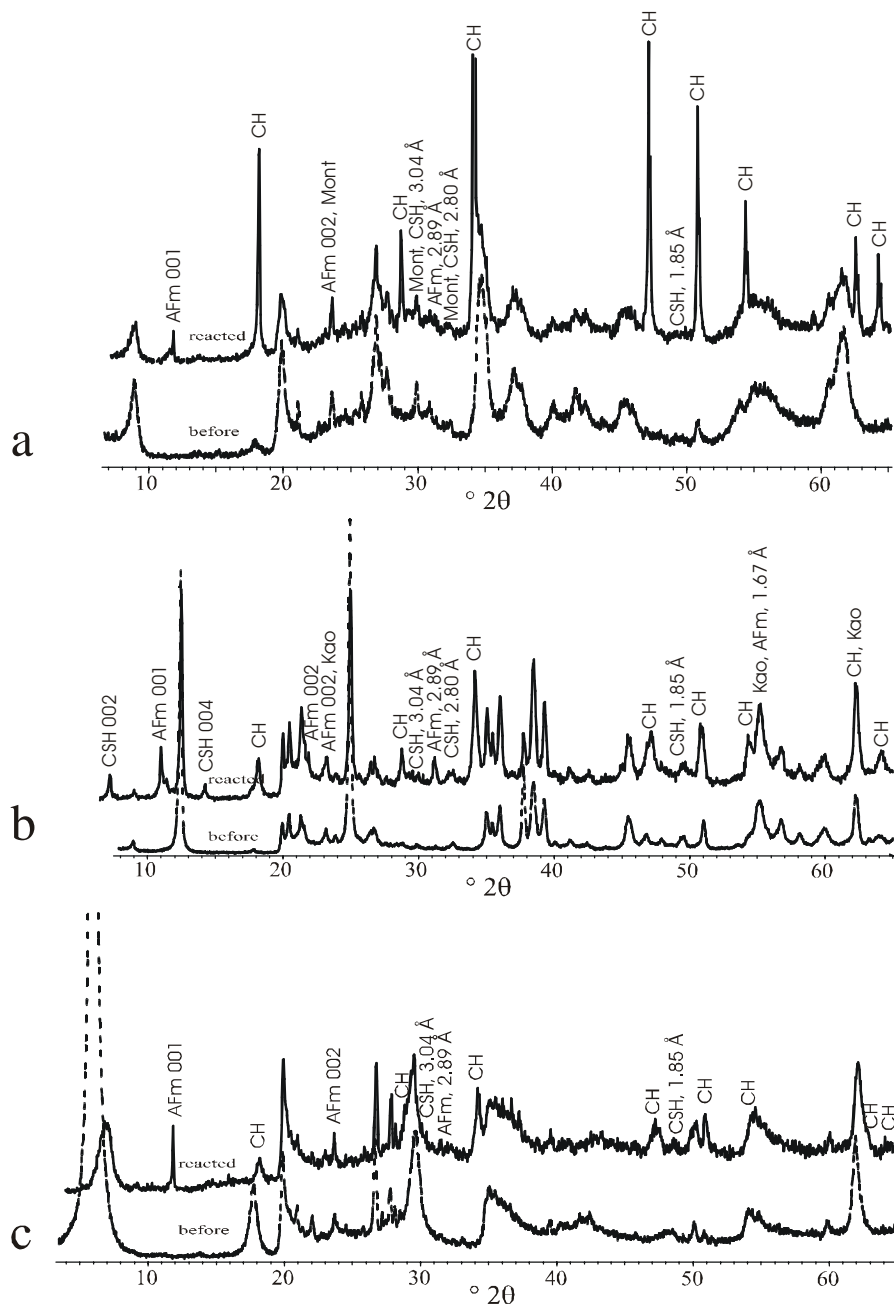
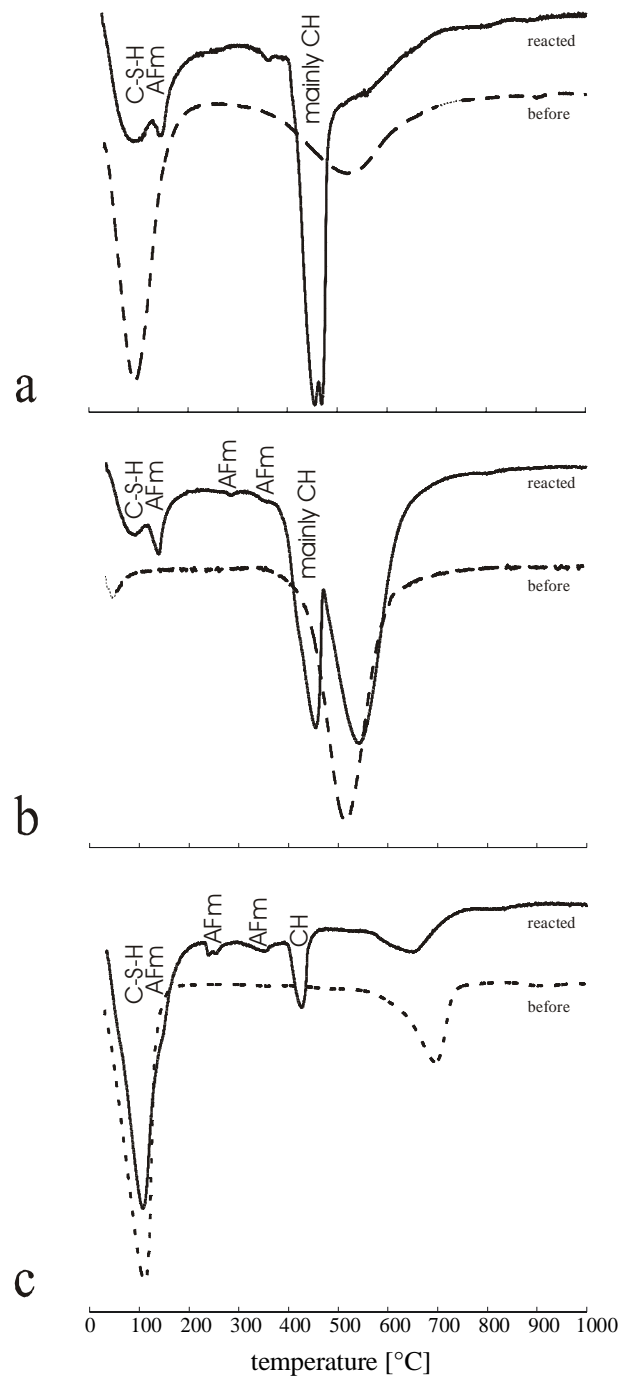


Fig. 6-5 shows the corresponding differential mass loss curves of these materials. Typical mass losses of AFm and C-S-H are indicated. The aqueous solution compositions of the clay-lime mixtures (Appendix IV to V) are also supportive. The Si and Al concentrations were mainly below 300 μM , which, together with the other evidence, is indicative of AFm and C-S-H phases by comparison with thermodynamical calculations in the pure $\text{CaO-Al}_2\text{O}_3\text{-SiO}_2\text{-H}_2\text{O}$ system [Damidot & Glasser, 1995].

Figure 6-5. TG-MS data of the initial and clay-lime mixtures in fig. 6-4: (a) illite MC, (b) China Clay and (c) Volclay. Y-axis: differential mass loss in arbitrary units.



6.1.3 Extent of pozzolanic reaction and passivation effects

The results on clay mineral and lime consumption are summarised in Appendix VI, VII and VIII. Consumption of clay minerals and lime were calculated by the difference in initial contents and those determined after reaction. No significant differences in mineral contents consumed were detected in the reacted mixtures. Table 6-2 summarises the averaged values for clay mineral and lime consumption in all of the clay-lime mixtures for

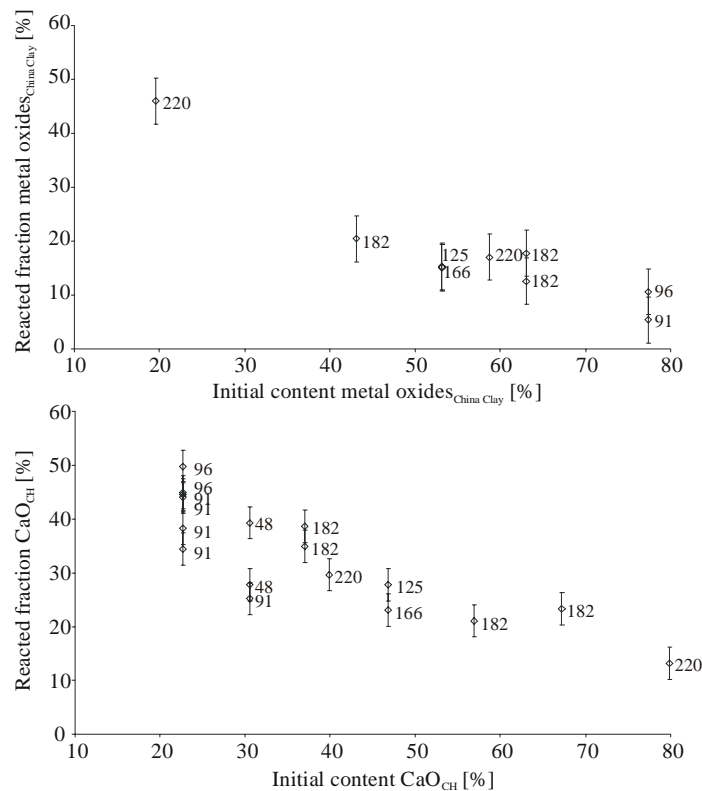
each clay. Consumption was independent of time between 1.5 and 6 months, of water to solid ratio between 1 and 13 and of mixing ratio between 0.5 and 3.5 (clay/CH) of the two components.

Table 6-2. Averaged consumption of clay minerals and lime in all of the clay-lime mixtures of each clay^a

mixture of clay with lime	consumption CaO_{CH}	consumption metal oxides _{clay}	mass ratio $\text{CaO}_{\text{CH}}/\text{oxide}_{\text{clay}}$
	[g/100g] from XRD	[g/100g] from extraction	
Illite Massif Central	8.9 ± 0.5	9.2 ± 1.3	1.0
China Clay	11.0 ± 0.6	8.0 ± 0.8	1.4
Volclay	20.0 ± 0.4	7.2 ± 0.7	2.8

^aThe consumption of clay minerals and lime was also determined by TA in order to check the more direct measurements (XRD, extraction). Results are considered to be the same when falling within the error limits of each method (Appendix VI, VII and VIII).

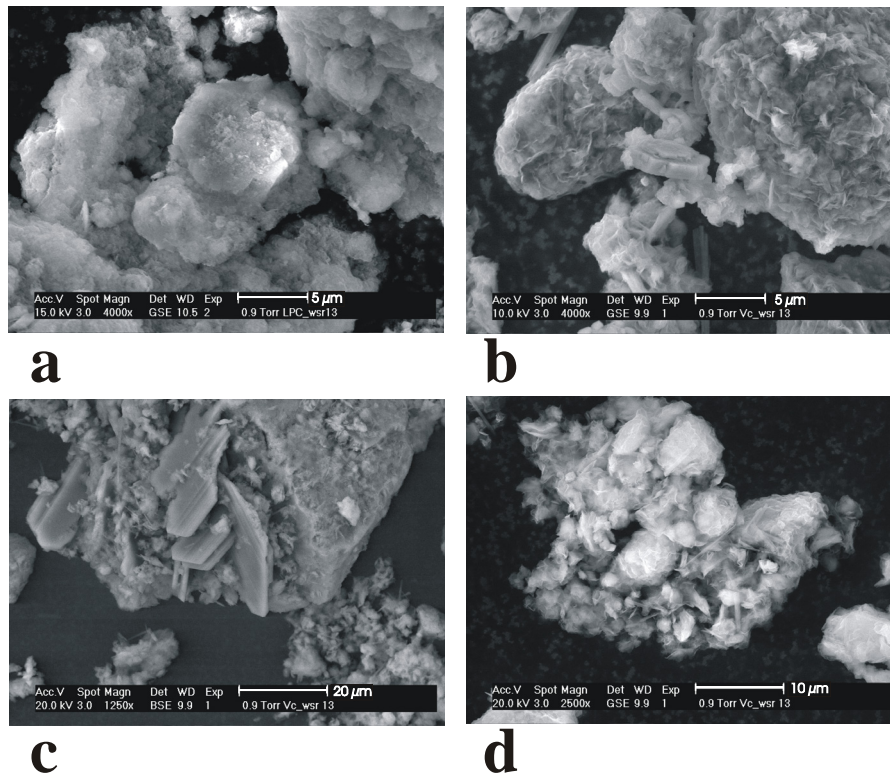
Figure 6-6. Reacted fractions of China Clay and lime with their initial contents in the solid mixture: upper figure metal oxides_{China Clay} from extract, lower figure CaO_{CH} from XRD. The number at each data point gives the reaction time in days.



As consumption was constant for the conditions investigated, it is clear that the reacted fractions of each initial mineral component decreases independent of reaction time with

the initial content of the respective component (exemplified by the China Clay-lime data in fig. 6-6). In a chemical reaction that is controlled by the dissolution rate and the surface area of one of the reactants, the reacted fractions would be constant for equal reaction time (independent of the mixing ratio) and would increase with reaction time. It is therefore concluded that the behaviour observed in the clay-lime mixtures is due to a cessation of the pozzolanic reaction. Between 1.5 to 6 months, the reaction does not proceed or just so slow that it was undetectable with the analytical approach undertaken.

Figure 6-7. Aggregates of reacted clay-lime mixtures after three months cemented and surrounded by pozzolanic reaction products (w/s = 13). (a) Illitic clay-lime mixture, (b)-(d) Volclay-lime mixture.



This cessation is explained by the passivation of the reactive surfaces of clay minerals and lime through the overgrowth of the pozzolanic reaction products. Fig. 6-7 shows examples of huge aggregates (up to ~80 μm in diameter) cemented and overgrown with reaction products. A similar cessation of the lime slaking reaction was observed by Xu et al. (1997) and attributed to the passivation of the reactive lime surfaces by calcium aluminate hydrates. Diffusion of reactive species from dissolving surfaces is however still expected to occur, but at a much reduced rate. Chemical species have to diffuse through the hydrated solids or the nano-pores of these solids.

Table 6-3. Chemical formulas of the minerals with the molar masses of the ignited dehydroxylated minerals

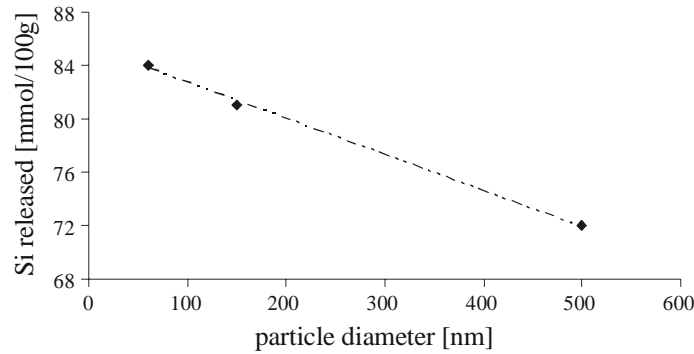
	Chemical formula	Molar mass of ignited mineral
CH^a	$\text{Ca}(\text{OH})_2$	56
Na-Volclay^b	$\text{Na}_{0.26}(\text{Al}_{1.54}\text{Fe}_{0.18}\text{Mg}_{0.26})\text{Si}_{3.95}\text{Al}_{0.05}\text{O}_{10}(\text{OH})_2 \cdot x\text{H}_2\text{O}$	352
Ca-Volclay^b	$\text{Ca}_{0.13}(\text{Al}_{1.54}\text{Fe}_{0.18}\text{Mg}_{0.26})\text{Si}_{3.95}\text{Al}_{0.05}\text{O}_{10}(\text{OH})_2 \cdot x\text{H}_2\text{O}$	351
Illite^c	$\text{Ca}_{0.04}\text{Na}_{0.12}\text{K}_{0.64}(\text{Al}_{1.17}\text{Fe}_{0.49}\text{Mg}_{0.33})\text{Si}_{3.52}\text{Al}_{0.48}\text{O}_{10}(\text{OH})_2$	384
China Clay^d	$\text{Al}_2\text{Si}_2\text{O}_5(\text{OH})_4$	222

^a ideal formula^b Mamy & Gaultier (1976)^c Müller-Vonmoss et al. (1991)^d ideal formula

The released amounts of structural silicon, aluminium and iron were calculated from the chemical formulas of the three clay minerals in Table 6-3 and their consumption data in Table 6-2. It is shown from these calculations that the amount of silicon released is very similar for the three clay minerals (Table 6-4) in contrast to the other two metals. This suggests that the major cementing and passivating phase is the C-S-H (which is plausible because of its gel character). Additionally, the released values of silicon show a correlation with the median particle diameter of the three clay minerals (fig. 6-8). This diameter is taken here as a relative indicator of edge surface area (the smaller a platelet gets, the higher the specific edge surface area). At least for the cessation of clay mineral dissolution, it is hypothesised that the C-S-H, which is formed from the silicon from the edges of the clay minerals, is the major passivating phase. However, this should be subject to further investigation and proof.

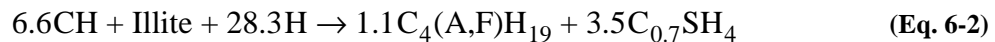
Table 6-4. Released amounts of silicon, aluminium and iron by clay mineral dissolution

clay	Si [mmol/100g]	Al [mmol/100g]	Fe [mmol/100g]
China Clay	72	72	-
Volclay	81	33	4
Illite Massif Central	84	40	12

Figure 6-8. Released silicon with median particle diameter of the clay mineral.

6.1.4 Estimation of reaction equations

In order to estimate porosity changes that occur during the pozzolanic reaction the chemical composition of the reaction products was calculated from the mineralogical data presented (proportion clay mineral and lime consumption). This is done using the chemical formulas and the molar masses of the clay minerals given in Table 6-3. Assuming a fixed Ca/(Al+Fe) ratio of two in the major aluminate reaction product (AFm), the Ca/Si ratio in the other major reaction product (C-S-H) may be estimated. According to these calculations, each mole of China Clay releases 2 moles of aluminium and silicon each, which react with 5.4 moles of calcium. 4 moles of this calcium are bound by the aluminium, the remaining calcium combines with 2 moles of Si to form a C-S-H phase with a Ca/Si ratio of 0.7. The same Ca/Si ratio is calculated for the illitic clay. The following equations are based on these calculations and are balanced with respect to water and water contents of an assumed AFm phase (C_4AH_{19}) and $C_{0.7}SH_4$ taken from Taylor (1997) (recall: H equals H_2O):



For the montmorillonite (Volclay) however, an unrealistic Ca/Si ratio of 3.6 is calculated. Ca/Si ratios of known C-S-H in cements range from 0.6 to 2.0 [Taylor 1997]. In order to decrease this value to a realistic one, another sink for CaO must be present. One sink is the ettringite identified in the Volclay products. Ettringite has a higher Ca/Al ratio than the AFm phases. However, even if all of the aluminate hydrates were ettringite, a realistic Ca/Si ratio would not be reached. An additional sink might be lime adsorbed as a monolayer on the clay minerals' external surfaces as proposed by Diamond & Kinter (1965).

The cation exchange experiment in this study has revealed also that a large amount of calcium hydroxide species may be bound to montmorillonite. After 4 days, 8.4% CaO (in samples with no adsorbed sodium) were extracted by the cation exchange technique. The sorption of lime might be responsible for the unrealistic result calculated on C-S-H composition. However, the sorption on the external surfaces only does not seem to be the proper explanation. Otherwise, the same effect as for Volclay should have been observed for the other clays as well. An alternative explanation might be inclusion of lime into the interlayers of expandable montmorillonite. This could only be verified by further investigations.

6.1.5 Pore refinement

It is known from the literature that addition of lime to clayey soils leads to immediate microstructural changes in the soil [Caprez, 1984]. This is evidenced by the sudden shift of a soil's grain size distribution to higher diameters, which appeared mainly for the grain size fractions $< 100\mu\text{m}$ [e.g. Croce & Russo, 2003]. Accordingly, the pore size distributions are also expected to change to larger pore sizes. It was concluded in a previous section that mainly the overgrowth of the aggregates' surfaces by reaction products leads to the cessation of the pozzolanic reaction. The size of the immediately formed aggregates must therefore increase with pozzolanic reaction progress due to the overgrowth, thereby, at sufficient low water contents, cementing the aggregates together and filling the macropore spaces.

Table 6-5. Phenomenological description of the specimen.

Hydration time [months]	kaolinite/lime/water [g]		montmorillonite/lime/water [g]	
	50/40/100 (A)	15/70/100 (B)	39/13/100 (C)	7/70/106 (D)
fresh	highly viscous paste, slowly flowing		thixotropic, capable of flowing when agitated	capable of flowing
1	shrunk, not hardened, breaks apart easily, but dimensionally stable, porous			
2	slightly hardened, withstands higher forces, dimensionally stable, porous			
3	hardened			
7	hardened, dense			

Various clay-lime specimens were prepared for the purpose of porosity measurements by mercury intrusion porosimetry (MIP). Table 6-5 gives a phenomenological description of the prepared specimen. All fresh pastes were capable of flowing. After reaction and

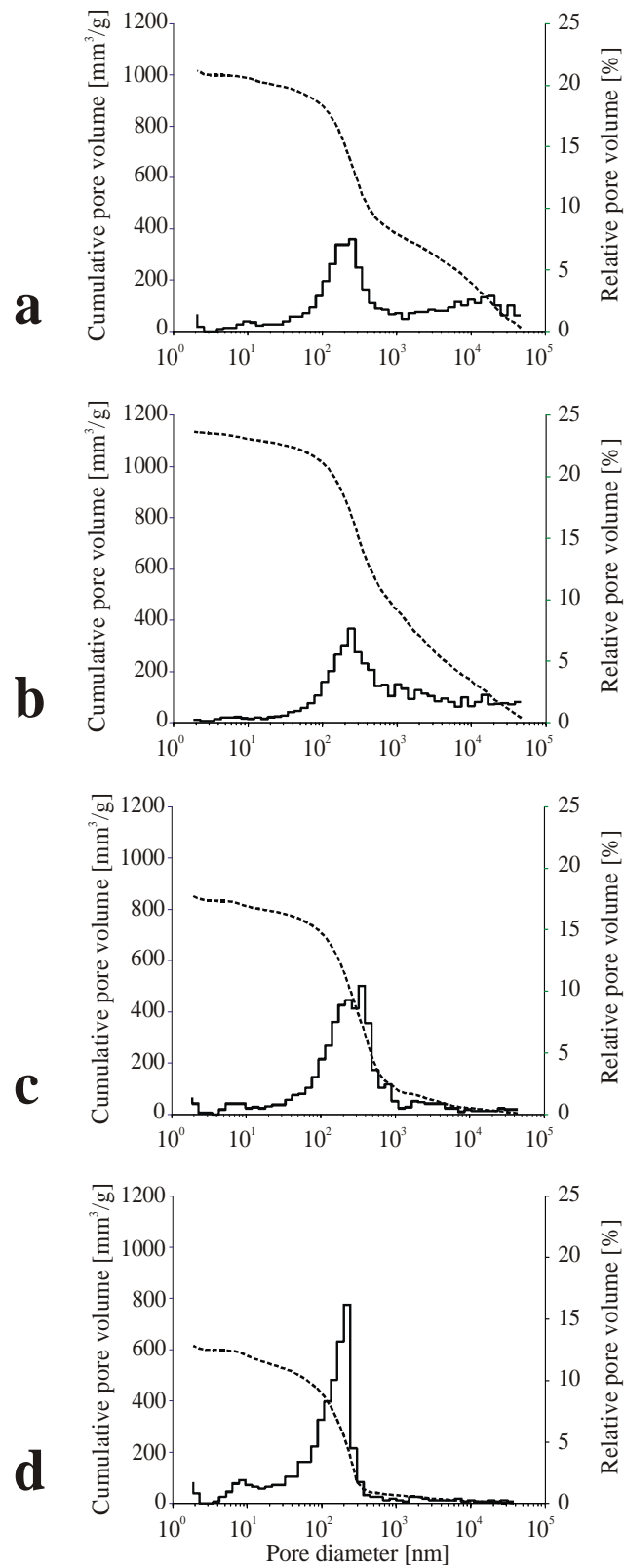
drying of the samples, the one- and two-month hydrated specimen showed an open porous structure that easily broke apart; the older specimen however, showed a dense appearance, a plane fractured surface and withstood higher forces (fig. 6-9).

Figure 6-9. Fragments of freeze-dried China Clay-lime specimens (15/70/100), reacted for 1 month (left), 2 months (middle) and 7 months (right); scale is in centimeters.



Fig. 6-10 shows the temporal development of selected pore properties exemplified on a China Clay-lime mixture. Total porosity, as indicated by the total specific pore volume, decreases with time, in accordance with the known pore refinement process [Mehta & Monteiro, 1993]. The lower pore volume of the sample in fig. 6-10a is probably due to sample preparation problems of the relatively fresh, weakly cemented material (reacted for one month). However, the pore size distribution of this sample shows marked differences to the one reacted for two months (fig. 6-10b). The first one is a bimodal distribution, the latter tends more to a broad unimodal distribution. The contribution of macropores (> 1000 nm) decreases generally with time. These pores are related to inter-aggregate pores in clays [Nüesch, 1992]. From 3 to 7 months (fig. 6-10c, d), the pores between 200 and 1000 nm start also to change, the pores with greater diameters disappear, the pore size distribution becomes more narrow and the main pore diameter shifts to lower values. The overgrowth of clay mineral-lime aggregates by reaction products leads to a decrease in porosity caused by either a filling of the inter-aggregate pores or a closure of the macropore entries. Later on, the smaller intra-aggregate pores become also filled or closed.

Figure 6-10. Temporal development of the pore size distribution in the China Clay-lime mixture (15/70/100); (a) 1 month, (b) 2 month, (c) 3 month, and (d) 7 month hydrated samples. Relative pore volume shown as histogram.



There is some debate in the cement literature regarding the mode of action of pozzolans in cements and the associated pore refinement [Taylor, 1997; Cook & Hover, 1999], whether the refinement is pore-filling or pore-closing. The results presented, rather point to a pore-closing action. It was shown that the dissolution reaction ceases due to the overgrowth. For sufficient low water to solid ratios, the overgrown aggregates will touch each other and this should be the reason for the cementation of the material. For concentrically growing aggregates it seems probable that inter-aggregate pores entries become first closed, before the pores become filled completely.

6.1.6 Porosity development

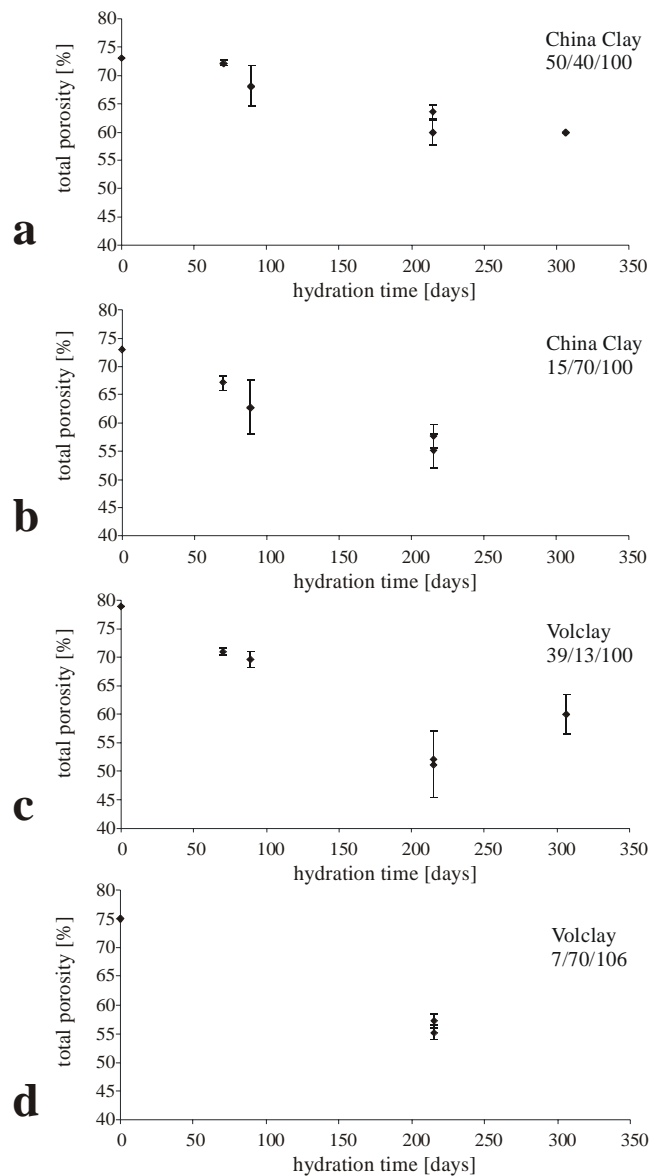
Fig. 6-11 shows the results of the total porosity measurements with time for the clay-lime specimens prepared. Their composition is given in Table 6-5. The calculated porosity of the fresh pastes at the beginning of the time scale is also indicated (calculation¹ from the initial mixing ratio and the densities given in Table 3-4). All the mixtures show a substantial decrease of the total porosity beginning in specimens hydrated over 2 or 3 months. Total porosity decreases by about 10% to 20% absolute, to values of 65% to 55%, irrespective of the mixing ratio or the clay used (China Clay or Volclay). The degree of porosity loss can be estimated from the molar volumes of the minerals (Table 3-4) and the chemical equations derived earlier (eq. 6-1 and eq. 6-2). The volume changes associated with the chemical equations are tabulated in Table 6-6. Volume changes are calculated from subtraction of product minus educt side. For complete reaction, there is no water left on the product side, however, the total volume of the solids after reaction is smaller than the water plus the solid volume before reaction. The specimens shrink (chemical shrinkage). In contrast, the solid volume increases, as water is incorporated into the solids.

Table 6-6. Estimated volume changes per mole of clay mineral due to the pozzolanic reaction.

	educt side [cm ³]		product side [cm ³]	product minus educt side [cm ³]	
	solids volume	water volume	solids volume	total	only solids
China Clay	274	389	609	-54	335
Volclay	367	509	825	-51	458

¹ Porosity is calculated as the total water porosity with the assumption of zero air void content.

Figure 6-11. Development of total porosity in mixtures with compositions given in Table 6-5; the error bars correspond to the standard error of the mean, missing error bars indicate a single determination only.



As an example, the porosity loss (until cessation occurs) of a China Clay-lime mixture (50/40/100) will be estimated with the volume changes given in Table 6-6. The initial porosity is calculated from the amount of solids divided by their density ($50 \text{ g}/2.7 \text{ g cm}^{-3} + 40 \text{ g}/2.24 \text{ g cm}^{-3}$), giving the volume of the solids, and with the volume of water added: 36.4 cm^3 solids are in 100 cm^3 water, which is equal to a total initial porosity of 73% (water volume divided by total volume assuming that pores are fully saturated with water). According to Table 6-6, the China Clay reaction consumes 389 cm^3 of pore water and produces 335 cm^3 of additional solid volume, both per mole of China Clay. China Clay equivalent to 8% of an ignited mixture will dissolve until cessation occurs (Table 6-

2). The dissolved China Clay species in this mixture (ignited mass 73.3g) are equal to 0.026 moles and consume 10.1 cm³ of pore water (0.026 moles times 389 cm³ per mole) and produce 8.7 cm³ of new solid volume (0.026 moles times 335 cm³ per mole). That is, the solid volume is increased from 36.4 cm³ to 45.1 cm³ and the water volume decreased from 100 cm³ to 89.9 cm³, which equals a total porosity of 66% with the assumption of water saturated pores. The calculated porosity loss from 73% to 66% can explain about one third of the maximum measured one (lowest value is 53%). The other two thirds might be due to shrinkage effects and the closure of the pore entries by cement hydrates (cf. previous section). If pores are closed and not accessible to the mercury during the intrusion experiment, the measured porosity will be lower than the actual one.

6.2 Conclusions

- (i) Addition of lime to clay minerals leads to immediate microstructural changes and shifts in the aggregate size distribution of clay minerals to larger sizes (this is concluded from literature data [Ho & Handy, 1963; Caprez, 1984; Croce & Russo, 2003]).
- (ii) Between 30 to 60 days following mixing, the prepared clay-lime specimen showed coherence due to cementation by the pozzolanic reaction. This was concluded from phenomenological observations of the specimen but also during porosity measurements.
- (iii) In the observed time range of 48 to 182 days, a cessation of the pozzolanic reaction of clay minerals and lime is observed. This was concluded from (i) the observation that clay mineral and lime consumption was independent of the solid's mixing ratio and of reaction time in that time range and (ii) from visual observations by ESEM/REM. The aggregates' surfaces become overgrown with pozzolanic reaction products. This markedly slows down further dissolution of reactants, the solid products form a diffusion barrier.
- (iv) Mass balance calculations showed that calculated product compositions were in a realistic range and that cessation of the pozzolanic reaction occurred when about the same amount of silicon was released from the clay mineral. This silicon was assumed to be exclusively precipitated as the C-S-H gel that was detected by TA, XRD and ESEM. This gel is regarded to be most effective in the formation of an overgrowth phase. The measured decline in porosity was partially explained by these calculations. An exception is found for montmorillonite-lime mixtures. Calculated product compositions are only realistic, if an additional large sink for lime is assumed. This sink may be lime contained in the interlayer spaces of the mineral.
- (v) The reaction mechanisms could not be elucidated completely. An effect of different total surface areas through variation of the clay-lime mixing ratio was not observed. Reaction yield (mineral consumption) was proportional to the whole mixtures' sur-

faces. The similarity of (reactive) surface areas of clay minerals and lime might explain this. A specific edge surface area of $8.5 \text{ m}^2/\text{g}$ for a montmorillonite in suspension is given by Tournassat et al. (2003), which is very close to the specific surface area of $12.2 \text{ m}^2/\text{g}$ of the dry lime powder in this study. Nevertheless, the correlation of released silicon with the median particle diameter of the clay minerals implies some contribution of the clay minerals' edges. The primary fast reaction might be an adsorption/surface precipitation type of reaction. Lime is deposited on the clay mineral's surfaces, leading to the formation of aggregates. This lime is transformed with at the edges's released silicon and aluminium into C-S-H and AFm. Simultaneously, the formation of the reaction product shells around the aggregates starts and causes cessation of further dissolution. For the three clay minerals, cessation occurs when about the same volume of reaction products is accumulated on the aggregates surfaces (inferred from the porosity measurements). By analogy to the last stage of cement hydration, the pozzolanic reaction is expected to proceed further much more slowly under diffusion control. This is also implied by the usual observed strength increase of lime stabilised soils. This increase may continue for several years [e.g. Taylor & Arman, 1960].

7 Relevance of results to geotechnics

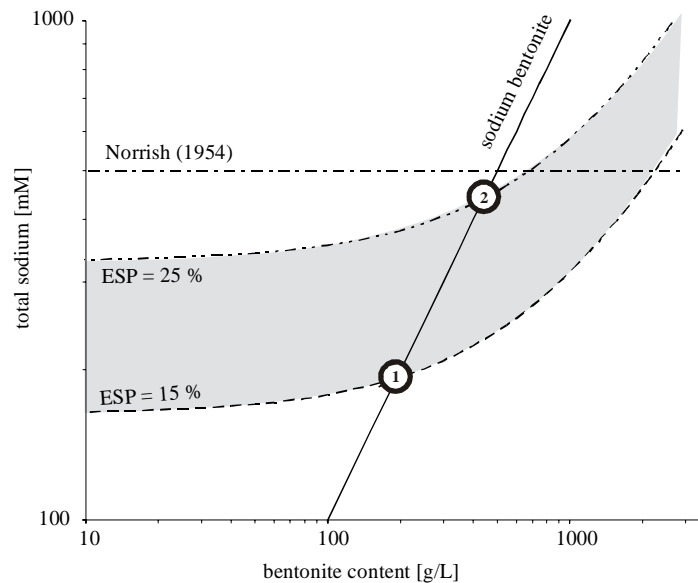
7.1 Pozzolanic reaction of clay minerals I: cation exchange, swelling and rheology

7.1.1 Cement-stable bentonites

When using a sodium bentonite in conjunction with cements or lime, it is desirable to utilise its beneficial properties and to prevent transformation to the calcium form with its unfavourable rheological properties, such as low dispersion stability and low yield point. Otherwise, a cheaper calcium bentonite would be preferred in the first place. This study has shown the importance of sodium-calcium cation exchange on describing the rheological behaviour of bentonite dispersions containing lime (note that Portland cement contains also a high proportion of lime). The solubility of lime defines the calcium concentration in solution. At a pH of 12.5, this calcium concentration is high (~20mM) and approximately constant. The sodium calcium cation exchange state of any bentonite dispersion containing lime will therefore mainly depend on the aqueous sodium concentration in the system. It follows that, for a fixed amount of sodium in the system, Na-Ca cation exchange state will depend on the water content or solid content of the bentonite dispersion. Loss of water will increase sodium in solution (but not calcium) and thereby also the amount of adsorbed sodium. The diagram in fig. 7-1 shows these interrelationships. It was calculated¹ from the isotherm data in Figure 5-1 on page 75 assuming that the relation obtained is independent of the bentonite's solid content (which may not be strictly true). The straight line "sodium bentonite" in fig. 7-1 shows the amount of sodium introduced to the system through the addition of a pure sodium montmorillonite with a CEC = 100 meq/100g. The two isolines show the total sodium concentration in the system necessary to maintain constant exchangeable sodium percentages (ESP) values of 15 and 25 % on the montmorillonite.

¹ These isolines for the exchangeable sodium percentage (ESP) were calculated from the sum of the sodium concentration in solution Na_{aq} [mM] and on the bentonite Na_{sorb} [meq/100g] multiplied with the solid content S [g/L], $Na_{tot} = Na_{aq} + Na_{sorb} \times S$, with Na_{sorb} for a specified ESP calculated from this ESP value and a total CEC [meq/100g], $Na_{sorb} = CEC \times ESP$.

Figure 7-1. Diagram showing the bentonite content versus the total amount of sodium (i) introduced through a pure sodium bentonite, (ii) necessary to maintain an exchangeable sodium percentage ESP of 15 or 25 % in the presence of lime.



The figure clearly shows that:

- (i) the cation exchange state in the presence of portlandite depends on the solid content of the bentonite as long as sodium is not added.
- (ii) without sodium additions, the montmorillonite reaches its ideal ESP at solid contents between point 1 and 2, i.e. between ~20 % and ~40 % bentonite content.
- (iii) below ~20% solid content, the additions of sodium necessary to obtain favourable ESP values may be read from the diagram.
- (iv) above ~40 % solid content, so much sodium is introduced to the system through the bentonite, that the boundary at 500 mM is crossed [Norrish, 1954]. From this point on, the effect observed on the yield point at an ESP of ~20% is expected to vanish due to volume decreases of the solids and the diffuse ion layer.

Such high solid contents of 20 to 40 % are not common for bentonite dispersions used in the construction industry. One can thus conclude that many dispersions used in conjunction with cements or lime would be, without sodium additions, in a cation exchange state that is calcium montmorillonite-like. In practical applications, additions are either applied in the form of soda (Na_2CO_3) or NaOH in order to raise the amount of adsorbed sodium. It is expected, that both additions might have similar effects on the rheology, but with quite different chemical mechanisms.

NaOH will increase pH, thereby decreasing the calcium concentrations in dispersion due to the decreased solubility of CH at higher pH [Duchesne & Reardon, 1995; Königsberger

et al., 1999]. This should favour desorption of calcium species from and adsorption of sodium onto the bentonite. To some extent, this might be impaired by the speciation of calcium as the fraction of CaOH^+ increases with pH.

Addition of Na_2CO_3 will force CaCO_3 to precipitate. The coexistence of portlandite and calcite markedly influences the calcium concentration, which will be governed by the partial pressure of CO_2 [Königsberger et al., 1999]. Total calcium concentration will be reduced from ~ 20 mM to values as low as 0.2 mM.

Interestingly, both additions act through the reduction of the aqueous calcium concentration. It was shown in this study that NaCl as an alternative sodium source can not improve rheological behaviour in a time relevant to practical applications (section 5.1.1). The cation exchange reaction is inhibited either due to a kinetic effect or to the irreversible sorption of calcium species at high pH. In order to avoid this inhibition, NaCl might be added to the bentonite dispersion prior to the cement addition. Taking into account all the sources of sodium immediately available in the system (bentonite, cement, water), the amount of NaCl needed can be estimated from fig. 7-1. It is worth mentioning here that the effects described might be modelled using common programs based on chemical equilibria and solubility data (except for the kinetic or irreversible effect).

In principle, the same conclusions apply to swelling soils, but also to such soils or bentonite dispersions containing gypsum or calcite instead of lime. CaSO_4 containing phases (gypsum) or calcite are very often present in natural systems. The main governing parameters are the CEC, the solubility of the Ca-containing phases, the partial pressure of CO_2 and the total amount of sodium and water present in the system.

These findings apply e.g. to the comparison of so-called activated calcium bentonites with natural sodium bentonite. Such activated bentonites were transformed by the addition of soda into a (partial) sodium bentonite, the released calcium is converted to calcite [Jas-mund & Lagaly 1993]. For a bentonite dispersion without calcite, the ESP value will remain more or less constant. For a dispersion with calcite however, the ESP value will increase with increasing solid content if sodium is only introduced through the bentonite. An activated bentonite is therefore expected to change its cation exchange state continuously to higher ESP values with increasing solid content. The activated bentonite contains calcite and will show a stronger dependency on solid content due to the continuous improvement of the ESP value.

7.2 Pozzolanic reaction of clay minerals II: dissolution, precipitation and pore refinement

7.2.1 Soil lime solidification

The results obtained allow conclusions to be drawn about the minimum lime content necessary for a sustainable and long-lasting lime-soil solidification. They may be also applicable to waste solidification problems with cement, as lime is always present in Portland cement and thought to be the major reaction partner of pozzolans in cements [Taylor, 1997]. The amount of lime necessary to obtain complete cementation and coating of the clay mineral-lime aggregates will be defined as the lime content sufficient for long-lasting solidification. The complete coating was reached when cessation of the pozzolanic reaction occurred. Consequently the lime contents (> 9%) determined in this study for three different clay minerals can be described as 'the sufficient lime content'. Thus the lime contents (~4%) defined as 'the lime fixation point' [Bergado, 1996] or minimal lime content [SN 640 503a] are not sufficient by far for achieving a sustainable solidification. Certainly, the influence of other grains that are always present in a soil (e.g. quartz grains in the silt fraction) and that may not participate in the pozzolanic reaction was not investigated. The presence of such relatively inert grains might lower the necessary lime content due to a dilution of the clay-lime mixture. By analogy to cement hydration however, it is inferred that the whole systems' surfaces are covered with reaction products. The interfacial zone between (inert) aggregate in concrete and the cement matrix is even of primary importance to the strength of the concrete as a whole [Taylor, 1997]. In order to prove this proposition, the effect of adding inert grains as e.g. quartz to clay-lime mixtures should be investigated.

7.2.2 Cut-off wall materials

The use of clay minerals in conjunction with cements raises some concern about the physico-chemical stability of clay minerals in the highly alkaline environment of cements. The results of this study show that clay minerals react significantly but not extensively until further dissolution is shut down. However, as clay contents in such barrier materials are usually high [Hermanns, 1993], the partial loss of these active components is not judged critical. It could not be established whether the dissolution proceeds slowly as long as lime is present, but it may be inferred from observed strength increases in soil-lime mixtures, which occurred for several years in some instances. It has to be emphasised when clay

mineral-lime aggregates become coated by cementitious reaction products, it will be these products that provide the direct sorption sites for contaminants diffusing into the barrier material. Only the slow diffusion of contaminants through these cementitious products will bring the contaminants into contact with the clay minerals. Efficiency of the sorption process in the whole barrier system is expected to be influenced mainly by the sorption behaviour of the cement hydrates. As those are also strong sorbents for many contaminants [Tits et al., 2006], the passivation of the active clay minerals' surfaces is not expected to critically affect the functionality of the technical barrier.

More important for permeation through the barrier is the pore refinement process associated with the pozzolanic reaction. Porosity, more precisely the main pore diameter [Hermanns, 1993], is closely related to permeability in such barrier materials and the lower these values are, the lower the transport of contaminants is. Marsh et al. (1985) demonstrated the effectiveness of fly ash substituted Portland cement on reducing the permeability. A 30% substitution of cement by fly ash resulted in a permeability reduction from $2 \times 10^{-12} \text{ m s}^{-1}$ in the control cement (no fly ash, only cement) to $4 \times 10^{-16} \text{ m s}^{-1}$ in the blended cement after 1 year. Historical sources even claim, that pozzolanic products grew out of the splices of underwater masonry [Ziegler, 2004], which indicates the dense nature of pozzolan-lime mortars.

For any substitution of cement by a pozzolan, it has to be emphasised that the higher the substituted fraction of cement is, the lower the lime content formed during cement hydration will be¹. Pore refinement potential due to the use of lime for the pozzolanic reaction will therefore be lower. So the options include (i) reducing the Portland cement content in barrier materials to as low values as necessary to fulfil given requirements for e.g. strength and (ii) adding lime in order to use the high pore refinement potential in the presence of high lime contents. Certainly, legal requirements should account for the slow progress of the pozzolanic reaction and the slow and difficult to quantify improvements of the parameter that is currently regulated as a minimum value by law (e.g. permeability).

¹ The hydration of tricalcium silicate may be used as an conservative estimate for the maximum lime content produced during cement hydration: $\text{C}_3\text{S} + 5.3\text{H} \rightarrow \text{C}_{1.7}\text{SH}_4 + 1.3\text{CH}$. From this equation and the data given in Table 3-4, it is calculated that up to 30% of CH may be produced from cement hydration. A mixture containing e.g. only 30% of cement, may then produce 9% of lime; i.e. lime becomes limiting for the pozzolanic reaction.

For example, prepared clay-lime specimens showed no strong cementation and coherence until after about one to two months.

However, by reducing the cement content in typical cut-off wall barrier materials, a common problem of such materials is also addressed. Barrier materials made of cement and clays are often too brittle to deform in the case of movement in the soil [Brinkmann, 2000]. Reducing the cement content should increase the contribution of the plastic deformation behaviour of the clays. The composite may be more adaptive to deformation. Ensuring a high pore refinement potential by the additional dosage of lime might ensure crack healing properties of these composites and continuous pore refinement due to the pozzolanic reaction. There must have been a reason why up to 43% of lime was mixed into mortars for the construction of underwater walls in e.g. the Netherlands in the 18th century, and this could provide an explanation.

8 Summary and outlook

8.1 Summary

The addition of lime to aqueous sodium-montmorillonite-dispersions results in a high aqueous calcium concentration and in the short-term in an equilibrium shift towards the calcium form of the montmorillonite. An intensifying effect due to the calcium speciation at high pH and preferred sorption of CaOH^+ appeared very probable. In either case, re-adsorption of sodium on lime-treated montmorillonite was hindered. The different sorption behaviour of the clay mineral's edge and outer surface sites on the one hand and interlayer sites on the other hand greatly influenced the crystalline swelling behaviour of the montmorillonite and the yield point of its dispersions. Calcium is preferentially sorbed into the interlayers and forces sodium to stay primarily on the outer surfaces of the clay mineral. Only after occupancy of these outer surfaces will sodium enter the interlayer space and cause interlayer expansion. These effects resulted in a significant increase of the dispersions' yield point at around 20% of adsorbed sodium. Further addition of sodium reduced the yield point again due to the contraction of interlayer space and of the diffuse ion layer in response to increasing ionic strength.

In practical applications, sodium-montmorillonite dispersions in the presence of lime are therefore in a calcium-montmorillonite-like state without additional sodium dosages. Even with subsequent sodium additions, this state is irreversibly fixed on the time-scale relevant for practical applications. Sodium salts, which reduce the calcium concentration in equilibrium with lime (e.g. Na_2CO_3 and NaOH), seem to be an exception. It is known from practice, that these salts are capable of increasing the yield point even after lime has been added. The inclusion of other sodium salts with no such effect (e.g. NaCl) prior to the addition of cement or lime would be an alternative approach to increase the dispersion's yield point. For this purpose, the necessary amount can be estimated from the cation exchange behaviour determined in this study.

The continuous dissolution of clay minerals in the presence of lime leads, in the long-term, to the cementation of the materials. The cementation has proceeded after one to two months until the surfaces of the clay mineral-lime aggregates were completely covered with reaction products. This led to the cessation of the dissolution reaction. Whether dissolution proceeds further after the seven months investigated (e.g. through the development of steady-state diffusion profiles), was not resolved in this study. In analogy to long-term investigations on the strength development of lime-stabilised soils, this seems however very probable. In either case, the precipitation of reaction products led to a reduction of porosity as a result of the filling or closure of the macro- respectively interaggregate pores. Mass balance calculations allowed reaction equations to be estimated for the three clay minerals. These equations show, that the composition of the reaction products is realistic in comparison with data from the literature and that a major part of the measured porosity reduction can be ascribed to the pozzolanic reaction.

It follows with respect to soil solidification techniques, at least for fine grained soils with mainly clay minerals, that the lime fixation point as defined for soil improvement (~4%) is not sufficient by far for a sustainable, long-lasting solidification. At least 9% of lime for illite and 11% for kaolinite have to be added in order to solidify the material sustainably. For montmorillonite, the necessary lime content is even 20%. Only a fraction of this 20% is actually used for the solidification by the pozzolanic reaction. However, the size of this fraction and the nature of the sink for the rest of the lime was not determined. Therefore, implications of this significantly increased lime demand can not be discussed with the results obtained.

With respect to barrier materials rich in clay minerals, it follows that no extensive dissolution of these active components is to be expected. The content of the three clay minerals was reduced in the first three to seven months by 7% to 9% in absolute terms which is not judged critical due to the usually higher clay mineral contents. Much more crucial for the choice of clay minerals as active components in barrier materials is the passivation of their reactive surfaces. Contaminants entering the barrier can only contact the clay minerals' surfaces by slow diffusion through the overgrown reaction products (cement hydrates). This has to be considered for the design of engineered barriers. The retention of contaminants by cement hydrates is therefore an important issue for such barrier materials next to their pore-filling and permeability-reducing properties.

For mixtures of clay and cement in general, there are consequences for further necessary lime addition in some instances. If the cement content in the mixture is chosen to be low (< 30%), the lime content produced during cement hydration (< 9%) may become limiting for the pozzolanic reaction. Thus, additional benefits arising from the cementing and pore refinement potential of the pozzolanic reaction can not be fully used. In that case, lime addition to the clay-cement mixture should be carried out.

8.2 Outlook

Methodology

- (i) One methodological goal of this study was the quantitative determination of clay minerals' content against an internal standard, without the need for calibration. This goal would simplify quantitative mineral analysis substantially, and might improve accuracy of results even in complicated studies. Such studies could be the observation of mineral reactions where structural parameters of minerals change while the reaction proceeds. In this case, traditional methods (which make use of calibration) might fail due to changes in the mineral's diffraction pattern. This study has shown that much more work on the real structures of clay minerals has to be done. Even for portlandite with a relative simple structure, quantification without calibration was not possible against the internal standard calcite. The use of flexible structure models developed in this study can account for a simplified, idealised description of translational disorder and anisotropic broadening of diffraction lines. The implementation of several (constrained) flexible structure models into existing subphase models is a promising way in order to improve quality of the fitting procedure. This should be subject to further work.
- (ii) This study has also shown that accuracy and precision of results obtained on weakly pozzolanic materials (such as clay minerals) should be improved. This could be done by inclusion of additional data on the chemistry of the extracted solutions and on the water bound inside the reaction products. Together with obtained results on portlandite and clay mineral consumption, an overdetermined equation system could be set up with all the information from the various analytical techniques. Solution of these equations substantially improves results [Allmann, 2003]. In order to determine the chemistry of the extracted solutions, the extractant should be changed (e.g. acid) to ease the analysis of the aqueous solution composition. The total amount of the cementitious reaction products may be determined by the non-evaporable water as termed in cement chemistry [Taylor, 1997].

Pozzolanic reaction of clay minerals I

- (i) The question whether a portlandite surface coating or the kinetically slow desorption of CaOH^+ species were responsible for the hindered sodium adsorption on lime-treated montmorillonite will be difficult to address. This question is probably also related to the open question on the nature of the calcium sink in the montmorillonite-

lime pozzolanic reaction. Long-term adsorption experiments could help to investigate whether the observed effect is due to reversible (adsorption) or irreversible (precipitation) processes. However, this will be complicated by the progression of clay mineral dissolution and the parallel cement hydrate precipitation, which was already indicated after four days. Spectroscopic techniques which are able to determine the chemical environment of calcium might offer a possibility for distinction of adsorbed or precipitated calcium. In either case, the separation of the two mineral compartments by dialysis bags is an appropriate way to investigate processes on montmorillonite in a lime-equilibrated system. Inclusion of a third empty dialysis bag helps to clarify whether calcium is solely sorbed on the montmorillonite surfaces or is also precipitated from the aqueous solution. Additionally, analysis of the lime's surfaces would give information on the precise passivation mechanism.

- (ii) With respect to practical applications, the cation exchange and rheological behaviour of different types of bentonites should be investigated in the presence of lime and also the temperature dependency of these phenomena. This would clarify if different bentonites behave in a similar way. Then, the amount of sodium needed in order to increase the yield point of bentonite dispersions is predictable in practical applications.

Pozzolanic reaction of clay minerals II

- (i) The proposition that C-S-H is the major phase responsible for the passivation observed could be addressed by using clay minerals of different chemistry and silicon content. Using magnesio- (e.g. serpentine minerals or talcum) instead of aluminosilicates could give additional information. Otherwise, this might be circumvented by reaction products of magnesium (magnesium hydroxide type minerals), which are also probable passivating phases.
- (ii) There are still open questions regarding the pozzolanic reaction progress of clay minerals: how does the reaction proceed in mixtures of different clay minerals? How does it proceed in the presence of Portland cement? And how would the presence of diluting mineral phases (e.g. silt grains of quartz), which hardly dissolve but also offer nucleation sites for pozzolanic reaction products, affect the reaction? How long does the reaction proceed, is it finished after six to seven months or does it continue and if, for how long is this significant? All these questions should be addressed in further research in order to reach the final goal of modelling clay-lime interactions in complex environmental geotechnical systems including soils or barrier materials. Then, questions concerning the minimum lime content in soil solidification or mixture design of barrier materials can be answered. Investigations can be performed using the methodology proposed in this study.

Bibliography

- ABEND S. and LAGALY G. (2000): Sol-Gel Transitions of Sodium Montmorillonite Dispersions. *Applied Clay Science*, 16(3-4):201-227.
- ALLMANN R. (2003): Röntgen-Pulverdiffraktometrie: Rechnergestützte Auswertung, Phasenanalyse und Strukturbestimmung. Berlin; Heidelberg: Springer-Verlag.
- ALTHER G.R. (1986): The Effect of Exchangeable Cations on the Physico-Chemical Properties of Wyoming Bentonites. *Applied Clay Science*, 1:273-284.
- AMANN P. (1997): Injektionen. In.: Weiterbildungskurs Institut für Geotechnik, ETH Zürich.
- AMBROISE J., GNIEWEK J., DEJEAN J. and PERA J. (1987): Hydration of Synthetic Pozzolanic Binders Obtained by Thermal-Activation of Montmorillonite. *American Ceramic Society Bulletin*, 66(12):1731-1733.
- AMBROISE J., MURAT M. and PERA J. (1985): Hydration Reaction and Hardening of Calcined Clays and Related Minerals. Extension of the Research and General Conclusions. *Cement Concrete Research*, 15(2):261-268.
- ARUJA E. (1960): Unit Cell and Space-Group Determination of Tetra-Calcium and Di-Calcium Aluminate Hydrates. *Acta Crystallographica*, 13(12):1018-1018.
- ARUJA E. (1961): Unit Cell and Space Group of $4\text{CaO} \cdot \text{Al}_2\text{O}_3 \cdot 19\text{H}_2\text{O}$ Polymorphs. *Acta Crystallographica*, 14(12):1213.
- ATKINS A. (1994): Physical Chemistry, 5th edn: New York : Freeman.
- BAERLOCHER C. (1993): Restraints and Constraints in Rietveld Refinement. In: *The Rietveld Method*. Edited by Young R.A. New York: Oxford University Press.
- Baes C.F. and Mesmer R.E. (1976): The hydrolysis of Cations. Wiley.
- BAUER A. and BERGER G. (1998): Kaolinite and Smectite Dissolution Rate in High Molar KOH Solutions at 35° and 80°C. *Applied Geochemistry*, 13(7):905-916.
- BERGADO D.T., ANDERSON L.R., MIURA N. and BALASUBRAMANIAM A.S. (1996): Soft Ground Improvement in Lowland and Other Environments. New York: American Society of Civil Engineers.
- BERGER G., BEAUFORT D. and LACHARPAGNE J.C. (2002): Experimental Dissolution of Sanidine under Hydrothermal Conditions: Mechanism and Rate. *American Journal of Science*, 302(8):663-685.
- BERGMANN J., FRIEDEL P. and KLEEBOEG R. (1998): BGMN - A New Fundamental Parameters Based Rietveld Program for Laboratory X-Ray Sources, It's Use in Quantitative Analysis and Structure Investigations. *Commission of Powder Diffraction, International Union of Crystallography, CPD Newsletter*, No. 20:5-8.

- BIERNACKI J.J., WILLIAMS P.J. and STUTZMAN P.E. (2001): Kinetics of Reaction of Calcium Hydroxide and Fly Ash. *ACI Materials Journal*, 98(4):340-349.
- BISH D.L. and REYNOLDS J. (1989): Sample Preparation for X-Ray Diffraction. In: *Modern Powder Diffraction*. Edited by Bish D.L., Post J.E., Vol. 20. Washington D.C.: Mineralogical Society of America: 101-145.
- BISH D.L. and VON DREELE R.B. (1989): Rietveld Refinement of Non-Hydrogen Atomic Positions in Kaolinite. *Clays and Clay Minerals*, 37(4):289-296.
- BODINE M.W. and FERNALLD T.H. (1973): EDTA Dissolution of Gypsum, Anhydrite, and Ca-Mg Carbonates. *Journal of Sedimentary Petrology*, 43(4):1152-1156.
- BONACCORSI E., MERLINO S. and TAYLOR H.F.W. (2004): The Crystal Structure of Jennite, $\text{Ca}_9\text{Si}_6\text{O}_{18}(\text{OH})_6 \cdot 8\text{H}_2\text{O}$. *Cement Concrete Research*, 34(9):1481-1488.
- BORCHARDT G. (1989): Smectites. In: *Minerals in Soil Environment. 2nd Ed.* Edited by Dixon J.B., Weed S.B. Madison, WI: Soil Science Society of America.
- BRANDL H. (1981): Alteration of Soil Parameters by Stabilization with Lime. In: *Proc. 10th Intl. Conf. Soil Mech. and Found. Eng'g., Stockholm: 1981: 587-594.*
- BRINDLEY G.W. and BROWN G. (eds.) (1980): Crystal Structures of Clay Minerals and their X-Ray Identification: Mineralogical Society. London United Kingdom. 1980.
- BRINKMANN A. (2000): Untersuchungen zum mechanischen Verhalten von Ton-Zementgebundenem Dichtwandmaterial für das Zweiphasenverfahren. *PhD Thesis*. Zürich: ETH.
- BROMS B.B. (1984): Stabilization of Soft Clay with Lime Columns. In: *Proc. Seminar on Soil Improvement and Construction Techniques in Soft Ground: 1984; Nanyang Technological Institute, Singapore.*
- BURROUGHS V.S. (2001): Quantitative Criteria for the Selection and Stabilisation of Soils for Rammed Earth Wall Construction. *PhD Thesis*.: University of New South Wales.
- CAPREZ, M. (1984): Stabilisierung mit Zement oder Kalk. Mitteilung 109 der SGBF.
- CASEY W.H. (1995): Surface Chemistry During the Dissolution of Oxide and Silicate Minerals. In: *Mineral Surfaces*. Edited by Vaughan D.J., Patrick R.A.D. London: Chapman & Hall.
- CHAIX-PLUCHERY O., PANNETIER J. and BOUILLOT J. (1987): Prereactional Transformations in $\text{Ca}(\text{OH})_2$. *Journal of Solid State Chemistry*, 67:225-234.
- CNR (2005) [Il molo. Consiglio Nazionale della Ricerca (CNR). Istituto di Cibernetica. <http://www.cib.na.cnr.it/CampiFlegrei/pozzuoli/molo.html>.]
- COOK R.A. and HOVER K.C. (1999): Mercury Porosimetry of Hardened Cement Pastes. *Cement and Concrete Research*, 29:933-943.

- COUTURE R.A. (1985): Steam Rapidly Reduces the Swelling Capacity of Bentonite. *Nature*, 318(6041):50-52.
- COWTAN K. (2005): BGMN - Coordinate Systems, Operators, and Transformations. *Commission on Crystallographic Computing, International Union of Crystallography, Newsletter No. 6, September 2005*:52-59.
- CROCE P. and RUSSO G. (2003): Soil-Water Characteristic Curves of Lime-Stabilised Soils. In: *Int. Workshop on Geotechnics of Soft Soils - Theory and Practice: 2003; Noordwijkerhout, Netherlands*: VGE.
- CSA A23.2-28a: Standard Practice for Laboratory Testing to Demonstrate the Effectiveness of Supplementary Cementing Materials and Chemical Admixtures to Prevent Alkali-Silica Reaction in Concrete. Canadian Standards Association.
- DAMIDOT D. and GLASSER F.P. (1995): Investigation of the CaO-Al₂O₃-SiO₂-H₂O System at 25°C by Thermodynamic Calculations. *Cement Concrete Research*, 25(1):22-28.
- DE SILVA P.S. and GLASSER F.P. (1992): Pozzolanic Activation of Metakaolinite. *Advances in Cement Research*, 4(16):167-178.
- DIAMOND S. and KINTER E.B. (1965): Mechanisms of Soil-Lime Stabilisation. *Highway Research Record*, 92:83-95.
- DIAMOND S. (1970): Pore Size Distributions in Clays. *Clays and Clay Minerals*, 18:7-23.
- DIAMOND S., WHITE JOE L. and DOLCH W.L. (1963): Transformation of Clay Minerals by Calcium Hydroxide Attack. In: *Clays and Clay Minerals, 12th Natl. Conf., Atlanta, GA, 1963, Proc.: 1963*: 359-379.
- DIN 1060-1:1995-03: Baukalk: Definitionen, Anforderung, Überwachung.
- DOSCH W. (1967): Interlamellar Reactions of Tetracalcium Aluminate Hydrates with Water and Organic Compounds. In: *Clays and Clay Minerals, 15th Natl. Conf., Pittsburgh, Pennsylvania, 1967, Proc.: 1967*: 121-142.
- DUCHESNE J. and REARDON E.J. (1995): Measurement and Prediction of Portlandite Solubility in Alkali Solutions. *Cement Concrete Research*, 25(5):1043-1053.
- DUNSTER A.M., PARSONAGE J.R. and THOMAS M.J.K. (1993): The Pozzolanic Reaction of Metakaolinite and Its Effects on Portland-Cement Hydration. *Journal of Materials Science*, 28(5):1345-1350.
- EADES J.L. and GRIMM R.E. (1960): Reaction of Hydrated Lime with Pure Clay Minerals in Soil Stabilization. *Bulletin No 262, Highway Research Board*:51-63.
- EMMERICH K. (2000): Die Geotechnische Bedeutung des Dehydroxylierungsverhaltens quellfähiger Tonminerale. IGT Band 213. *PhD Thesis*. Zürich: ETH.
- FRANCOIS M., RENAUDIN G. and EVRARD O. (1998): A Cementitious Compound with Composition 3CaO Al₂O₃ CaCO₃ 11H₂O. *Acta Crystallographica C*, 54(9):1214-1217.

- GAO H.X. and PENG L.M. (1999): Parameterization of the Temperature Dependence of the Debye-Waller Factors. *Acta Crystallographica A*, 55:926-932.
- GARTNER E.M., GAIDIS J.M. and GRACE W.R. (1989): Hydration Mechanisms, I. In: *Materials Science of Concrete I*. Edited by Skalny J.P. Westerville, OH: American Ceramic Society.
- GHORAB H.Y., ABDELALIM A.M.K. and AHMED O.M. (1991): Hardening Characteristics of some Clay-Minerals. *Zement-Kalk-Gips*, 44(11):578-581.
- GILES D.E., RITCHIE I.M. and XU B.A. (1993): The Kinetics of Dissolution of Slaked Lime. *Hydrometallurgy*, 32(1):119-128.
- GLENN G.R. and HANDY R.L. (1963): Lime-Clay Mineral Reaction Products. *Highway Research Board Record*, 29:240-249.
- GUGGENHEIM S. and VAN GROOS A.F.K. (2001): Baseline Studies of the Clay Minerals Society Source Clays: Thermal Analysis. *Clays and Clay Minerals*, 49(5):433-443.
- HASENPATT R., DEGEN W. and KAHR G. (1989): Flow and Diffusion in Clays. *Applied Clay Science*, 4(2):179-192.
- HASLAM R.T., CALINGAERT G. and TAYLOR C.M. (1924): The Hydrates of Lime. *Journal of the American Chemical Society*, 46:308-311.
- HE C. (1994a): Thermal Stability and Pozzolanic Activity of Calcined Clays. In: *16th General Meeting of the International Mineralogical Association (abstracts): 1994b*: 169-170.
- HE C., MAKOVICKY E. and OSBAECK B. (1994b): Thermal Stability and Pozzolanic Activity of Calcined Kaolin. *Applied Clay Science*, 9(3):165-187.
- HE C., MAKOVICKY E. and OSBAECK B. (1995): Thermal Stability and Pozzolanic Activity of Calcined Illite. *Applied Clay Science*, 9(5):337-354.
- HE C., MAKOVICKY E. and OSBAECK B. (1996a): Thermal Treatment and Pozzolanic Activity of Na- and Ca-Montmorillonite. *Applied Clay Science*, 10(5):351-368.
- HE C., MAKOVICKY E. and OSBAECK B. (1996b): Thermal Treatment and Pozzolanic Activity of Sepiolite. *Applied Clay Science*, 10(5):337-349.
- HE C., MAKOVICKY E. and OSBAECK B. (2000): Thermal Stability and Pozzolanic Activity of Raw and Calcined Mixed-Layer Mica/ Smectite. *Applied Clay Science*, 17(3-4):141-161.
- HEATHCOTE K.A. (1995): Durability of Earthwall Buildings. *Construction and Building Materials*, 9(3):185-189.
- HEIDE M., BÖTTGER K.G. and KNÖFEL D. (1996): Reaktivität von Gebrannten Tonen in Weisskalkhydrat. In: *Werkstoffwissenschaften und Bauinstandsetzen, Berichtsband zum Vierten Internationalen Kolloquium, Band 2*. Edited by Wittmann F.H., Gerdes A.: 817-835.

- HERMANN R. (1993): Sicherung von Altlasten mit Vertikalen Mineralischen Barrieresystemen im Zweiphasen-Schlitzwandverfahren. IGT Band 204. *PhD Thesis*. Zurich: ETH.
- HERMANN R. and BUCHER F. (1990): Sicherung von Altlasten durch Vertikale Künstliche Barrieren. *Zeitschrift der Deutschen Geologischen Gesellschaft*, 141:348-353.
- HERMANN STENGELE R. (2005): Einsatz der Mischungsverfahren im Raum Zürich. In.: Baugrundverbesserung - Weiterbildungskurs Institut für Geotechnik, ETH Zürich.
- HERMANN STENGELE R. and PLÖTZE M. (2000): Suitability of Minerals for Controlled Landfill and Containment. *EMU Notes in Mineralogy*, 2:291-331.
- HERZOG A. and MITCHELL J.K. (1962): X-Ray Evidence for Cement-Clay Interactions. *Nature*, 195:989-990.
- HERZOG A. and MITCHELL J.K. (1963): Reactions Accompanying Stabilization of Clay with Cement. *Highway Research Board Record*, 36:146-171.
- HIGHT R., SCHMIDT P.W., DARLEY H.C.H. and HIGDON W.T. (1962): Small Angle X-Ray Scattering from Montmorillonite Clay Suspensions. *Journal of Chemical Physics*, 37(3):502.
- HILL R.J. and MADSEN I.C. (1987): Data Collection Strategies for Constant Wavelength Rietveld Analysis. *Powder Diffraction*, 2(3):146-162.
- HILT G.H. and DAVIDSON D.T. (1960): Lime Fixation in Clayey Soils. *Bulletin No 262, Highway Research Board, Washington DC*:20-32.
- HILT G.H. and DAVIDSON D.T. (1961): Isolation and Investigation of a Lime-Montmorillonite Crystalline Reaction Product. *Bulletin No 304, Highway Research Board, Washington DC*:51-64.
- HO C. and HANDY R.L. (1963): Electrokinetic Properties of Lime-Treated Bentonites. In: *Clays and Clay Minerals, 12th Natl. Conf., Atlanta, GA, 1963, Proc.: 1963*: 267-281.
- HOFMEISTER F. (1888): On the Understanding of the Effects of Salts. *Arch. Exp. Pathol. Pharmakol. (Leipzig)*, 24: 247-260.
- HUDER J. (1972): Stability of Bentonite Slurry Trenches with Some Experiences in Swiss Practice. In: *5. Europ. Conf. Soil Mech. and Found. Eng'g.: 1972; Madrid*: 517-522.
- HULL A.W. (1919): A New Method of Chemical Analysis. *Journal of the American Chemical Society*, 41:1168-1175.
- ICSD - Inorganic Crystal Structure Database [<http://www.fiz-informationsdienste.de/en/DB/icsd/>]

- JACKSON M. (2004): Reactive Components of Roman Pozzolane in the Pozzolanitic Cements of Ancient Rome. In: *Annual Meeting Geological Society of America: 2004; Denver, CO*: 308.
- JASMUND K. and LAGALY G. (eds.) (1993): Tonminerale und Tone: Struktur, Eigenschaften, Anwendungen und Einsatz in Industrie und Umwelt. Darmstadt: Steinkopff.
- JESCHKE A.A. and DREYBRODT W. (2002): Dissolution Rates of Minerals and their Relation to Surface Morphology. *Geochimica Cosmochimica Acta*, 66(17):3055-3062.
- JOHANNSEN K. and RADEMACHER S. (1999): Modelling the Kinetics of Calcium Hydroxide Dissolution in Water. *Acta hydrochimica hydrobiologica*, 27(2):72-78.
- KAHR G. and PLÖTZE M. (2000): Korngrößenmessung von Tonen mit dem Quecksilberdruckporosimeter? In: *Tone in der industriellen Anwendung. Beiträge zur Jahrestagung der DTTG, Band 8: 2000; Limburg*.
- KARSTEDT J. (1980): Untersuchungen zum aktiven räumlichen Erddruck in rolligem Boden bei hydrostatischer Stützung der Erdwand. *PhD Thesis*.
- KLEMM W.A. (1989): Cementitious Materials: Historical Notes. In: *Materials Science of Concrete I*. Edited by Skalny J.P. Westerville, OH: American Ceramic Society.
- KLUG H.P. and ALEXANDER L.E. (1974): X-Ray Diffraction Procedures for Polycrystalline and Amorphous Materials. 2nd Ed. New York: Wiley.
- KÖNIGSBERGER E., KÖNIGSBERGER L.-C. and GAMSJAGER H. (1999): Low-Temperature Thermodynamic Model for the System $\text{Na}_2\text{CO}_3\text{-MgCO}_3\text{-CaCO}_3\text{-H}_2\text{O}$. *Geochimica Cosmochimica Acta*, 63(19-20):3105-3119.
- KÖSTER H.M., KOHLER E.E., KRAHL J., KROEGER J. and VOGT K. (1973): Veränderungen am Montmorillonit durch Einwirkung von 0,1 M EDTA-Lösungen, 1 N NaCl-Lösung und 0,1 N Salzsäure. In: *Neues Jahrbuch fuer Mineralogie. Abhandlungen*. Vol. 119: E. Schweizerbart'sche Verlagsbuchhandlung. Stuttgart Federal Republic of Germany: 83-100.
- KRAEHENBUEHL F., STOECKLI H., BRUNNER F., KAHR G. and MULLER-VONMOOS M. (1987): Study of the Water-Bentonite System by Vapour Adsorption, Immersion Calorimetry and X-Ray Techniques: I. Micropore Volumes and Internal Surface Areas, Following Dubinin's Theory. *Clay Minerals*, 22:1.
- KRAUS W. and NOLZE G. (2000): Powdercell for Windows. [http://www.bam.de/service/publikationen/powdercell_i.htm]
- LAGALY G. (1981): Characterization of Clays by Organic-Compounds. *Clay Minerals*, 16(1):1-21.
- LAGALY G. (1989): Principles of Flow of Kaolin and Bentonite Dispersions. *Applied Clay Science*, 4(2):105-123.

- LAGALY G., SCHULZ O. and ZIMEHL R. (eds.) (1997): Dispersionen und Emulsionen: Eine Einführung in die Kolloidik feinverteilter Stoffe einschliesslich der Tonminerale. Darmstadt: Steinkopff.
- LANG H.-J. (1989): Preface. *Applied Clay Science*, 4(2):95.
- LIEBIG E. (1997): Gebrannte Tonminerale und Trassmehle als puzzolanische Komponenten in Kalkmörteln. *PhD Thesis*. Universität Karlsruhe.
- LIEBIG E. and ALTHAUS E. (1997): Kaolinite and Montmorillonite as Pozzolanic Components in Lime Mortars - Untreated and after Thermal Activation. *Zement-Kalk-Gips*, 50(5):282-290.
- MACKENZIE R.C. (1951): A Micromethod for Determination of Cation-Exchange Capacity of Clay. *Journal of Colloid Science*, 6:219-222.
- MADSEN F.T. and MÜLLER-VONMOOS M. (1989): The Swelling Behaviour of Clays. *Applied Clay Science*, 4(2):143-156.
- MALHORTA V.M. and MEHTA P.K. (1996): Pozzolanic and Cementitious Materials: Lightning Source Inc.
- MAMY J. and GAULTIER J.P. (1976): Les Phenomenes De Diffraction des Rayonnements X et Electroniques par les Reseaux Atomiques; Application a l'etude de l'ordre Cristallin dans les Mineraleux Argileux. Evolution Structurale de la Montmorillonite Associee au Phenomene de Fixation Irreversible du Potassium. *Annales agronomiques*, 27(1):1-16.
- MARCUS Y. (1985): Ion Solvation: John Wiley and Sons Ltd.
- MARSH B.K., DAY R.L. and BONNER D.G. (1985): Pore Structure Characteristics Affecting the Permeability of Cement Paste Containing Fly Ash. *Cement Concrete Research*, 15(6):1027-1038.
- MEHTA P.K. and MONTEIRO O.J.M. (1993): Concrete: Microstructure, Properties and Materials: McGraw Hill.
- MERLINO S., BONACCORSI E. and ARMBRUSTER T. (1999): Tobermorites: Their Real Structure and Order-Disorder (Od) Character. *American Mineralogist*, 84(10):1613-1621.
- MERMUT A.R. and CANO A.F. (2001): Baseline Studies of the Clay Minerals Society Source Clays: Chemical Analyses of Major Elements. *Clays and Clay Minerals*, 49(5):381-386.
- MEZGER T. (2000): Das Rheologie-Handbuch. Hannover: Vincentz Verlag.
- MITCHELL J.K. and DERMATAS D. (1992): Clay Soil Heave Caused by Lime-Sulfate Reactions, Innovations and Uses of Lime. *ASTM STP 1135, DD Walker, Jr, TB Hardy, DC Hoffman, and DD Stanley, Eds American Society for Testing and Materials, Philadelphia:41-64.*

- MOORE D.M. and REYNOLDS R.C. (1997): X-Ray Diffraction and the Identification and Analysis of Clay Minerals: Oxford University Press.
- MÜLLER C.J., DELVILLE A., KAHR G., PLÖTZE M. and HERMANN STENGELE R.H. (2002): Quantitative Mineral Analysis of Clays - an Approach with Rietveld Analysis. In: *Clay Minerals Society 39th Annual Meeting (CMS2002)*; Boulder, CO.
- MÜLLER C.J., DELVILLE A., KAHR G. and PLÖTZE M. (2004a): Interlayer Cation Arrangement and Hydration Shells in Sodium and Calcium Montmorillonite obtained by Monte Carlo Simulations. In: *Clay Minerals Society 41st Annual Meeting (CMS2004)*: 2004; Richland, WA.
- MÜLLER C.J., DELVILLE A., KAHR G. and PLÖTZE M. (2004b): Surface Complexes of Sodium and Calcium on Montmorillonite obtained by Monte Carlo Simulations. In: *The Third International Conference "Interfaces Against Pollution" 2004*: 2004; Jülich, Germany.
- MÜLLER C.J. and PLÖTZE M. (2005): Flexible structure models applied to swelling montmorillonite. In: Reiner Dohrmann R. and Kaufhold S. (Eds.): *Berichte der DTTG Bd.11, Beiträge zur Jahrestagung Celle*: 41-46.
- MÜLLER-VONMOOS M., BUCHER F., KAHR G., MADSEN F. and MAYOR P.-A. (1991): Wechsellagerung und Quellverhalten von Kalium-Bentoniten. In: Baden (Schweiz): NAGRA: 44.
- MÜLLER-VONMOOS M. and LOKEN T. (1989): The Shearing Behaviour of Clays. *Applied Clay Science*, 4(2):125-141.
- MURAT M. (1983): Hydration Reaction and Hardening of Calcined Clays and Related Minerals. Preliminary Investigation on Metakaolinite. *Cement Concrete Research*, 13(2):259-266.
- MURPHY W.M., OELKERS E.H. and LICHTNER P.C. (1989): Surface Reaction Versus Diffusion Control of Mineral Dissolution and Growth Rates in Geochemical Processes. *Chemical Geology*, 78(3-4):357-380.
- NORRISH K. (1954a): Manner of Swelling of Montmorillonite. *Nature*, 173(4397):256-257.
- NORRISH K. (1954b): The Swelling of Montmorillonite. *Discussions of the Faraday Society*, (18):120-134.
- NORRISH K. and QUIRK J.P. (1954): Crystalline Swelling of Montmorillonite - Use of Electrolytes to Control Swelling. *Nature*, 173(4397):255-256.
- NÜESCH R. (1992): Das Mikrogefüge in Tongesteinen. In: *Tonmineralogie für die Geotechnische Praxis*. Edited by Gartung E.: LGA, Heft 64: 35-44.
- OATES J.A.H. (1998): Lime and Limestone, 1. edn. Weinheim: Wiley-VCH.
- OKAMURA T. and TERASHI M. (1975): Deep Lime Mixing Method of Stabilisation for Marine Clays. In: *Proc. 5th Asian Reg. Conf. Soil Mech. and Found. Eng'g., Bangalore, India: 1975*: 69-75.

- PARKER S.P. (ed.) (1997): McGraw Hill Dictionary of Earth Science. New York: McGraw Hill.
- PARKHURST D. L. and APPELO C. A. J. (1999). Phreeqc2 User's Manual and Program, U.S. Geological Survey. [<http://www.geo.vu.nl/users/posv/phreeqc/index.html>]
- PENNER D. (1998): Das Aggregationsverhalten von Montmorillonitdispersionen unter dem Einfluss organischer und anorganischer Elektrolyte. *PhD Thesis.*: University Kiel.
- PETCH H.E. (1961): Hydrogen Positions in Portlandite, $\text{Ca}(\text{OH})_2$, as indicated by Electron Distribution. *Acta Crystallographica*, 14(9):950-&.
- PLÖTZE M. and KAHR G. (2003): Swelling Pressure and Suction of Clays. In: *Euroclay Proc.: 2003; Modena: 228-229.*
- POINSSOT C., BAEYENS B. and BRADBURY M.H. (1999): Experimental and Modelling Studies of Caesium Sorption on Illite. *Geochimica Cosmochimica Acta*, 63(19-20):3217-3227.
- PÖLLMANN H. (1991): Solving X-Ray Powder Pattern Problems Dealing with Layer Structures in the Field of Calcium Aluminum Hydroxy Salts. *Materials Science Forum*, 79-82:679-684.
- Powder Diffraction File (PDF), Copyright by International Centre for Diffraction Data (ICDD).
- POWERS, T.C. and BROWNYARD, T.L. (1948): Studies on the Physical Properties of Hardened Portland Cement Paste (Bull. 22), 992pp., Portland Cement Association, Chicago, IL; reprinted from *Journal of the American Concrete Institute (Proc.)* (1947) 43.
- PREZZI M., MONTEIRO P.J.M. and SPOSITO G. (1997): The Alkali-Silica Reaction - Part 1: Use of the Double-Layer Theory to Explain the Behaviour of Reaction-Product Gels. *ACI Materials Journal*, 94(1):10-17.
- PREZZI M., MONTEIRO P.J.M. and SPOSITO G. (1998): Alkali-Silica Reaction - Part 2: The Effect of Chemical Admixtures. *ACI Materials Journal*, 95(1):3-10.
- PUIGDOMENECH I. (2000): Windows Software for the Graphical Presentation of Chemical Speciation. In: *219th ACS National Meeting. Abstracts of Papers: March 26-30 2000; San Francisco, CA: U760-U760.*
- PULSFORT M. and WALZ B. (2000): Skriptum zur Vorlesung: Spezialgrundbau, Teil A - Schlitzwandbauweise. In. Bergische Universität, Gesamthochschule Wuppertal.
- QUIRK J.P. (2001): The Significance of the Threshold and Turbidity Concentrations in Relation to Sodicity and Microstructure. *Australian Journal of Soil Research*, 39(6):1185-1217.
- RAPIN J.-P. and FRANCOIS M. (2001): The Double-Layered Hydroxide $3\text{CaO} \cdot \text{Al}_2\text{O}_3 \cdot 0.5\text{CaBr}_2 \cdot 0.5\text{CaCl}_2 \cdot 10\text{H}_2\text{O}$. *Acta Crystallographica C*, 57(2):137-138.

- RAPIN J.-P., NOOR N.M. and FRANCOIS M. (1999a): The Double Layered Hydroxide $3\text{CaO Al}_2\text{O}_3 \text{ CaBr}_2 \cdot 10\text{H}_2\text{O}$. *Acta Crystallographica C*, 55(8):.
- RAPIN J.-P., RENAUDIN G., ELKAIM E. and FRANCOIS M. (2000): Synchrotron Powder Diffraction Study of the Structural Phase Transition of Friedel Salt $\text{Ca}_2\text{Al}(\text{OH})_6^+\text{Cl}^- \cdot 2\text{H}_2\text{O}$. *Acta Crystallographica A*, 56(1):348.
- RAPIN J.-P., WALCARIUS A., LEFEVRE G. and FRANCOIS M. (1999b): A Double-Layered Hydroxide, $3\text{CaO Al}_2\text{O}_3 \text{ CaI}_2 \cdot 10\text{H}_2\text{O}$. *Acta Crystallographica C*, 55(12):1957-1959.
- REDDI L.N. and INYANG H.I. (2000): *Geoenvironmental Engineering: Principles and Applications*. New York, Basel: Marcel Dekker, Inc.
- RENAUDIN G. and FRANCOIS M. (1999): The Lamellar Double-Hydroxide (LDH) Compound with Composition $3\text{CaO Al}_2\text{O}_3 \text{ Ca}(\text{NO}_3)_2 \cdot 10\text{H}_2\text{O}$. *Acta Crystallographica C*, 55(6):835-838.
- REYNOLDS R.C. and REYNOLDS R. (2005): Newmod for Windows: The Calculation of One-Dimensional Diffraction Patterns of Mixed Layered Clay Minerals. [<http://www.angelfire.com/md/newmod>]
- RIETVELD H.M. (1969): A Profile Refinement Method for Nuclear and Magnetic Structures. *Journal of Applied Crystallography*, 2:65-71.
- RITCHIE I.M. and XU B.A. (1990): The Kinetics of Lime Slaking. *Hydrometallurgy*, 23(2-3):377-396.
- RODRIGUES F.A., MONTEIRO P.J.M. and SPOSITO G. (1999a): Surface Charge Density of Silica Suspended in Water-Acetone Mixtures. *Journal of Colloid and Interface Science*, 211(2):408-409.
- RODRIGUES F.A., MONTEIRO P.J.M. and SPOSITO G. (1999b): The Alkali-Silica Reaction - the Surface Charge Density of Silica and Its Effect on Expansive Pressure. *Cement Concrete Research*, 29(4):527-530.
- RODRIGUES F.A., MONTEIRO P.J.M. and SPOSITO G. (2001): The Alkali-Silica Reaction - the Effect of Monovalent and Bivalent Cations on the Surface Charge of Opal. *Cement Concrete Research*, 31(11):1549-1552.
- SALVADOR S. (1995): Pozzolanic Properties of Flash-Calcined Kaolinite - A Comparative-Study with Soak-Calcined Products. *Cement Concrete Research*, 25(1):102-112.
- SCHOONHEYDT R.A. (1995): Clay Mineral Surfaces. In: *Mineral Surfaces*. Edited by Vaughan D.J., Patrick R.A.D. London: Chapman & Hall.
- SCHRAMM L.L. and KWAK J.C.T. (1982): Influence of Exchangeable Cation Composition on the Size and Shape of Montmorillonite Particles in Dilute Suspension. *Clays and Clay Minerals*, 30(1):40-48.
- SCRIVENER K.L. (1989): The Microstructure of Concrete. In: *Materials Science of Concrete I*. Edited by Skalny J.P. Westerville, OH: American Ceramic Society.

- SERRY M.A., TAHA A.S., ELHEMALY S.A.S. and ELDIDAMONY H. (1984): Metakaolin Lime Hydration Products. *Thermochimica Acta*, 79(SEP):103-110.
- SHAINBERG I. and KEMPER W.D. (1966): Electrostatic Forces between Clay and Cations as Calculated and Inferred from Electrical Conductivity. In: *Proc. 14th Natl. Conf., Clays and Clay Minerals: 1966; Berkeley, CA*: 117-132.
- SHAINBERG I. and OTOH H. (1968): Size and Shape of Montmorillonite Particles Saturated with Na/Ca Ions (Inferred from Viscosity and Optical Measurements). *Israel Journal of Chemistry*, 6(3):251.
- SN 640 500a: Schweizer Norm: Stabilisierung, VSS (1985).
- SN 640 503a: Schweizer Norm: Stabilisierung mit Weisskalk, VSS (1987).
- SNYDER R.L. and BISH D.L. (1989): Quantitative Analysis by X-Ray Powder Diffraction. In: *Modern Powder Diffraction*. Edited by Bish D.L., Post J.E., Vol. 20. Washington D.C.: Mineralogical Society of America: 101-145.
- SPOSITO G., HOLTZCLAW K.M., CHARLET L., JOUANY C. and PAGE A.L. (1983a): Sodium Calcium and Sodium Magnesium Exchange on Wyoming Bentonite in Perchlorate and Chloride Background Ionic Media. *Soil Science Society of America Journal*, 47(1):51-56.
- SPOSITO G., HOLTZCLAW K.M., JOUANY C. and CHARLET L. (1983b): Cation Selectivity in Sodium - Calcium, Sodium - Magnesium, and Calcium - Magnesium Exchange on Wyoming Bentonite at 298-K. *Soil Science Society of America Journal*, 47(5):917-921.
- SCRIVENER K.L. (1989). In: *Materials Science of Concrete I*. Edited by Skalny J.P. Westerville, OH: American Ceramic Society: 127.
- STANJEK H. and SCHNEIDER J. (2000): Anisotropic Peak Broadening Analysis of a Biogenic Soil Greigite (Fe_3S_4) with Rietveld Analysis and Single Peak Fitting. *American Mineralogist*, 85:839-846.
- STRÄTLING W. and ZUR STRASSEN H. (1940): Die Reaktion zwischen gebranntem Kaolin und Kalk in wässriger Lösung, Teil 1 und 2. *Zeitschrift für anorganische und allgemeine Chemie*, 245(3):257-278.
- SVERDRUP H. and HOLMQVIST J. (1999): Kinetics, Steady State or Equilibrium ? Reversibility or Irreversibility in Chemical Weathering Rate Modelling. In: *Mineral/water interactions close to equilibrium: 1999; Speyer*: Forschungszentrum Karlsruhe GmbH.
- TAMBACH T.J., BOLHUIS P.G. and SMIT B. (2004): A Molecular Mechanism of Hysteresis in Clay Swelling. *Angewandte Chemie Int. Ed.*, 43(20):2650-2652.
- TAYLOR H.F.W. (1985): The Reactions of Cement Compounds with Water. In: *Reactivity of Solids, Mater. Sci. Monogr. 28A: 1985; Dijon, France*: Elsevier Science Publishers B.V.: 39-45.
- TAYLOR H.F.W. (1997): *Cement Chemistry*: Thomas Telford Publishing, London.

- TAYLOR W.H. and ARMAN A. (1960): Lime Stabilization Using Preconditioned Soils. *Bulletin No 262, Highway Research Board, Washington DC*:1-11.
- The Society of Rheology: [<http://www.rheology.org/sor/info/default.htm>]
- TITS J., WIELAND E., MÜLLER C.J., LANDESMAN C. and Bradbury M. H. (2006): Strontium Binding by Calcium Silicate Hydrates. Submitted to *Journal of Colloid and Interface Science*.
- TOURET O., PONS C.H., TESSIER D. and TARDY Y. (1990): Study on Distribution of Water in Saturated Mg²⁺ Clays with High Water-Content. *Clay Minerals*, 25(2):217-233.
- TOURNASSAT C., GRENECHE J.-M., TISSERAND D. and CHARLET L. (2004a): The Titration of Clay Minerals: I. Discontinuous Backtitration Technique Combined with CEC Measurements. *Journal of Colloid Interface Science*, 273(1):224-233.
- TOURNASSAT C., FERRAGE E., POINSIGNON C. and CHARLET L. (2004b): The Titration of Clay Minerals: II. Structure-Based Model and Implications for Clay Reactivity. *Journal of Colloid Interface Science*, 273(1):234-246.
- TOURNASSAT C., NEAMAN A., VILLIERAS F., BOSBACH D. and CHARLET L. (2003): Nanomorphology of Montmorillonite Particles: Estimation of the Clay Edge Sorption Site Density by Low-Pressure Gas Adsorption and AFM Observations. *American Mineralogist*, 88(11-12):1989-1995.
- TSIPURSKY S.I. and DRITS V.A. (1984): The Distribution of Octahedral Cations in the 2-1 Layers of Dioctahedral Smectites Studied by Oblique-Texture Electron-Diffraction. *Clay Minerals*, 19(2):177-193.
- UN (1992): Earth Construction Technology. United Nations Centre For Human Settlements, Nairobi.
- VULAVA V.M. (1998): Cation Competition in Soil Materials : Adsorption Equilibria and Transport. *PhD Thesis*.: ETH Zürich.
- WASHBURN E.W. (1921): Note on a Method of Determining the Distribution of Pore Sizes in a Porous Material. *Proceedings National Academy Sciences*, 7:115–116.
- WEISS A. (1989): About Sealing of Waste Disposals by Clays with Special Consideration of Organic Compounds in Percolating Water. *Applied Clay Science*, 4(2):193-209.
- WILLIAMS P.J., BIERNACKI J.J., WALKER L.R., MEYER H.M., RAWN C.J. and BAI J.M. (2002): Microanalysis of Alkali-Activated Fly Ash-Ch Pastes. *Cement Concrete Research*, 32(6):963-972.
- WINSLOW, N.M. and SHAPIRO, J.J. (1959): An Instrument for the Measurement of Pore-Size Distribution by Mercury Penetration. *ASTM Bull.*, 236, 39-54.
- XU B.A., GILES D.E. and RITCHIE I.M. (1997): Reactions of Lime with Aluminate-Containing Solutions. *Hydrometallurgy*, 44(1-2):231-244.
- XU B.A., GILES D.E. and RITCHIE I.M. (1998): Reactions of Lime with Carbonate-Containing Solutions. *Hydrometallurgy*, 48(2):205-224.

YOUNG R.A. (1993): Introduction to the Rietveld Method. In: *The Rietveld Method*. Edited by Young R.A. New York: Oxford University Press.

ZIEGLER C.L. (2004): Von dem Tarras, der Puzzolana und deren Substitutionsarten. *International Journal for Restoration*, 10(2):133-162 (original publ.: Hannoverisches Magazin, 1773).

Appendices

Chemical composition of the three clay materials as determined by X-ray fluorescence spectroscopy

	China Clay			illite Massif Central		Volclay			
	XRF	from ^a	ideal ^b	XRF	from ^c	from ^d	<20 µm XRF	total XRF	<2µm ^e
SiO ₂	47.43 (8)	47.66	46.54	50.26 (4)	51.70	57.3	57.10 (61)	57.86	56.17
TiO ₂	0.02 (0)	0.03	-	0.69 (7)	0.72	0.13	0.14 (5)	0.17	0.08
Al ₂ O ₃	37.08 (6)	37.3	39.49	20.10 (2)	28.55	18.5	18.94 (5)	19.00	20.15
Fe ₂ O ₃ /FeO	0.58 (4)	0.51	-	7.08 (7)	2.73/0.52	3.5	3.41 (9)	3.37	3.99
MgO	0.26 (0)	0.26	-	3.84 (13)	4.70	2.6	2.21 (6)	2.16	2.69
MnO	-	-	-	0.05 (0)	0.03	0.01	-	-	-
P ₂ O ₅	0.09 (0)	-	-	0.09 (0)	0.24	0.06	0.04 (0)	0.03	0.00
CaO	0.03 (0)	0.03	-	0.64 (0)	0.88	0.5	1.03 (0)	1.04	1.08
SrO	0.01 (0)	-	-	0.02 (0)		-	0.03 (0)	0.03	-
Na ₂ O	0.04 (0)	0.06	-	0.08 (1)	0.10	2.0	2.12 (5)	2.07	1.34
K ₂ O	1.06 (4)	1.53	-	7.77 (1)	8.45	0.6	0.43 (0)	0.52	0.18
Rb ₂ O	0.01 (0)	-	-	0.06 (0)		-	-	-	-
SO ₃	-	-	-	-	-	-	0.40 (5)	0.43	-
LOI	13.83 (15)	12.38	13.96	8.55 (7) ^f	6.6	14.9	13.90 (17)	13.7	13.89
sum	100.43 (8)	99.76	100	99.23 (1)	99.4	100.1	99.77 (54)	100.38	99.59

^aJasmund & Lagaly (1993) and references therein

^bfrom the ideal formula Al₂[Si₂O₅(OH)₄] or Al₂O₃ 2 SiO₂ 2 H₂O

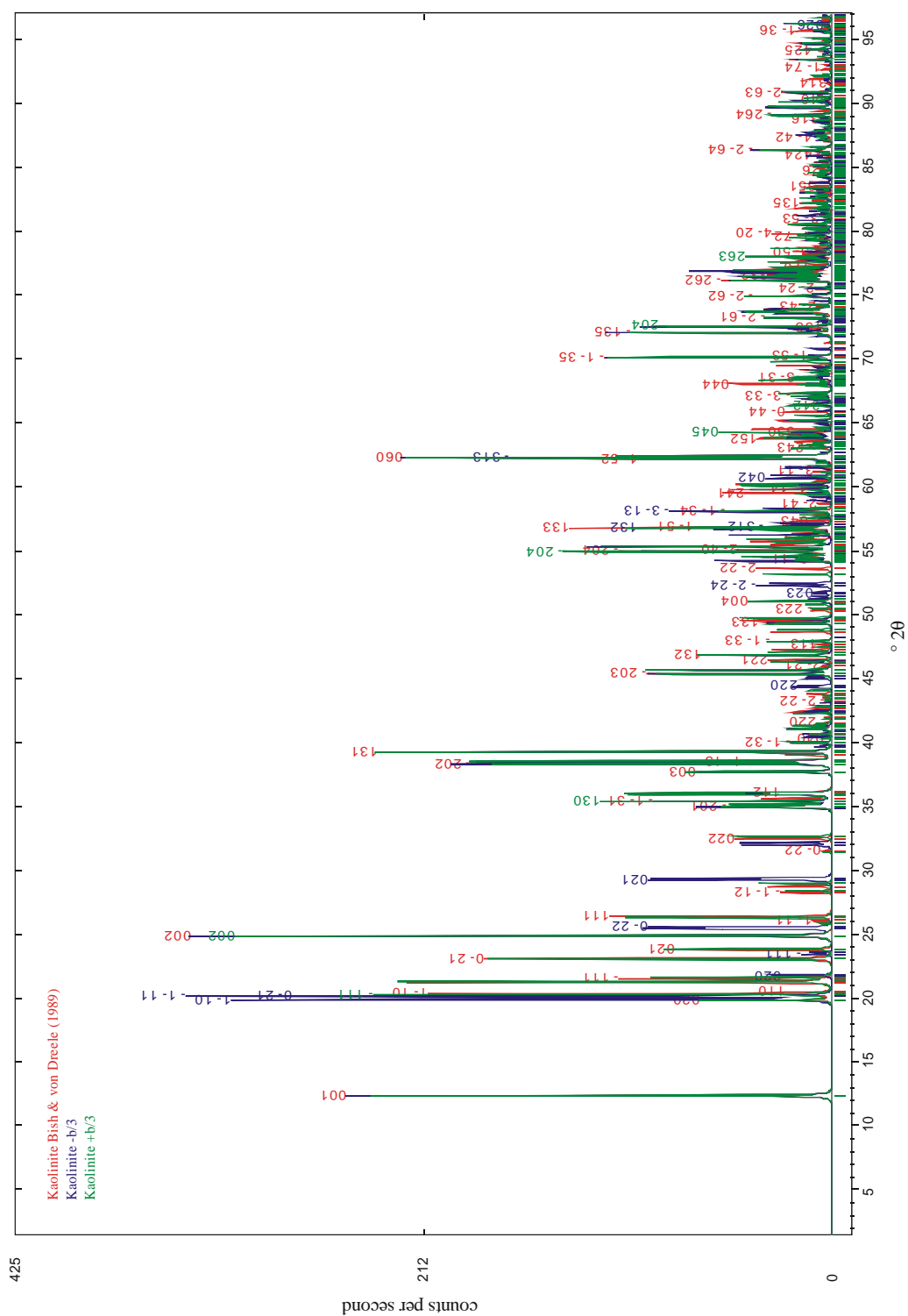
^cMüller Vonmoos et al. (1991)

^dOld laboratory analysis of the < 2 µm fraction

^eData from Mermut & Cano (2001) for the SWy-2 standard clay recalculated with the water content from TG data [Guggenheim & Koster Van Groos, 2001].

^fdetermined at 750°C

Diffraction patterns of the original kaolinite structure of Bish & von Dreele (1989) and the two flexible structure models with perfect $\pm b/3$ shifts (Bragg-Brentano, variable slit)



Sodium and calcium concentrations after 4 days inside and outside the dialysis bag for two independent series measured with ICP-AES

Na⁺ outside [mM]	Na⁺ inside [mM]	standard error [%]	Ca²⁺ outside [mM]	Ca²⁺ inside [mM]	standard error [%]
3.4	3.2	2.6	21.5	18.6	7.3
5.8	5.1	5.9	21.3	18.0	8.3
6.5	6.4	0.5	20.2	17.7	6.7
13.1	12.5	3.4	18.3	14.9	10.2
18.5	20.1	4.1	19.3	16.9	6.8
32.3	25.1	12.5	19.6	16.6	8.3
51.0	51.6	0.6	22.3	19.2	7.5
80.0	74.0	3.9	23.4	18.7	11.2
238.4	211.6	5.9	30.5	23.9	12.1
622.3	575.5	3.9	36.6	29.5	10.8
634.4	611.3	1.9	26.2	21.5	9.7
870.9	849.8	1.2	25.6	24.0	3.3
1085.8	1061.6	1.1	25.0	22.5	5.1
1245.4	1244.1	0.1	23.5	21.7	4.0
1329.2	1257.9	2.8	36.6	28.8	12.0
1329.9	1272.9	2.2	23.1	21.6	3.3
1630.3	1453.7	5.7	22.4	19.2	7.7

Chemical analysis of the solutions in contact with the pristine bentonite Volclay

concentration ^a	contact time				
	45 days	90 days	120 days	150 days	180 days
Na [mM]	- ^b				
K [mM]	-				
Ca [mM]	c				
Mg [μM]	4 (3)	2 (1)			-
Sr [μM]	56 (0)	75 (12)			74 (3)
Al [μM]	132 (78)	149 (81)			63 (9); 382 (64)
Fe [μM]	6 (4)	9 (5)			-
Si [μM]	112 (73)	171 (20)			262 (56); 2435 (521)

^a first values are averaged values, the values inside the brackets indicates the standard error of the mean of the last digits; the value after the semicolon is that of the sample with the highest clay content

^b varying values, depending on the cation exchange state

^c the calcium concentration is also a function of the system's pH; when sodium is exchanged from the bentonite, the pH increases which is responsible for the decrease in the calcium concentration

Chemical analysis of the solutions in contact with the Ca-form of the bentonite Volclay

concentration ^a	contact time				
	45 days	90 days	120 days	150 days	180 days
Na [mM]	0.4 (0)	0.8 (2)	0.48	0.53	0.57
K [mM]	0.2 (0)	0.3 (1)	0.41	0.46	0.49
Ca [mM]	20.4 (5)	19.9 (6)	20.8	20.0	21.1
Mg [μM]	32 (24)	9 (2); 106	3	1	37
Sr [μM]	36 (0)	41 (4)	99	98	100
Al [μM]	118	115 (24); 3758	241	183	326
Fe [μM]	24 (16)	7 (1); 227	12	8	23
Si [μM]	137	161 (25); 2198	61	48	430

^a first values are averaged values, the values inside the brackets indicates the standard error of the mean of the last digits; the value after the semicolon is that of the sample with the highest clay content

Chemical analysis of the solutions in contact with the illitic clay from Massif Central

concentration ^a [mM]	contact time				
	45 days	90 days	120 days	150 days	180 days
Na [mM]	0.2 (0)	0.2 (0)	0.35	0.40	0.44
K [mM]	2.3 (0)	3.0 (3)	4.85	5.81	6.60
Ca [mM]	20.2 (4)	19.3 (1)	18.4	18.4	19.4
Mg [μM]	46 (29)	3 (1); 29	5	3	70
Sr [μM]	103 (0)	93 (10)	147	155	155
Al [μM]	86	88 (3); 259	42	42	235
Fe [μM]	30 (18)	2 (0); 23	3	3	44
Si [μM]	137	64 (9); 303	92	56	456

^a first values are averaged values, the values inside the brackets indicates the standard error of the mean of the last digits; the value after the semicolon is that of the sample with the highest clay content

Chemical analysis of the solutions in contact with the kaolin China Clay

concentration [mM]	contact time				
	45 days	90 days	120 days	150 days	180 days
Na [mM]	1.5 (0)	2.7 (8)	1.51	1.58	1.4 (1)
K [mM]	0.9 (0)	1.5 (3)	1.31	1.40	0.9 (1)
Ca [mM]	20.2 (2)	21.3 (5)	19.6	19.5	21.1 (9)
Mg [μM]	3 (2)	3 (1)	11	4	31 (17)
Sr [μM]	84 (0)	69 (11)	150	152	167 (33)
Al [μM]	345 (0)	359 (69)	1063	390	305 (80); 1751
Fe [μM]	2 (0)	5 (1)	10	2	3 (1); 17
Si [μM]	203 (4)	177 (59)	831	293	810 (84); 3505

Consumption of China Clay oxides and CaO from CH in China Clay-lime mixtures at varying water to solid, varying lime to clay ratios and also different hydration times

	Initial amount of minerals [g/100mL]		mineral oxides used per ignited mass [g/100g]				
	clay	CH	content [%]	oxide _{clay}	CaO _{CH}		
hydration time [days]			CaO _{CH}	TA	extract	XRD	TA
48	10	5	30.6	4.4		8.5	6.1
48	10	5	30.6	4.7		12.0	6.6
96	39	13	22.7	4.9	8.2	11.3	7.0
96	39	13	22.7	4.8		10.1	6.8
91	24	8	22.7	5.6		8.7	7.7
91	12	4	22.7	5.2		7.8	7.3
91	9	3	22.7	5.0		10.2	6.8
91	6	2	22.7	4.3		10.0	6.3
125	9	9	46.8	4.8	8.0	13.0	6.7
166	9	9	46.8	6.2	8.0	10.8	8.6
182	39	26	37.0	7.2	7.9	14.3	10.1
182	6	14	67.3	8.1		15.7	11.1
182	6	9	56.9	7.2	8.8	12.0	9.8
182	6	4	37.0	7.4	11.2	12.9	10.4

Consumption of Volclay oxides and CaO from CH in Volclay-lime mixtures at varying water to solid, varying lime to clay ratios and also different hydration times (data in the upper part of the table are reported for the Ca-form, in the lower part for the pristine Volclay)

	Initial amount of minerals [g/100mL]		content [%]	mineral oxides used per ignited mass [g/100g]			
	Ca-clay	CH		oxide _{Volclay}	TA	extract	CaO _{CH}
hydration time							
[days]							
48	10	5	30.8	7.1			16.8
48	10	5	30.8	6.5			14.6
93	40	20	30.8	8.3	6.2	20.6	20.6
93	20	10	30.8	8.1		17.2	20.6
93	10	5	30.8	7.8	6.1	18.2	20.2
93	6	3	30.8	8.4	5.7	18.3	21.7
125	6	10	59.7	7.2	10.3	20.1	18.0
166	6	10	59.7	7.7	5.1	16.3	18.9
182	6	10	59.7	8.8		23.1	22.4
	clay						
97	6	13	65.6	7.8			19.7
97	6	10	59.5	7.9		19.5	19.8
97	6	5	42.3	7.8		21.2	19.1
97	6	4	37.0	7.9		18.4	20.1
95	39	13	22.7	7.8	8.9	19.8	20.6
95	15	5	22.7	7.8	8.4	20.2	21.2
97	12	4	22.7	7.7		20.6	22.6
97	9	3	22.7	7.9		20.6	22.9
97	7.5	2.5	22.7	7.9		20.6	23.4
95	6	2	22.7	7.8	10.2	20.7	23.7
182	39	39	46.8	7.8	4.1	23.4	18.8
182	15	15	46.8	7.9	6.8		22.1

Consumption of Illite oxides and CaO from CH in Illite-lime mixtures at varying water to solid, varying lime to clay ratios and also different hydration times

hydration time [days]	Initial amount of minerals [g/100mL]		content [%]	mineral oxides used per ignited mass [g/100g]				
	clay	CH		oxide _{clay}	CaO _{CH}	TA	extract	XRD
48	10	5	29.6	10.4			8.3	10.5
93	6	2	21.9	10.2	10.5		8.9	9.5
93	6	2	21.9	9.6				9.3
93	9	3	21.9	8.8				8.8
93	9	3	21.9	9.1				8.7
93	12	4	21.9		5.6			
93	15	5	21.9	10.4				9.7
93	24	8	21.9	9.2				9.1
93	39	13	21.9	9.0	9.5		8.0	9.1
125	9	9	45.7	12.5			10.2	11.9
166	9	9	45.7	12.2	11.3			11.5

Curriculum Vitae

Christian Müller

- 1969 born in Esslingen (Germany)
- 1980-1989 High School Schelztorgymnasium Esslingen
- 1989-1990 Civil Service in Stetten im Remstal
- 1991-1993 Restorer for archeological objects in Schwäbisch Gmünd and Karlsruhe
- 1993-1997 Studies in Mineralogy at the University of Karlsruhe
- 1997-1999 Studies in Water Chemistry and Earth Sciences at the ETH Zurich
- 1999-2000 Diploma Thesis at the EAWAG, ETH Zürich
- 2000-2002 Scientific Assistant at the IGT, ETH Zurich
- 2002-2005 Ph.D. Thesis at the IGT, ETH Zurich